Competing Demands for a Complex System: Photosystem II Repair, Photoprotection and Quantum Yield

John Veerman, Ph.D Thesis

Biology Program

Submitted in partial fulfillment

of the requirements for the degree of

Ph.D Biology

Faculty of Mathematics and Science, Brock University

St. Catharines, Ontario

DEDICATION

I dedicate this work to the friends and family who have always supported me. Foremost of these people are my parents Jeannie and Eddie as well as my brother Mark. I truly know what it is to be accepted and encouraged by the people in my life, such moral support lends to perseverance which is much of what this thesis represents.

ACKNOWLEDGEMENTS

Although some may speak otherwise, the accomplishment of goals is rarely, if ever, an exercise of the individual. Starting as an undergraduate student at Brock University, I received patient and valued instruction from many Professors, lab demonstrators and teaching assistants. I was essentially molded into a disciplined observer and analyst. Upon commencement of graduate studies I was further supported by my supervisor Professor Douglas Bruce who mentored me while allowing for a degree of autonomy mixed with valued guidance to keep me on track. Dr. Sergei Vasil'ev also served as a mentor in the laboratory and through the course of my graduate studies I learned it is the questions that matter rather than the answers.

I would also like to thank international collaborators Professor Julian Eaton-Rye, Professor Conrad Mullineaux, Dr. Fikret Mamedov, Professor Stenbjörn Styring and Fiona Bently. I am also greatly appreciative of the work performed by students in our lab at Brock University: Michael McConnell, Gavin Patton, Abdullah Mahboob and Justin Ramanauskas. Along with Sergei and Doug, this list represents the people who collaborated with me during my studies. They are the co-authors of the publications associated with this thesis and their precise contributions are outlined in the preface of each chapter. I feel it important to reiterate that research is truly a cooperative exercise and I am exceedingly grateful for being fortunate enough to be a member of good 'teams'.

I am thankful for all the constructive input from my committee members: Professor Art van der Est, Professor Douglas Campbell, Professor Edward Sternin, Professor Jeffrey Atkinson, Professor Gary Pickering and my supervisor Professor Douglas Bruce.

Besides direct collaborators I also worked with many good people in the laboratory, among them Allen Derks, Pascal Comte and Matt Scott whom I will always remember for his creativity and honesty. We always had interesting conversations in the lab, covering just about every subject but also sometimes related to our actual research. I would also be remiss if I did not include Abdullah on this list of 'lab mates'.

I am also grateful for the funding received from Brock University, the Government of Ontario (in the form of an OGS scholarship) and grants from the National Sciences and Engineering Research Council of Canada to Professor Bruce's laboratory.

" In the series of things those which follow are always aptly fitted to those which have gone before; for this series is not like a mere enumeration of disjointed things, which has only a necessary sequence, but it is a rational connection: and as all existing things are arranged together harmoniously, so the things which come into existence exhibit no mere succession, but a certain wonderful relationship."

- Marcus Aurelius

Table of Contents

Table of Figures

Tables

ABSTRACT

Photosynthesis in general is a key biological process on Earth and Photosystem II (PSII) is an important component of this process. PSII is the only enzyme capable of oxidizing water and is largely responsible for the primordial build-up and present maintenance of the oxygen in the atmosphere. This thesis endeavoured to understand the link between structure and function in PSII with special focus on primary photochemistry, repair/photodamage and spectral characteristics. The deletion of the PsbU subunit of PSII in cyanobacteria caused a decoupling of the Phycobilisomes (PBS) from PSII, likely as a result of increased rates of PSII photodamage with the PBS decoupling acting as a measure to protect PSII from further damage. Isolated fractions of spinach thylakoid membranes were utilized to characterize the heterogeneity present in the various compartments of the thylakoid membrane. It was found that the pooled PSII-LHCII pigment populations were connected in the grana stack and there was also a progressive decrease in the reaction rates of primary photochemistry and antennae size of PSII as the sample origin moved from grana to stroma. The results were consistent with PSII complexes becoming damaged in the grana and being sent to the stroma for repair. The dramatic quenching of variable fluorescence and overall fluorescent yield of PSII in desiccated lichens was also studied in order to investigate the mechanism by which the quenching operated. It was determined that the source of the quenching was a novel long wavelength emitting external quencher. Point mutations to amino acids acting as ligands to chromophores of interest in PSII were utilized in cyanobacteria to determine the role of specific chromophores in energy transfer and primary photochemistry. These results indicated that the H114 ligated chlorophyll acts as the 'trap' chlorophyll in CP47 at low temperature and that the Q130E mutation imparts considerable changes to PSII electron transfer kinetics, essentially protecting the complex via increased non-radiative charge

recombination and also apparently exhibiting increased charge stabilization. Overall, the results demonstrate the challenge of studying the link between structure and function in PSII. The results also indicate that PSII structure and function are in large part a product of PSII repair/photoprotection based factors as well as that of photochemical yield. This complexity is compounded by the association of PSII with other components of the photosynthetic apparatus as well as the heterogeneity necessitated by PSII protection/repair. It would appear that the study of PSII requires the development of a more comprehensive model of the PSII supercomplex. The MD simulation as utilized in this thesis is a nascent step toward such a model.

List of Abbreviations:

AP = Allophycocyanin

AP_B = Allophycocyanin Terminal Emitter

ATP = Adenosine-5'-triphosphateCCD = Charge Coupled Device

Chl *a* = Chlorophyll a

Chl *b* = Chlorophyll b

D1:1 = D1 protein type 1

D1:2 = D1 protein type 2

D1:Ph = D1 Pheophytin

DAS = Decay Associated Spectra

DCMU = 3-(3,4-dichlorophenyl)-1,1-dimethylurea

E_m = Electromotive Force

F_D = fluorescence yield of desiccated *Parmelia sulcata*

F_m = dark-adapted fluorescence yield when photosystem II traps are closed

F_o = dark-adapted fluorescence yield when photosystem II traps are open

FRAP = Fluorescence Recovery After Photobleaching

F_v = Fm – Fo

H114Q = CP47 protein substitution mutation, Histidine to Glutamine at 114 position

HEPES = 4-(2-hydroxyethyl)-1-piperazineethanesulfonic acid

IRF = Instrument Response Function

LHCII = Light Harvesting Complex II

MD = Molecular Dynamic

MDS = Molecular Dynamic Simulation

NPQ = Non-Photochemical Quenching

OEC = Oxygen Evolution Complex

PAM = Pulse Amplitude Modulated

PBS = Phycobilisome(s)

PDB = Protein Data Bank

PC = Phycocyanin

PC = Plastocyanin

PCC = Pasteur Culture Collection

PCR = Polymerase Chain Reaction

PE = Phycoerythrin

Ph = Pheophytin

PS = Photosystem

PSI = Photosystem I

PSII = Photosystem II

Q130E = D1 protein substitution mutation, Glutamine to Glutamate at 130 position

Q_A = primary Quinone electron acceptor in photosystem II

Q_B = Quinone B

Q_B = secondary Quinone electron acceptor in photosystem II

qP = Photochemical Quenching

RC = Reaction Center

P680 = primary electron donor in photosystem II

TES = 2-[tris(hydroxymethyl)methyl]amino-1-ethanesulfonic acid

UV-B = Ultra Violet type B radiation, 280-315nm wavelength

INTRODUCTION

Significance of Photosynthesis

The capturing of light energy from the sun to drive chemical reactions was an early innovation during the history of life on Earth, with initial forms of the process thought to have first occurred as long ago as 3.5 billion years (1). Although the precise life forms and chemical processes involved in the early evolution of photosynthesis remains uncertain (2); the initial paradigm of photosynthetic activity is presumed to have involved the use of compounds such as hydrogen sulfide as an electron source (3). Since these compounds were in limited supply on primordial Earth, while water was ubiquitous; selective pressures highly favored the subsequent nascence of photosynthetic organisms capable of oxidizing water for use as an electron source (4). The use of water as a reactant resulted in the production of molecular oxygen, representing a pivotal point in the evolution of life on Earth (*4*), as the early atmosphere to this point was both anaerobic and reducing (*5*). Oxygenic photosynthesis progressively increased the oxygen content of the atmosphere over billions of years which has been correlated with the advent of complex aerobic eukaryotic life forms (*3*). Since the supply of water, carbon dioxide and sunlight were essentially unlimited for the purposes of oxygenic photosynthesis, the process also resulted in a substantial increase in the biomass present on the planet as well as a decreased level of carbon dioxide through carbon fixation (*6*). These changes resulted in conditions amenable to complex aerobic life using oxygen as a reactant and producing carbon dioxide as a waste product (*6*). This dynamic extends to the present day with the current situation of an atmosphere containing life sustaining oxygen, ozone that shields the surface of the planet from UV radiation and carbon dioxide present at a relatively low concentration that serves to mitigate the greenhouse effect on the Earth's temperature (*5*). In addition, most of the biomass and bioavailable energy on the

planet can be ultimately attributed to oxygenic photosynthesis (*7*).

As indicated above, oxygenic photosynthesis remains an intriguing phenomenon in regards to the formation and evolution of life on Earth. In addition, the nebulous beginnings of photosynthesis and the evolutionary steps required for the apparatus to evolve as seen in the present day remain interesting(*4*), even in isolation. However, oxygenic photosynthesis is also a process that remains both remarkably efficient and chemically unique (*3;8*). In particular, Photosystem II (PSII) represents such efficiency, with a quantum yield of approximately 0.95 for charge separation of the primary radical pair per photon absorbed by PSII(*9*) as well as the ability to oxidize water. Water oxidation is unique to PSII: no other enzyme is able to split water (*3*); while PSII performs this feat repeatedly when active. There is a good reason why water, while plentiful, is not utilized as an electron source by any other enzyme: the midpoint reduction potential required for water oxidation is 0.82 volts (*3*). However, the reaction center of PSII produces a potential in excess of 1 volt (*10*), the highest potential produced by any enzyme.

Although PSII remains interesting because of its unique and complex abilities, mysterious evolutionary history and importance regarding the evolution of life on Earth; the research of PSII has many potential applications. Since photosynthesis is the source of the world's food supply, PSII function and overall efficiency have potential applications in farming and by extension the growing biofuel sector (*11*). Since PSII generates such a high redox potential and is light driven, the complex has also generated interest for possible roles in industrial chemistry, with the idea being that PSII could be modified so as to perform a variety of chemical reactions. Similarly, PSII has also been identified as a candidate for possible use in solar cells; as such cells would use water as a reactant and produce oxygen as a waste product. In addition, the entire photosynthetic apparatus might be modified to produce hydrogen as well as

oxygen (*12;13;13*). At the very least, the principles gleaned from studying PSII could result in the development of artificial systems inspired by the complex, and researchers are presently working in such a capacity (*14*). Although these potential innovations are long-term overriding goals, they still provide impetus for research into how PSII functions.

Focus: Key Factors Affecting Photosystem II Photochemistry

The high redox potentials produced by PSII cause the complex to operate with a relatively high chance of damage due to the complex oxidizing or reducing itself (*15*). Interestingly, PSII incurs such a high rate of damage and the energy cost is such that the rate of repair is limited by the ATP produced by photosynthesis (*16*). The light harvesting process of PSII is a delicate balance between excitation energy and electron transport. In order to mediate this balance photosynthetic organisms have evolved energy dissipation mechanisms known as quenching as well as excitation energy redistribution mechanisms such as state transitions to protect PSII from damage and balance the activity of PSII and PSI (*17*). As a result, both quenching and PSII damage/repair mechanisms remain an area of intense interest due to the importance of each to the overall yield of photosynthesis and what they can reveal about PSII photochemisty.

The overall efficiency of PSII within the context of the photosynthetic apparatus is essentially a function of the amount of energy required to maintain the population of active PSII centers as compared to the photochemical yield of the population per photon absorbed. While such efficiency is highly dependent on the aforementioned repair/protective mechanisms, the structure of the complex is perhaps the key to understanding how PSII functions. In PSII, function follows forms, where the location and presence of various cofactors, pigments, proteins, metal ions and lipids all contribute to how the complex works (*18*). The structure directly relates

to PSII light harvesting efficiency, damage and repair as well as quenching and thus has been an area under considerable investigation, with crystal structures being pursued and produced with vigor (*19-21*).

Photosystem II Structure and Function

PSII is a membrane bound pigment protein complex consisting of 35 chlorophyll a (Chl *a*) molecules, 12 cartenoid pigment molecules, 20 protein subunits along with various cofactors, ions and lipids(*18*). The subunits CP43 and CP47 both contain pigment molecules and serve to funnel energy into the reaction center of PSII. The reaction center consists of the D1 and D2 subunits, which host cofactors involved in the electron transport chain as well as the oxygen evolving complex (OEC). The luminal side of the complex consists of three subunits, PsbU, PsbO and PsbV, these serve to shield the OEC and also support oxygen evolution (*22*).

When the energy derived from an absorbed photon in the form of the lowest stable excited state, or exciton, enters the reaction center via exciton transfer (Figure 1); charge separation occurs at P680 (Figure 2), the electron is transferred to the D1 pheophytin then Quinone A (Q_A) then Quinone B (Q_B). On the donor side, Tyrosine Z is oxidized to the Tyrosine Z+ radical which in turn oxidizes the manganese cluster of the OEC. The oxidation of the manganese cluster occurs successively four times then two water molecules are oxidized resulting in the release of molecular oxygen and protons.

Although PSII includes integral Chl *a* based antennae in CP43 and CP47, these are supplemented by auxiliary antennae; in cyanobacteria this antennae takes the form of the phycobilisome (PBS) as shown in Figure 1. The PBS complex consists of phycobilin chromophores covalently bonded to linker proteins to form phycobiliproteins: Allophycocyanin (AP), Phycocyanin (PC) and Phycoerythrin (PE) (*23*). The superstructure of the PBS consists of

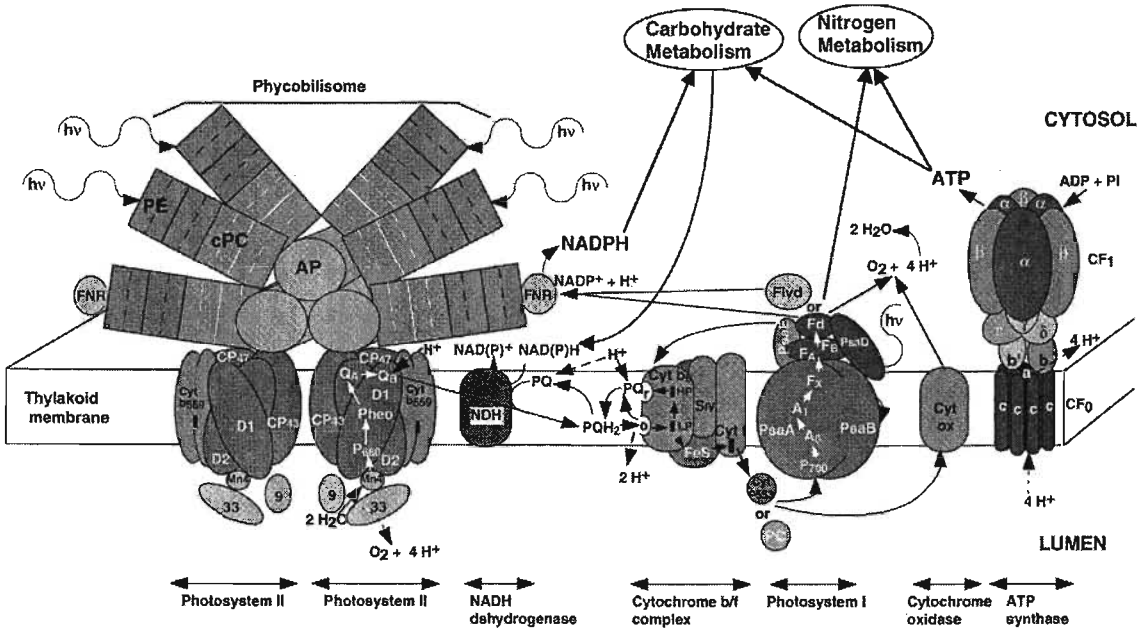

Figure 1. The photosynthetic apparatus in cyanobacteria, showing PBS, PSII dimer and PSI as well as the enzymes involved with the electron transport chain as well as various metabolic pathways both central and peripheral to the photosynthetic apparatus. Figure reproduced from (*46*) used with permission.

a AP core with PC 'rods' extending outward, with some species of cyanobacteria also incorporating PE into the ends of 'rods'. The energy transfer interlink between the PBS and PSII is facilitated by the Allophycocyanin terminal emitter (AP_E)(*24*), which is excitonically coupled to PSII. The exciton energy levels of the phycobiliproteins decrease in a classic 'downhill' energy transfer scheme with the energy successively decreasing from outer rod to the core and AP_E (Table 1 and Figure 1). It should be noted that most of the experiments on cyanobacteria presented in this thesis were carried out exclusively on *Synechocystis* PCC 6803, which possess PBS with AP and PC but without PE.

In higher plants, light harvesting complex II (LHCII) serves as an auxiliary antennae and contains both Chl *a* and *b* pigment molecules. These antennae complexes have known quenching properties (*25;26*) and serve to supplement the light harvesting capacity of PSII under low light level conditions. PSII-LHCII super complexes include CP24, CP26 and CP29 monomers as well as LHCII trimers as shown in Figure 2.

Photosynthetic Apparatus

In order to fully understand the role of PSII, the complex must be appreciated in the context of the entire photosynthetic apparatus. As shown in Figure 3, PSII operates in concert with Photosystem I (PSI), the Cyt b_6f complex and ATP synthase. As mentioned earlier, PSII absorbs light and uses the energy to split water and drive the electron transport chain. This leads to Q_B being reduced and after accepting two electrons and being protonated the molecule migrates to the Cyt b_6f complex, reducing the complex and transferring electrons further down the chain. The Cyt b_6f complex then reduces and subsequently releases plastocyanin (PC) which travels to PSI, acting as an electron donor. PSI then uses light energy to reduce ferredoxin and ultimately convert $NADP^+$ to NADPH for use in carbon fixation reactions. These reactions also

Table 1. Absorbance and fluorescence maxima for PBS constituent phycobiliproteins (*23;24*).

Phycobiliprotein	**≈A_{max} (nm)**	**≈F_{max} (nm)**
PE	498*, 560	575
PC	620	640-650
AP	650	660
AP_E	657	676

*Alternate Forms of PE with shorter wavelength absorbance maxima are present in a few types of marine cyanobacteria

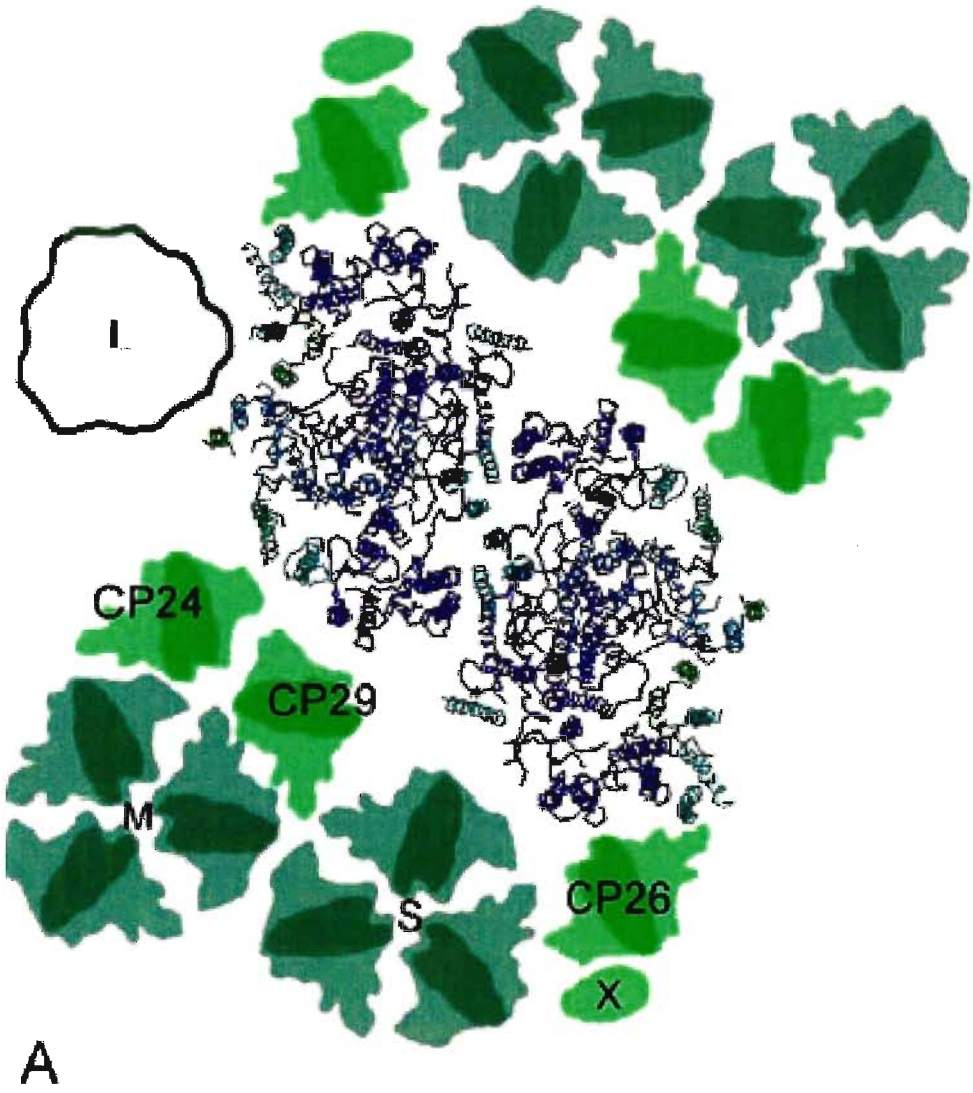

Figure 2. Schematic of PSII-LHCII supercomplex from spinach, PSII protein backbone alpha helixes shown in center with adjacent LHCII monomers and trimers on the periphery. M and S denote medium and strongly associated LHCII, with L assigned to trimer found in spinach only. Figure reproduced from (*47*) used with permission.

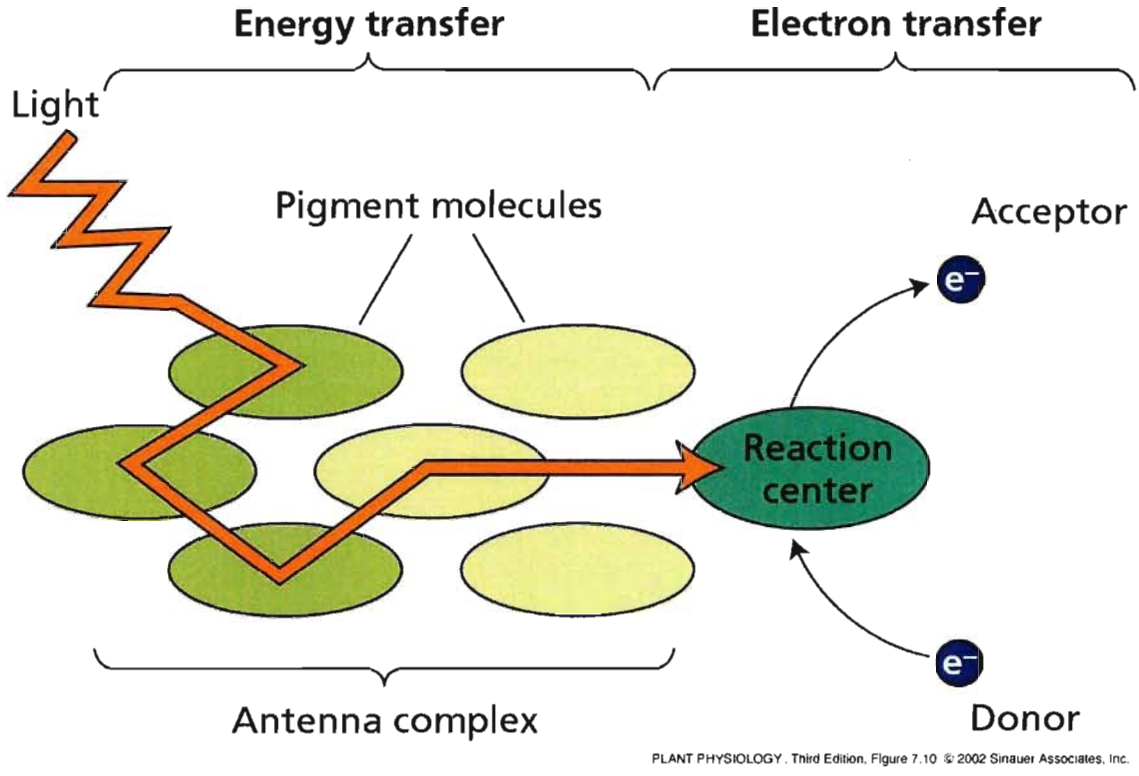

Figure 3. Schematic representation of exciton transfer from pigment to pigment and the resulting energy being used for electron transfer. Figure reproduced from (*48*) used with permission.

facilitate the generation of a proton gradient across the thylakoid membrane that is utilized by ATP synthase to produce ATP.

Since PSII works in tandem with PSI, the overall quantum yield of the photosynthetic apparatus is thought to be maximized when both complexes are operating synergistically (*27*). The rate at which each complex performs photochemistry is highly dependent on the distribution of the aforementioned auxiliary antennae, with LHCII in higher plants or PBS in the case of cyanobacteria redistributing with respect to connectivity to PSII and PSI based on light conditions so as to balance the excitation energy and thus activity of the PSII and PSI populations (*27*). These changes in distribution of auxiliary antennae are known as state transitions and are an important factor in both the efficiency of PSII and the overall efficiency of photosynthesis.

Photosystem II Repair System

As mentioned earlier, the structure of PSII coupled with the high redox potential produced, results in a high rate of damage to the complex during charge separation (*15*). PSII repair predominantly consists of D1 subunit replacement (*28*) as shown in Figure 4 and requires a complex repair apparatus to facilitate the disassembly, replacement of damaged subunits and reassembly (*15*).

In higher plants, the repair of PSII is known to be compartmentalized with the grana stacks of the chloroplast representing a region where PSII is active, while the stroma portion acts as the site of PSII repair (*29*). Existing models of PSII repair proceed as follows: PSII damaged in the grana stack is progressively disassembled while being transported to the stroma lamellae where subunits are replaced and the complex is subsequently reassembled and reinserted into the grana stack (*30*). The reactivation and reassembly phase of the repair system is schematically

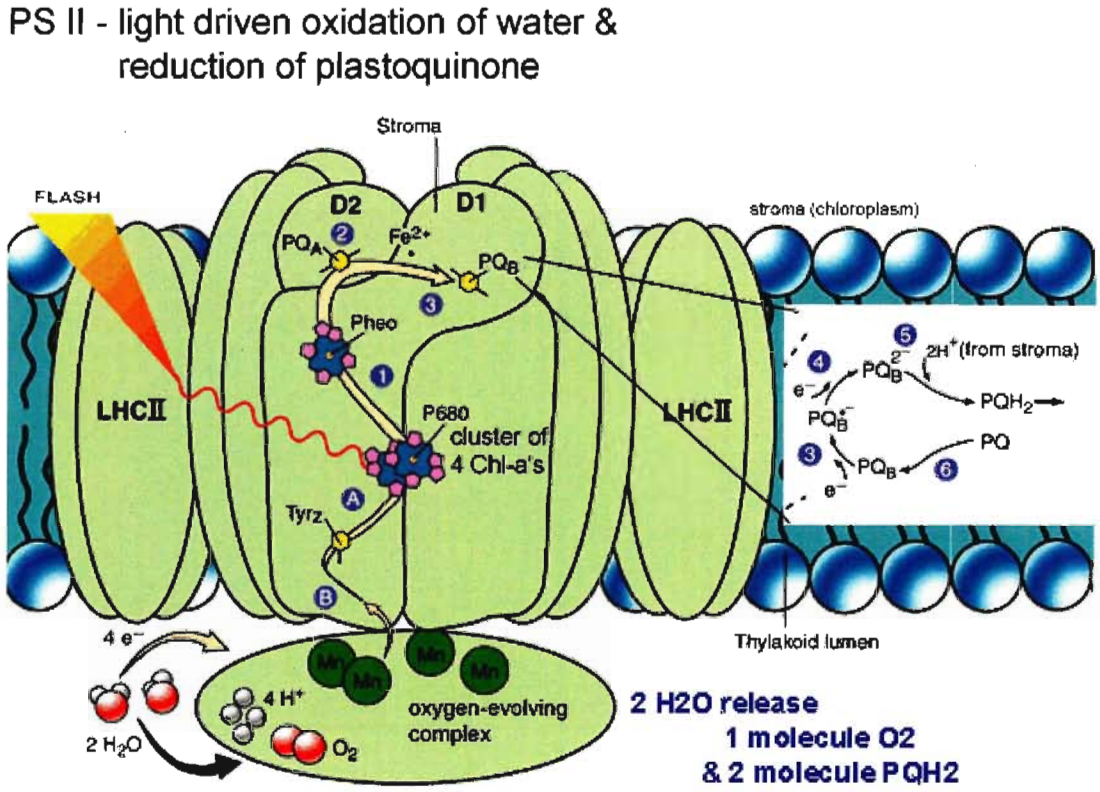

Figure 4. PSII complex embedded in lipid bilayer with the major cofactors of the reaction center and OEC being represented as well. Figure reproduced from (*49*) used with permission.

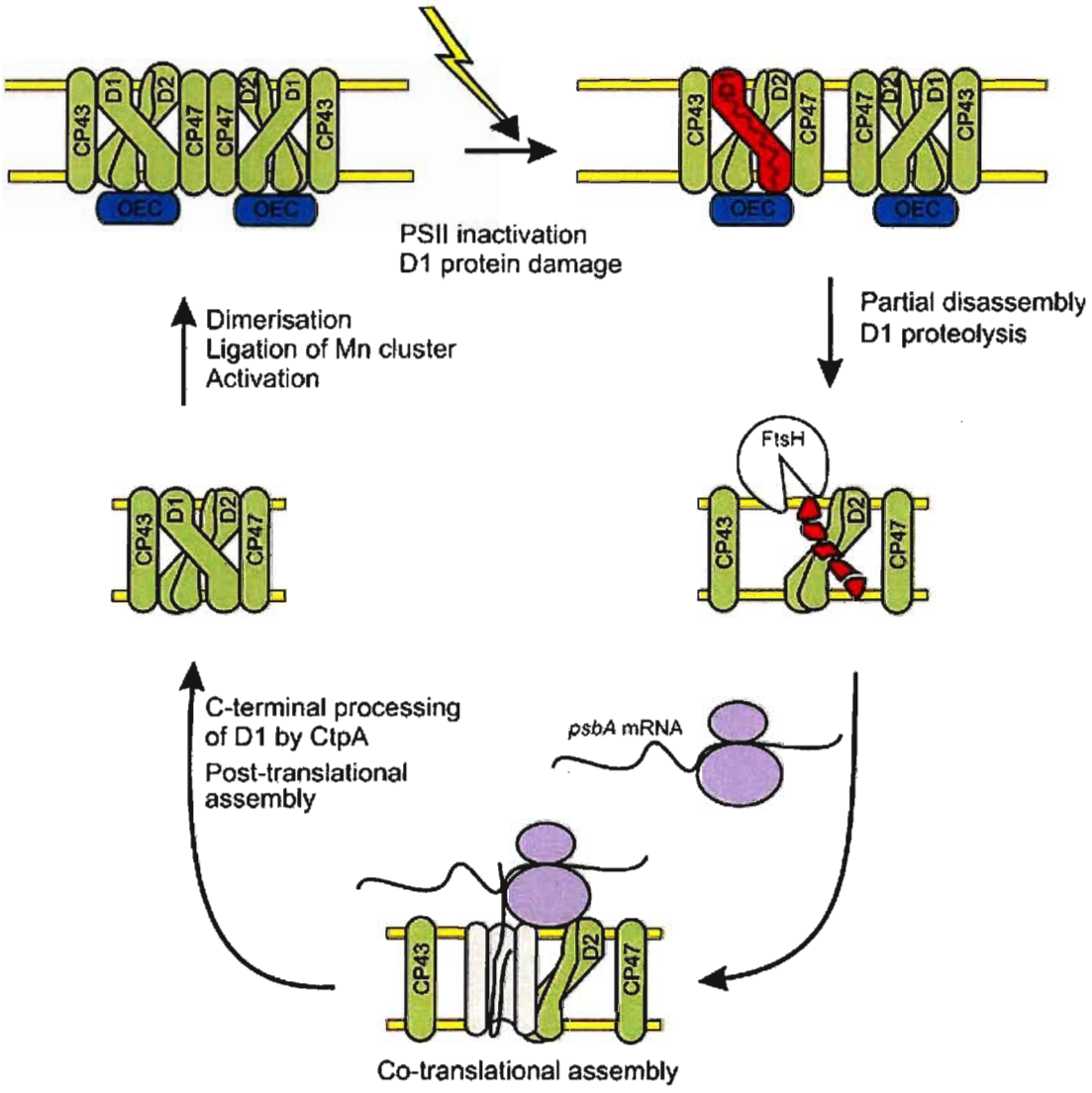

Figure 5. Schematic of PSII repair: light driven inactivation via D1 protein damage is followed by partial disassembly of PSII and D1 degradation by the protease FtsH. The *psbA* transcript and ribosome complex directly insert the D1 protein as the gene is translated. D1 subunit then undergoes C-terminal processing followed by reassembly, reactivation and dimerization. Figure reproduced from (*50*) used with permission.

represented in Figure 5: which is essentially the opposite of the damage/inactivation and disassembly process leading up to D1 and/or other protein subunit replacement.

PSII Quenching

Since PSII is highly vulnerable to damage under unfavorable conditions, mechanisms and specific structures present in PSII have evolved to protect the complex. Thus decreasing the energetic investment required by the PSII repair system as a means to maximize the overall photochemical yield of photosynthesis. These include the detachment of auxiliary antennae from PSII under high light level conditions or the evolution of certain subunits present in PSII such as PsbU and PsbV which serve to reduce the chance of damage occurring by shielding the OEC. However, perhaps the most important protective aspect of PSII is the aforementioned quenching (*31*). There exist two types: non-photochemical quenching (NPQ) and photochemical quenching (qP). qP denotes the quenching of the excited state through photochemical means (*32*). Such reactions include primary photochemistry: the transfer of electrons from P680* to Pheophytin and down the electron transport chain. In the case of NPQ, energy derived from light in the form of an exciton is transferred to a quencher then dissipated as heat (*33*).

NPQ quenching mechanisms generally occur when PSII is subjected to high light levels, is damaged in some other manner via heat or oxidizing agents or is exposed to unfavorable physiological conditions such as desiccation (*33*). Perhaps the most striking example of effective NPQ is in the special case of lichens, which are organisms containing both a fungal portion and photosynthetic portion which includes cyanobacteria or algae (*34*). Lichens are immobile and often inhabit harsh environments where they are exposed to unshielded sunlight, temperature extremes and desiccation (*33*). Many species of lichen can withstand extended periods completely desiccated and exposed to direct sunlight and still retain substantial PSII activity

upon hydration. This is accomplished largely through quenching of PSII, with a variety of mechanisms involved, both intrinsic to PSII and mediated by other proteins or antennae (*35*).

As alluded to above, excitation energy quenching is an integral part of PSII function and is heavily related to PSII repair and efficiency. Quenching mechanisms are also, as with PSII repair and damage mechanisms, dependent on PSII structure. Thus, determining the mechanisms of PSII quenching aids in ascertaining how the structures within PSII operate and perhaps how they can be improved. It should also be noted that PSII quenching is thought to be both native to PSII and a result of activity by auxiliary antennae or perhaps other complexes evolved specifically for quenching PSII (*32*). As such, studies involving PSII quenching provide potential for a better understanding of how PSII operates within the context of the photosynthetic apparatus as well as providing a means to discover new complexes associated with PSII.

PSII Mutation Studies and Modeling

Researchers often use mutations of genes encoding the protein subunits of PSII in order to determine the role of specific structures. Point mutations to Chl or pheophytin ligands are capable of altering the redox potentials, spectral properties and the orientation/position of the ligated pigment molecules. Observing the effect of such alterations to pigment properties on PSII light harvesting function serves to reveal the function of the specific pigment molecule and as such have been widely used previously to investigate PSII (*36*). While point mutations are meant to have a very specific effect on a single molecule, deletion mutations omitting an entire subunit from PSII have also been used such as in the case of PsbU and PsbV (*37;38*). Although the scale and location of the mutations involved in such research can be highly disparate ranging from an entire pigment protein complex such as in PSI-less mutants (*39*) to point mutations (*40*), the objective is the same: to determine the functional role of a specific structure in PSII.

Mutation studies, when combined with crystal structures of PSII, readily facilitate forming a link between the structure of PSII and the function of each component. However, this approach remains limited because the number of combinations of mutations required to elucidate how all the components in PSII work together is prohibitively high. Computer modeling represents an elegant solution to this problem, whereby a simulation of PSII is created using information from various experiments and models (*41*). The computer model can then be tested for validity by attempting to predict experimental results and revised as needed, providing a more accurate model with each successive revision. Simple kinetic models have been used to simulate PSII photochemistry (*42*), and auxiliary antennae can also be included in such a model (*29*). However, one of the most comprehensive and complex models used to date is the molecular dynamic simulation of PSII as generated by Sergei Vassilev (*43*). The model includes the lipid bilayer, water molecules, PSII complex in dimer form and can be paired with a variety of other programs to obtain useful data.

The ultimate goal of such a model would be to include the various aspects of PSII function such as PSII photochemistry, interactions with auxiliary antennae and the rest of the photosynthetic apparatus, PSII damage and repair and the facility of each structure in PSII. At this point existing models include light harvesting and photochemical aspects of PSII with some level of ability to include auxiliary antennae and quenching when paired with kinetic models (*29;41;44*).

Putting it all together: Investigating Photosystem II

Since the link between structure and function remains an intense area of interest in photosynthesis research, this thesis involved studying the effect of alterations to the structure of PSII on light harvesting efficiency and photochemical function. In Chapters 1 and 4 mutations

were utilized to target structures in PSII for removal or replacement in order to determine the role of the structure or related structures. To this end, ligands of the D1 pheophytin and the most red-shifted chlorophyll present in CP47 were altered by point mutations and a mutation featuring the deletion of PsbU from the luminal side of PSII was utilized. Deletion of PsbU was found to impair PSII photochemistry and to disrupt the association of PSII with the PBS and had been shown previously to increase the probability of PSII damage rates (*38*). It is also interesting to note that a recent study indicated that the observed decoupling of the PBS from PSII represents a mechanism which serves to protect PSII from photo damage by regulating the influx of excitation energy (*45*). The point mutations shifted the Q_Y transition of the red shifted chlorophyll in CP47 and the Q_Y absorbance band in the D1 pheophytin. The D1 pheophytin point mutation produced profound effects on PSII photochemistry. The Q130E mutation increased the rate of non-radiative dissipation of the radical pair in the reaction center of PSII, protecting the complex from photodamage. Interestingly, the fluorescence decay kinetics of open cyanobacteria PSII reaction centers became similar to those of higher plant PSII complexes. In addition, a molecular dynamic simulation (*43*) of PSII was also used to model the point mutations. The simulation was able to reasonably predict the shifts in the energy level of the D1 pheophytin as a result of the Q130E mutation to the pheophytin ligand.

Compartmentalized PSII repair in thylakoid membranes was also studied since the repair system involves the progressive disassembly then reassembly of PSII and leaves different compartments in the thylakoid membrane with populations of PSII complexes in various states of assembly as shown in Figure 6. These various states of assembly exemplify modified PSII structures that occur naturally. Many of these structures are comprised of damaged or quenched states, which represent significant regulation of PSII light harvesting and photochemical

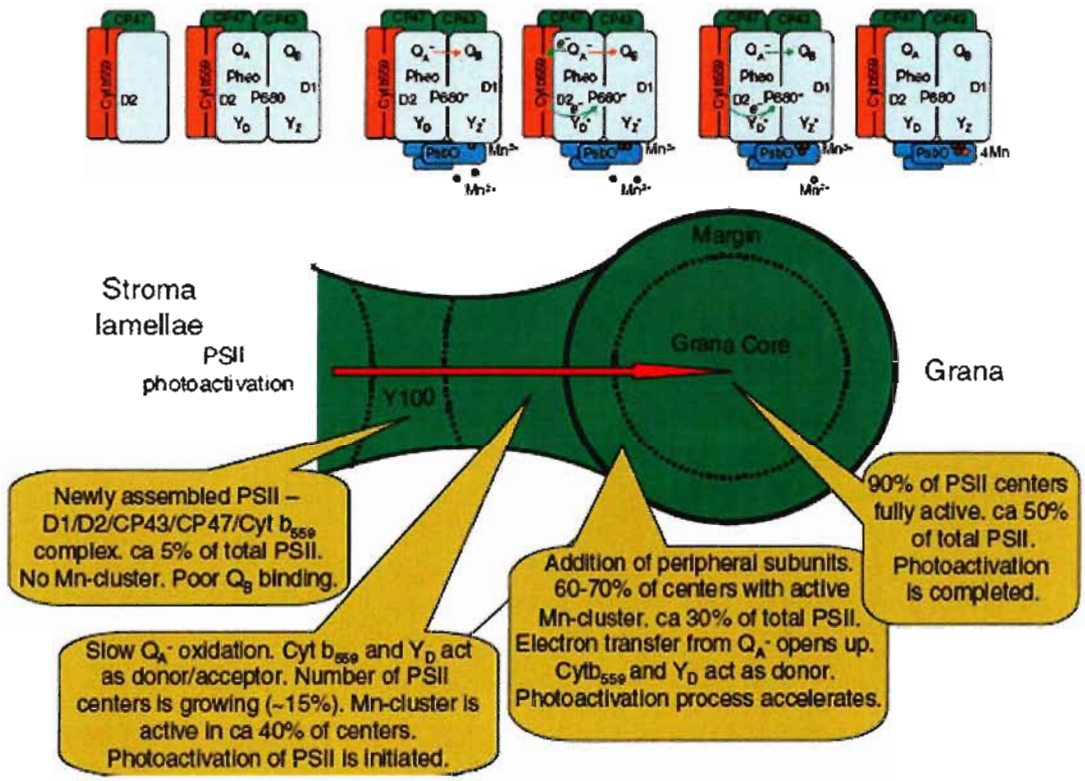

Figure 6. PSII location dependent activation and assembly involved in compartmentalized repair in higher plant thylakoid membranes is illustrated. Figure reproduced from (*51*) used with permission.

function. This system of compartmentalized PSII repair was investigated, as reported in Chapter 2, using isolated fractions of the thylakoid membrane representing different compartments. The results revealed that PSII was progressively disassembled while being moved from grana to stroma, and that PSII possessed profoundly altered kinetics when damaged and/or under repair. Although it was unclear whether the altered kinetics were due to damage or a novel state of PSII when the complex is inactivated during repair. An antennae based kinetic model was also used to determine PSII functional antennae size, reaction rates and quantum yield of primary photochemistry in the different compartments of the thylakoid membrane.

In Chapter 3 the special case of lichen quenching was studied. PSII exists in a unique state in desiccated lichens, likely both with respect to the native structure of PSII and also the association of PSII with auxiliary antennae. It is also true that the quenched state of PSII under desiccated conditions denotes one of the most pronounced alterations in PSII light harvesting function known. Thus, as in the case of PSII compartmentalized repair, desiccated lichens allowed for the study of PSII in an altered/unique structural and functional configuration. PSII quenching was investigated in the lichen *Parmelia sulcata*, where it was found that a novel long wavelength quencher appeared responsible for the NPQ. The identity of the long wavelength quencher was not determined but it is probable that it is an as yet unsequenced antennae complex.

The approaches outlined above are articulated in this thesis in the following four chapters, but the overriding goals and objectives remain the same: to highlight the role of structure to the function of PSII and to derive how the complex operates as a light harvesting enzyme. In addition, many of the altered structures investigated are also physiologically significant and thus merit investigation.

References

1. Elomaa, P., Joensuu, J. J., Korpelainen, H., Makinen, K., Niklander-Teeri, V., Pirhonen, M., Seppanen, M. M., Teeri, T. H., and Valkonen, J. P. T. (2008) *Agricultural and Food Science 17*, 307-324.

2. Xiong, J., Fischer, W. M., Inoue, K., Nakahara, M., and Bauer, C. E. (2000) *Science 289*, 1724-1730.

3. Blankenship, R. E. and Hartman, H. (1998) *Trends in Biochemical Sciences 23*, 94-97.

4. Blankenship, R. E. (2001) *Trends in Plant Science 6*, 4-6.

5. Kasting, J. F. (1993) *Science 259*, 920-926.

6. Barber, J. (2009) *Chemical Society Reviews 38*, 185-196.

7. Mussgnug, J. H., Thomas-Hall, S., Rupprecht, J., Foo, A., Klassen, V., McDowall, A., Schenk, P. M., Kruse, O., and Hankamer, B. (2007) *Plant Biotechnology Journal 5*, 802-814.

8. Zhu, X. G., Long, S. P., and Ort, D. R. (2008) *Current Opinion in Biotechnology 19*, 153-159.

9. Vasil'ev, S. and Bruce, D. (2004) *Plant Cell 16*, 3059-3068.

10. Debus, R. J. (1992) *Biochimica et Biophysica Acta 1102*, 269-352.

11. Faller, P., Pascal, A., and Rutherford, A. W. (2001) *Biochemistry 40*, 6431-6440.

12. Bernat, G., Waschewski, N., and Rogner, M. (2009) *Photosynthesis Research 99*, 205-216.

13. Youngblood, W. J., Lee, S. H. A., Kobayashi, Y., Hernandez-Pagan, E. A., Hoertz, P. G., Moore, T. A., Moore, A. L., Gust, D., and Mallouk, T. E. (2009) *Journal of the American Chemical Society 131*, 926-+.

14. Gust, D., Moore, T. A., and Moore, A. L. (2001) *Accounts of Chemical Research 34*, 40-48.

15. Aro, E. M., Suorsa, M., Rokka, A., Allahverdiyeva, Y., Paakkarinen, V., Saleem, A., Battchikova, N., and Rintamaki, E. (2005) *Journal of Experimental Botany 56*, 347-356.

16. Murata, N., Takahashi, S., Nishiyama, Y., and Allakhverdiev, S. I. (2007) *Biochimica et Biophysica Acta-Bioenergetics 1767*, 414-421.

17. Ivanov, A. G., Hurry, V., Sane, P. V., Oquist, G., and Huner, N. P. A. (2008) *Journal of Plant Biology 51*, 85-96.

18. Guskov, A., Kern, J., Gabdulkhakov, A., Broser, M., Zouni, A., and Saenger, W. (2009) *Nature Structural & Molecular Biology 16*, 334-342.

19. Muh, F., Renger, T., and Zouni, A. (2008) *Plant Physiology and Biochemistry 46*, 238-264.

20. Barber, J. (2008) *Inorganic Chemistry 47*, 1700-1710.

21. Zouni, A., Jordan, R., Schlodder, E., Fromme, P., and Witt, H. T. (2000) *Biochimica et Biophysica Acta-Bioenergetics 1457*, 103-105.

22. Enami, I., Okumura, A., Nagao, R., Suzuki, T., Iwai, M., and Shen, J. R. (2008) *Photosynthesis Research 98*, 349-363.

23. Grossman, A. R., Schaefer, M. R., Chiang, G. G., and Collier, J. L. (1993) *Microbiological Reviews 57*, 725-749.

24. Lundell, D. J., Yamanaka, G., and Glazer, A. N. (1981) *Journal of Cell Biology 91*, 315-319.

25. Mozzo, M., Passarini, F., Bassi, R., van Amerongen, H., and Croce, R. (2008) *Biochimica et Biophysica Acta-Bioenergetics 1777*, 1263-1267.

26. Bailey, S. and Grossman, A. (2008) *Photochemistry and Photobiology 84*, 1410-1420.

27. McConnell, M. D., Koop, R., Vasil'ev, S., and Bruce, D. (2002) *Plant Physiology 130*, 1201-1212.

28. Baena-Gonzalez, E., Barbato, R., and Aro, E. M. (1999) *Planta 208*, 196-204.

29. Veerman, J., McConnell, M. D., Vasil'ev, S., Mamedov, F., Styring, S., and Bruce, D. (2007) *Biochemistry 46*, 3443-3453.

30. Danielsson, R., Suorsa, M., Paakkarinen, V., Albertsson, P. A., Styring, S., Aro, E. M., and Mamedov, F. (2006) *Journal of Biological Chemistry 281*, 14241-14249.

31. Berera, R., van Stokkum, I. H. M., d'Haene, S., Kennis, J. T. M., van Grondelle, R., and Dekker, J. P. (2009) *Biophysical Journal 96*, 2261-2267.

32. Baker, N. R. (2008) *Annual Review of Plant Biology 59*, 89-113.

33. Veerman, J., Vasil'ev, S., Paton, G. D., Ramanauskas, J., and Bruce, D. (2007) *Plant Physiology 145*, 997-1005.

34. Heber, U. (2008) *Planta 228*, 641-650.

35. Heber, U., Azarkovich, M., and Shuvalov, V. (2007) *Journal of Experimental Botany 58*, 2745-2759.

36. Polivka, T., Kroh, P., Psencik, J., Engst, D., and Komenda, J. (1997) *Journal of Luminescence 72-4*, 600-602.

37. Veerman, J., Bentley, F. K., Eaton-Rye, J. J., Mullineaux, C. W., Vasil'ev, S., and Bruce, D. (2005) *Biochemistry 44*, 16939-16948.

38. Shen, J. R., Qian, M., Inoue, Y., and Burnap, R. L. (1998) *Biochemistry 37*, 1551-1558.

39. Shen, G. Z. and Vermaas, W. F. J. (1994) *Biochemistry 33*, 7379-7388.

40. Giorgi, L. B., Nixon, P. J., Merry, S. A. P., Joseph, D. M., Durrant, J. R., Rivas, J. D., Barber, J., Porter, G., and Klug, D. R. (1996) *Journal of Biological Chemistry 271*, 2093-2101.

41. Vassiliev, S. and Bruce, D. (2008) *Photosynthesis Research 97*, 75-89.

42. Vassiliev, S., Lee, C. I., Brudvig, G. W., and Bruce, D. (2002) *Biochemistry 41*, 12236-12243.

43. Vasil'ev, S. and Bruce, D. (2006) *Biophysical Journal 90*, 3062-3073.

44. Raszewski, G. and Renger, T. (2008) *Journal of the American Chemical Society 130*, 4431-4446.

45. Hwang, H. J., Nagarajan, A., McLain, A., and Burnap, R. L. (2008) *Biochemistry 47*, 9747-9755.

46. Campbell, D., Hurry, V., Clarke, A. K., Gustafsson, P., and Oquist, G. (1998) *Microbiology and Molecular Biology Reviews 62*, 667-+.

47. Dekker, J. P. and Boekema, E. J. (2005) *Biochimica et Biophysica Acta-Bioenergetics 1706*, 12-39.

48. Taiz, L. and Zeiger, E. "Plant Physiology". 3rd Edition (2002). Sunderland, Sinauer Associates.

49. Mallery, C. "Biology 255 Cell & Molecular Biology". http://www.bio.miami.edu/~cmallery/255/255phts/gk6x10.PSII.gif (2009). Retrieved on 6-25-2010.

50. Mulo, P., Sicora, C., and Aro, E. M. (2009) *Cellular and Molecular Life Sciences 66*, 3697-3710.

51. Mamedov, F. and Styring, S. (2003) *Physiologia Plantarum 119*, 328-336.

Biochemistry 44, 16939-16948 (2005)

Chapter 1: The PsbU subunit of Photosystem II stabilizes energy transfer and primary photochemistry in the Phycobilisome-Photosystem II assembly of Synechocystis sp. PCC 6803 Biochemistry 44, 16939-16948 (2005) †

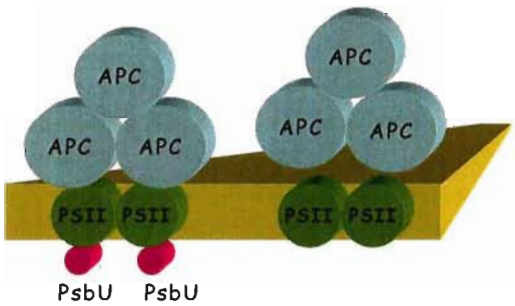

John Veerman[‡], *Fiona K. Bentley*[§], *Julian J. Eaton-Rye*[§], *Conrad W. Mullineaux*[⊥], *Sergei Vasil'ev*[‡], *and Doug Bruce*[‡*]

[‡]Department of Biological Sciences, Brock University, St. Catharines, Ontario, L2S 3A1, Canada. [§]Department of Biochemistry, University of Otago, P.O. Box 56, Dunedin, New Zealand. [⊥]School of Biological Sciences, Queen Mary, University of London, Mile End Road, London E1 4NS, UK

†This work was supported by grants from the Natural Sciences and Engineering Research Council of Canada to DB, by a New Zealand Marsden grant (UOO309) to JE-R and by grants from the Biotechnology and Biological Sciences Research Council (UK) to CWM.

*Address correspondence to this author. Telephone: (905) 688-5550 ext. 3826. Fax: (905) 688-1855. Email: dbruce@ brocku.ca[1]Abbreviations: DCMU, 3-(3,4-dichlorophenyl)-1,1-dimethylurea; DAS, decay associated spectra; Fo, dark-adapted fluorescence yield when photosystem II traps are open; Fm, dark-adapted fluorescence yield when photosystem II traps are closed; Fv, Fm – Fo; FRAP, fluorescence recovery after photobleaching; HEPES, 4-(2-hydroxyethyl)-1-piperazineethanesulfonic acid; OEC, oxygen-evolving complex; PBS, phycobilisome(s); PCC, Pasteur Culture Collection; PCR, polymerase chain reaction; PSI, photosystem I; PSII, photosystem II; TES, 2-[tris(hydroxymethyl)methyl]amino-1-ethanesulfonic acid

Preface

This chapter was published in the high impact Journal *Biochemistry* in 2005. I wrote the first draft of this article and was heavily involved in revisions and addressing the concerns and critique of both reviewers and the editor of *Biochemistry*.

The mutant cells were generated at the University of Otago in New Zealand, by Professor Julian Eaton-Rye and Fiona Bently. Thus, Figure 1.1 was produced by Professor Eaton-Rye. Professor Conrad Mullineaux, of the University of London noticed that the PBS may be decoupled in the PsbU mutant and in this capacity produced Figure 1.3. I produced all other figures and collected and analyzed the data contained therein.

It should also be noted that Professor Doug Bruce and Dr. Sergei Vasil'ev both guided me through all aspects of the research, from hypothesis formation, data collection, and analysis to writing/revising the article.

ABSTRACT

The PsbU subunit of photosystem II (PSII) is one of three extrinsic polypeptides associated with stabilizing the oxygen evolving machinery of photosynthesis in cyanobacteria. We investigated the influence of PsbU on excitation energy transfer and primary photochemistry by spectroscopic analysis of a PsbU-less (or ΔPsbU) mutant. The absence of PsbU was found to have multiple effects on the excited state dynamics of the phycobilisome and PSII. ΔPsbU cells exhibited decreased variable fluorescence when excited with light absorbed primarily by allophycocyanin, but not when excited with light absorbed primarily by chlorophyll *a*. 77K fluorescence emission spectra showed evidence for impaired energy transfer from the allophycocyanin terminal phycobilisome emitters to PSII. Picosecond fluorescence decay kinetics revealed changes in both allophycocyanin and PSII associated decay components. These changes were consistent with a decrease in the coupling of phycobilisomes to PSII and an increase in the number of closed PSII reaction centers in the dark-adapted ΔPsbU mutant. Our results are consistent with the assumption that PsbU stabilizes both energy transfer and electron transport in the PBS/PSII assembly.

INTRODUCTION

Photosystem II (PSII)[1] is the site of water splitting and oxygen evolution during oxygenic photosynthesis (*1*). This pigment-protein complex consists of at least 19 proteins, with ~16 being integral membrane subunits, and the complex contains ~36 chlorophyll (Chl) molecules (*2*). Two Chl *a*-binding core antenna subunits known as CP43 and CP47 (*3,4*) serve to absorb incident light and funnel the energy into the reaction center of the complex. The reaction center is composed of the D1 and D2 protein subunits which contain a Chl dimer known as P680, that serves as primary donor for electron transport (*1,2*). Oxidation of P680 results in the successive oxidation of the inorganic core of the oxygen-evolving complex (OEC). This incorporates a manganese cluster containing Ca^{2+} and Cl^- co-factors (*2,5*) that exists in five oxidation or S-states which undergo a cyclic pathway of univalent oxidation steps from states S_o to S_4, returning to S_o after O_2 release (*6*). The OEC is located on the lumenal side of the thylakoid membrane and in cyanobacteria the surrounding environment additionally contains the extrinsic PsbO, PsbU and PsbV (or cytochrome *c*-550) protein subunits (*7*).

The efficiency of primary photochemistry is largely dependent on the ability of the organism to absorb photons and direct the energy into the PSII reaction center so that charge separation and plastoquinone reduction can take place (*1*). This is achieved by transferring energy through peripheral antenna complexes to the core antenna pigment proteins. In cyanobacteria, the peripheral complex is the phycobilisome (PBS), which serves as antenna to both PSII and photosystem I (PSI). Changes in the distribution of absorbed energy between PSII and PSI are regulated via the light state transition. (*8,9,10*).

The mechanism(s) by which the PBS physically binds to the thylakoid membrane and/or photosystems are unclear as are the details of PBS energy coupling to PSII and PSI. An

exogenous hydrophobic linker polypeptide consisting of 54 amino acid residues, and referred to as the PB-loop, has been implicated in PBS/thylakoid interactions (*9,10*). However, there is also evidence that indicates that PSII has a native binding affinity for the PBS, even in the absence of the PB-loop (*11,12*) and it is possible that the PBS may associate with the membrane through interactions with lipid head groups (*13*). It has been suggested that the terminal emitter or the PBS ApcE anchor polypeptide is required for PBS assembly and PBS/PSII energy coupling (*14*). Fluorescence recovery after photobleaching (FRAP) measurements support a transient binding of PBS to PSII, as they show diffusion rates for the PBS to be much higher than for PSII (*10,13*). Despite the lack of agreement on the precise mechanism of binding and energy coupling, it is clear that changes in orientation or distance of the PBS from PSII would greatly affect energy transfer efficiency (*8*).

The 12 kDa PsbU protein, encoded by *psbU*, is thought to impart structural stability to the OEC and to shield the manganese complex from cellular reductants. Inactivation of the *psbU* gene in *Synechococcus* sp. PCC 7002 demonstrated that PsbU stabilized oxygen evolution at elevated temperatures and was also required for the acquisition of cellular thermo-tolerance (*15,16*). Similar results were obtained with *Synechocystis* sp. PCC 6803 although the requirement of PsbU was less stringent in this strain (*17*). In addition, *in vivo,* the removal of PsbU also resulted in reducing oxygen evolution to ~80% of the wild-type rate and photoautotrophic growth was slowed in the absence of either Ca^{2+} or Cl^- and abolished under $CaCl_2$-limiting conditions (*17-19*). Moreover, thermoluminescence measurements have demonstrated that the S_2-state of the OEC is modified in ΔPsbU cells where the recombination reactions are shifted to higher temperatures for both the Q and B-bands (*18*).

The importance of PsbU for optimal rates of oxygen evolution was also observed *in vitro* where full reconstitution of PSII activity required the re-binding of PsbU to isolated PSII complexes from *Thermosynechococcus vulcanus* and removal of PsbU in ΔPsbO cells prevented photoautotrophic growth in a ΔPsbO:ΔPsbU strain of *Synechocystis* sp. PCC 6803 (*20,21*). Despite the importance of PsbU for PSII activity the number of PSII centers assembled in ΔPsbU cells was found to be similar to wild type when assayed using 3-(3,4-dichlorophenyl)-1,1-dimethylurea (DCMU)-replaceable [^{14}C]-atrazine binding to detect assembled photosystems (*22*). Unexpectedly, assays of PSII abundance using variable Chl *a* fluorescence yield measurements indicated that fluorescence was quenched in the ΔPsbU strain (*22*). The present study was undertaken to determine the origin of the quenched variable fluorescence and ascertain the effect of PsbU removal on energy transfer and primary photochemistry in PSII. To this end the *psbU* gene in *Synechocystis* sp. PCC 6803 was interrupted to produce a ΔPsbU strain which was then characterized by room temperature, low temperature and picosecond time-resolved fluorescence spectroscopy. Our results indicate that both energy transfer from the PBS to PSII and primary photochemical processes within PSII were altered in the ΔPsbU mutant.

MATERIALS AND METHODS

Growth of Synechocystis sp. PCC 6803 strains. Cultures were maintained on BG-11 plates containing 5 mM glucose and 20 μM atrazine and, when required, chloramphenicol was present at a concentration of 15 μg/mL in both solid and liquid BG-11 media. The solid media were supplemented with 10 mM TES-NaOH (pH 8.2) and 0.3% sodium thiosulfate (*23*) and liquid cultures were grown photoautotrophically unless otherwise noted. Cells were grown under a continuous illumination of 30 μE m^{-2} s^{-1} and the temperature in the growth chamber was 30^0C.

The *Synechocystis* sp. PCC 6803 strain used in this study was the glucose-tolerant strain from Williams (*24*) and this is referred to throughout as wild type.

Construction of a Synechocystis sp. PCC 6803 strain lacking PsbU. The open-reading frame sll1194, encoding the PsbU protein, was obtained by PCR using the forward primer 5'-CCCAAAATCGGATCCGTCGGCATAATTTTC-3' and the reverse primer 5'-AAAGGGTACGCAATGGAATTCGGTTAGCAG-3'. The underlined bases correspond to introduced *Bam*HI and *Eco*RI sites, respectively, that were incorporated into the primer design and used to clone the PCR product into pUC19 (New England BioLabs, USA). The cloned *psbU* gene was interrupted at a unique intragenic *Swa*I site by a chloramphenicol-resistance cassette derived from pBR325 (*25,26*) and then used to transform *Synechocystis* sp. PCC 6803 according to established protocols (*23,24*). Complete segregation for the introduced antibiotic-resistance cassette was verified by PCR using the forward and reverse primers described above.

Photoinactivation and Oxygen Evolution Assays. For these measurements cells were grown in BG-11 containing 5 mM glucose before being harvested for the experiments. Following the removal of glucose, cells, maintained at 30 °C and at a Chl *a* concentration of 10 μg/mL, were inactivated by 2.0 mE m^{-2} s^{-2} white light provided by a Kodak Ektalite 1000 slide projector. Oxygen evolution was measured with a Clark-type electrode (Hansatech, UK) at 30 °C in BG-11 containing 25 mM HEPES-NaOH, pH 7.5. Saturating actinic light (2 mE m^{-2} s^{-1}) was provided by an FLS1 light source (Hansatech, UK) passed through a Melis Griot OG 590 sharp cutoff red glass filter. The electron acceptors were 3.0 mM $K_3Fe(CN)_6$ and 0.6 mM 2,5-dimethyl-*p*-benzoquinone. When added, lincomycin was at 250 μg/mL

Room temperature fluorescence. Cell cultures were place in a 1 cm path glass cuvette at a volume of ~3 mL and dark adapted to state 2 (*27*) and measurements made with a PAM

fluorometer (model Pam 101, H.Walz, Effeltrich, Germany). The minimal Chl *a* fluorescence yield, Fo, was determined by exposing dark-adapted cells to a low intensity modulated measuring light of either 655 nm or 440 nm (*28*). To obtain the variable Chl *a* fluorescence yield, Fv, saturating white light pulses of 600 ms duration were used to close the PSII reaction centers and determine the maximum fluorescence yield, Fm, from which Fv was calculated as Fm – Fo.

77K fluorescence emission spectra. Cells were harvested during exponential growth phase and the ΔPsbU mutant and wild-type samples were adjusted to equal absorbance at 435 nm as determined with an Aminco DW-2 absorbance spectrometer equipped with a light scattering correcting frosted glass between the sample and photomultiplier tube. Samples were dark-adapted to state 2 and then transferred to glass tubes that were ~5 mm in radius and 10 cm in length with one end sealed. Tubes were placed in a dewar filled with liquid N_2 and positioned so that the glass tube could be manually turned about its lengthwise axis while retaining its position and orientation. Fluorescence emission spectra were collected using an EG&G 1461 diode array detector (E.G. & G., Salem, MA, USA) as described previously (*29*). In order to account for position sensitive variation in fluorescence yield from the frozen samples, each sample tube was rotated incrementally and measured a total of sixteen times to generate one averaged emission spectra. Three independent repeats of this procedure were used to generate the final emission spectrum for each sample.

Fluorescence decay kinetics. Fluorescence decay kinetics were measured with dark-adapted whole cell cultures at a Chl *a* concentration of 10 μg/mL using the single photon timing apparatus previously described (*30-32*). Both the 407 nm and 650 nm picosecond pulsed diode lasers (Picoquant, Berlin, Germany) used for excitation were operated at 10 MHz. For each

measurement a 200 mL sample was circulated at a flow rate of ~4 mL s^{-1}. The detector was a Hamamatsu R3809 microchannel plate (Hamamatsu, Japan). Decay data were collected in 4096 channels over 50 ns with a Becker & Hickl SPC-630 single photon timing card (Berlin, Germany) in a Pentium PC. Decay data were collected at Fo from dark-adapted samples and Fm from preilluminated samples in the presence of DCMU as described in (32).

Global lifetime analysis. Global lifetime analyses of fluorescence decays at multiple emission wavelengths were done as described previously (*32*). The detection wavelength ranges were 640-730 nm for 650 nm excitation, and 660-730 nm for 407 nm excitation, taken at 10 nm increments. All programs used for data manipulation and global analysis were written by Sergei Vassiliev.

Chlorophyll and phycocyanin determination. Chlorophyll concentrations were determined from methanol extracts by the method of MacKinney (33). Phycocyanin concentrations were determined from whole cell absorption by the method of Myers et al (34).

RESULTS

Construction and physiology of the ΔPsbU mutant.

The strategy to construct the ΔPsbU mutant used in this report is shown in Figure 1.1A. Also shown is the result of a PCR using primers specific for the *psbU* gene and confirming full segregation of the inactivated *psbU* carrying a 2.0 kb chloramphenicol-resistance cassette in the ΔPsbU strain. The rates of oxygen evolution for the ΔPsbU mutant were found to be ca. 52% of the wild-type rate (Figure 1.1B). In addition the effect of 45 min illumination at 2 mE m^{-2} s^{-1} is shown. In wild-type cells the initial rate of oxygen evolution was reduced by 20% while the

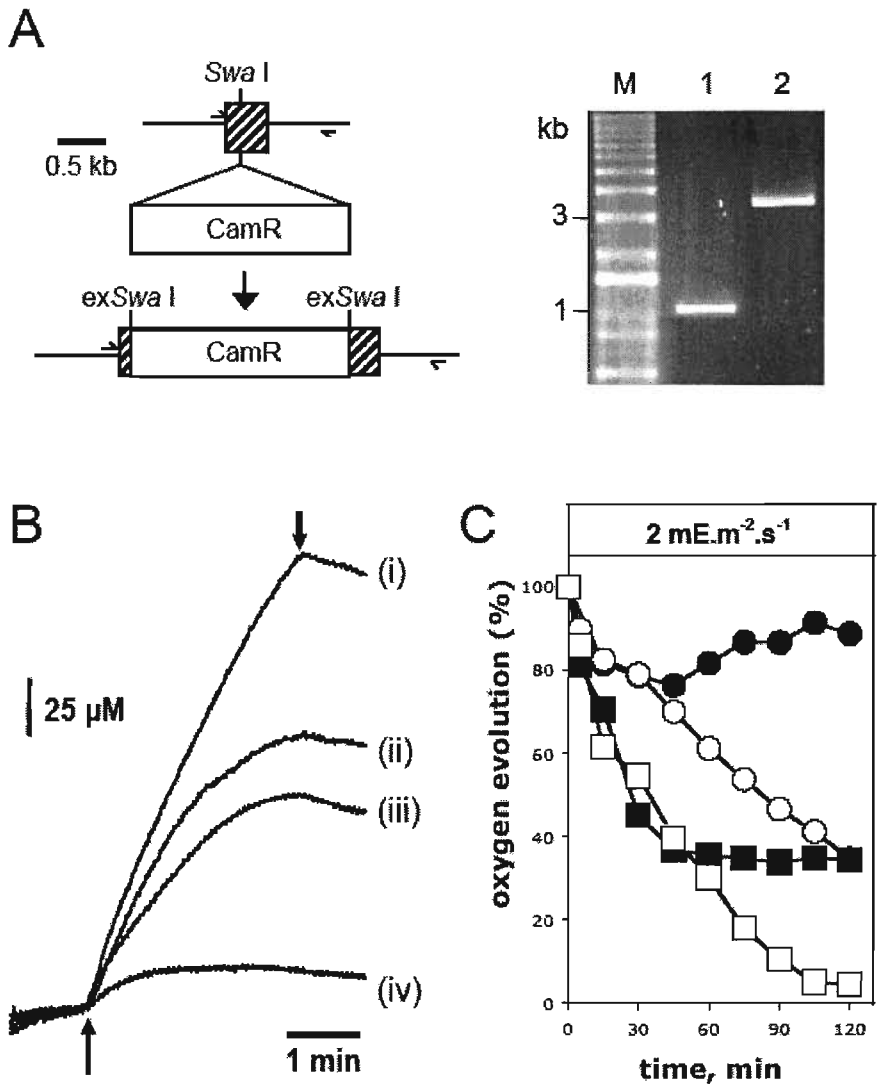

Figure 1.1. Construction of the ΔPsbU mutant. (A) Diagram of the *psbU* region in the *Synechocystis* sp. PCC 6803 genome with or without the insertion of a 2.0 kb chloramphenicol-resistance marker (CamR) inserted at a *SwaI* site 160 bp from the initial base of the start codon. A PCR was run that confirmed complete replacement of *psbU* with the interrupted gene in the ΔPsbU strain. The primers used in the reaction are indicated with arrows. The lanes on the gel are: M, 1 Kb Plus DNA ladder, supplied by Invitrogen; Lane 1, PCR product from wild type, and Lane 2, PCR product from the ΔPsbU strain. (B) Oxygen evolution traces before and after illumination at 2 mE m^{-2} s^{-1} with white light. Trace (i) wild type at 0 min: 503 µmoles O_2 (mg of Chl)$^{-1}$ h^{-1}; trace (ii) wild type after 45 min illumination: 402 µmoles O_2 (mg of Chl)$^{-1}$ h^{-1}; trace (iii) ΔPsbU at 0 min: 262 µmoles O_2 (mg of Chl)$^{-1}$ h^{-1}, and trace (iv) ΔPsbU after 45 min illumination: 84 µmoles O_2 (mg of Chl)$^{-1}$ h^{-1}. The data in panel (B) were repeated in three independent experiments with similar results. (C) Time course of photoinactivation of oxygen evolution in wild type (circles) and ΔPsbU (squares). Open symbols contain lincomycin. The results from two independent experiments are shown. The Chl concentration was 10 µg mL^{-1} during exposure to 2 mE m^{-2} s^{-1} white light and during the oxygen evolution assays in panels (B) and (C).

ΔPsbU strain exhibited only 32% of its initial rate and underwent rapid photoinactivation during the period that the actinic light was on. The susceptibility of the ΔPsbU mutant to high light was investigated in the time course shown in Figure 1.1C. Rates of oxygen evolution in ΔPsbU cells exposed to 2 mE m^{-2} s^{-1} illumination fell by ca. 50% within 30 min. In contrast, oxygen-evolution rates in the wild type initially decline by ca. 25% but then were able to acclimate to the high light conditions. These data suggest that the rate of repair of photodamaged PSII was able to keep up with the rate of inactivation in the wild type but not in the ΔPsbU mutant under these conditions. This interpretation was supported by the addition of lincomycin before the onset of the high light treatment. Under these conditions oxygen evolution in the wild type was reduced by 50% in ca. 80 min, although in the ΔPsbU cells PSII activity declined at a similar rate in the presence or absence of lincomycin. However, without the protein synthesis inhibitor, PSII activity of the ΔPsbU mutant remained at ca. 30% of the initial level before exposure to high light, whereas PSII activity was completely abolished in the presence of lincomycin. We also found that photoinactivated ΔPsbU cells recovered oxygen-evolving activity to the level observed before exposure to 2 mE m-2 s-1 illumination following a further incubation at 0.07 mE m-2 s-1 over 2 h, and that this recovery was completely prevented by the presence of lincomycin (data not shown).

The results obtained in Figure 1.1 therefore confirm that the ΔPsbU cells created for this study represented a homoplasmic line and that oxygen-evolving activity was impaired in agreement with earlier studies (17,22). These cells were therefore used to evaluate the anomalously low estimates of PSII abundance measured in ΔPsbU cells using Chl a variable fluorescence yield measurements as previously reported (22).

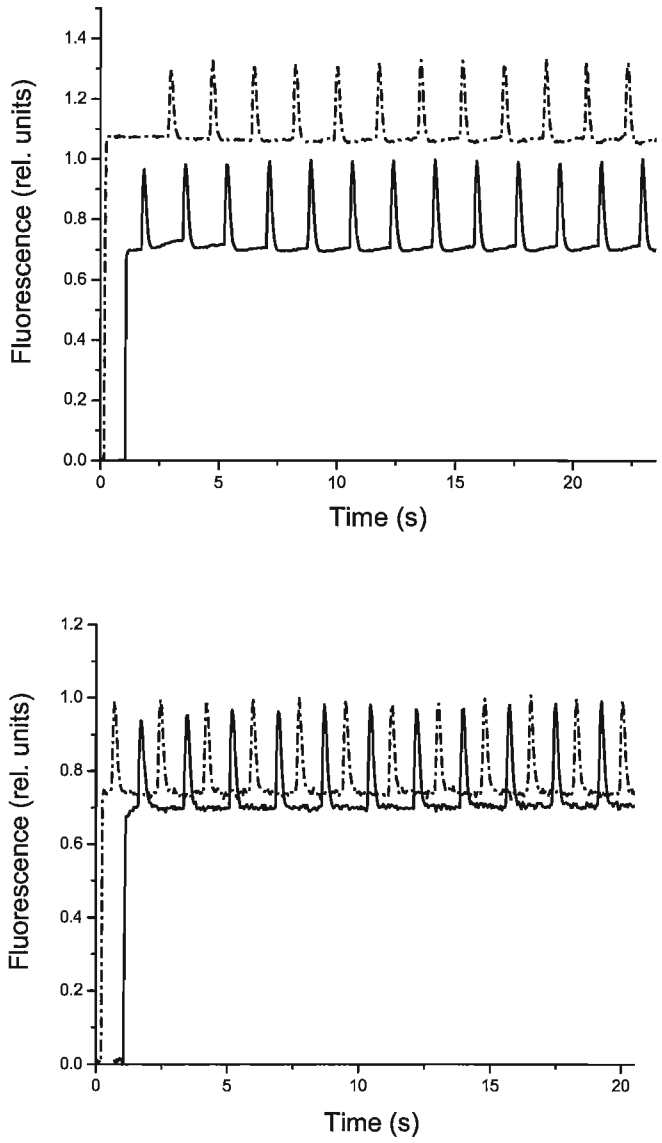

Figure 1.2. Pulse amplitude modulated (PAM) room temperature fluorescence kinetic traces. Upper panel, excitation wavelength 665 nm; lower panel, excitation wavelength 440 nm. Solid traces are wild type, dashed traces for the the ΔPsbU strain. Wild-type and ΔPsbU cells were at equal Chl concentrations. Multiple turnover saturating white light flashes (600 ms duration) were used to determine Fm (spikes on traces). Traces are not normalized. This experiment was repeated 5 times, a representative trace is shown. Repeated measures of Fo and Fm between individual experiments were within 10%.

Room temperature fluorescence. Steady-state room temperature variable fluorescence (Fv) was measured using a PAM fluorometer. Figure 1.2 clearly indicates that variable fluorescence (Fv/Fm) of the ΔPsbU mutant was decreased when compared to the wild-type when using a 655 nm measuring light (preferentially exciting allophycocyanin). The data in Figure 1.2 were not normalized and wild-type and ΔPsbU mutant samples were at equal Chl concentrations. This revealed that much of the decrease observed in Fv/Fm arose from a large increase in Fo in the ΔPsbU mutant relative to wild-type cells. Interestingly, the Fv/Fm of the ΔPsbU mutant was not smaller that that of the wild-type when variable fluorescence was determined with 440 nm measuring light (preferentially exciting Chl *a*) although both the Fo and Fm levels of the wild-type were slightly lower than those of the ΔPsbU strain. Observation of the decreased Fv/Fm in the ΔPsbU mutant was thus dependent on excitation of the phycobilisome. These data suggest that the decreased Fv/Fm in the mutant arises from an increase in phycobilin fluorescence contributing to the Fo yield and not necessarily to an intrinsic change in PSII photochemistry. This was confirmed with room temperature emission spectra at Fo and Fm, shown in Figure 1.3. For excitation of the PBS at 600 nm the emission spectra of both Fo and Fm in the ΔPsbU mutant and wild-type are dominated by phycobilin fluorescence. The data from mutant and wild-type are similar, however the relative contribution of phycobilin to Chl emission is higher in the ΔPsbU mutant. In both wild-type and mutant the contribution of Chl to the Fo emission spectra is minimal. The Fo spectra are also characterized by a long wavelength tail, a characteristic of phycobilin emission, that extends beyond 740nm.

From the shape of the room temperature emission spectra it is clear that the amplitude of Fv/Fm, determined with a PAM type fluorometer, will depend heavily on the detection wavelength and the excitation wavelength of the instrument. The emission filter used in the

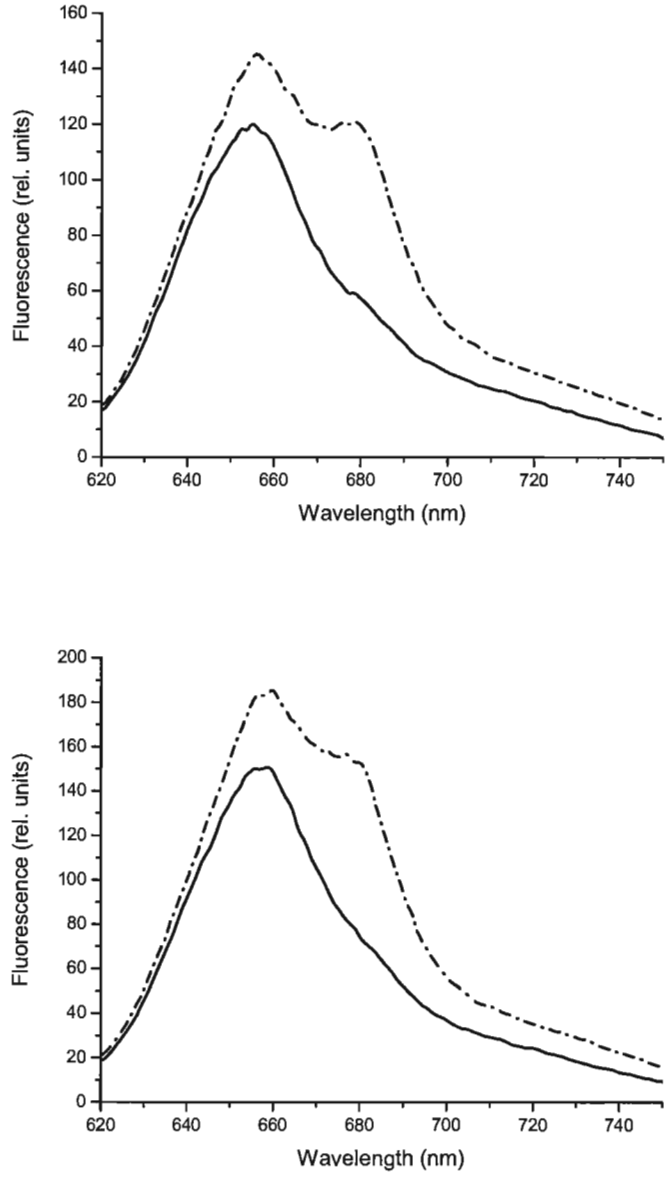

Figure 1.3. Room temperature fluorescence emission spectra. Excitation wavelength was 600 nm. Upper panel is wild type and lower panel is the ΔPsbU strain. All samples were measured at equal phycocyanin concentrations. Solid lines are cells at Fo and dashed lines are cells at Fm (see text for details).

standard PAM fluorometer is a long pass (> 710 nm) red filter which will unfortunately block the bulk of the Chl *a* variable fluorescence and allow detection of much of the long wavelength phycobilin emission. This will have the effect of decreasing the apparent Fv/Fm when determined with phycobilisome excitation wavelengths. As the contribution of phycobilin fluorescence relative to Chl fluorescence is higher in the ΔPsbU mutant than in the wild type (Figure 1.2) the Fv/Fm as measured with the PAM appears lower in the mutant cells for excitation at 650 nm. Chlorophyll fluorescence

makes a much larger relative contribution to the room temperature emission for Chl *a* excitation (data not shown) and Fv/Fm determinations with the PAM for excitation at 440

nm are not as confounded by phycobilin emission and are thus more similar in mutant and wild-type cells. However, at either excitation wavelength the multiple components contributing to the steady state PAM fluorescence measurements complicate the interpretation of variable fluorescence and limit the conclusions made possible by simple comparisons of Fv/Fm.

Absorbance spectra of the ΔPsbU mutant and wild-type cells show similar relative contributions from Chl *a* and phycobilin pigments (data not shown). The fluorescence yield of phycobilin pigments is, however, consistently higher in the ΔPsbU mutant than in the wild type when samples are measured at either equal Chl (data not shown) or equal phycocyanin concentrations (Figure 1.2). This increased phycobilin fluorescence may be characteristic of a partially decoupled PBS.

To investigate energy transfer from the PBS to Chl *a* in the thylakoid membrane, 77K fluorescence emission spectra were determined (Figure 1.4). The 77K fluorescence spectra of the ΔPsbU mutant and wild type were similar when 435 nm light was used to preferentially excite Chl *a* (Figure 1.4, upper panel). In contrast, excitation of the PBS with 600 nm light

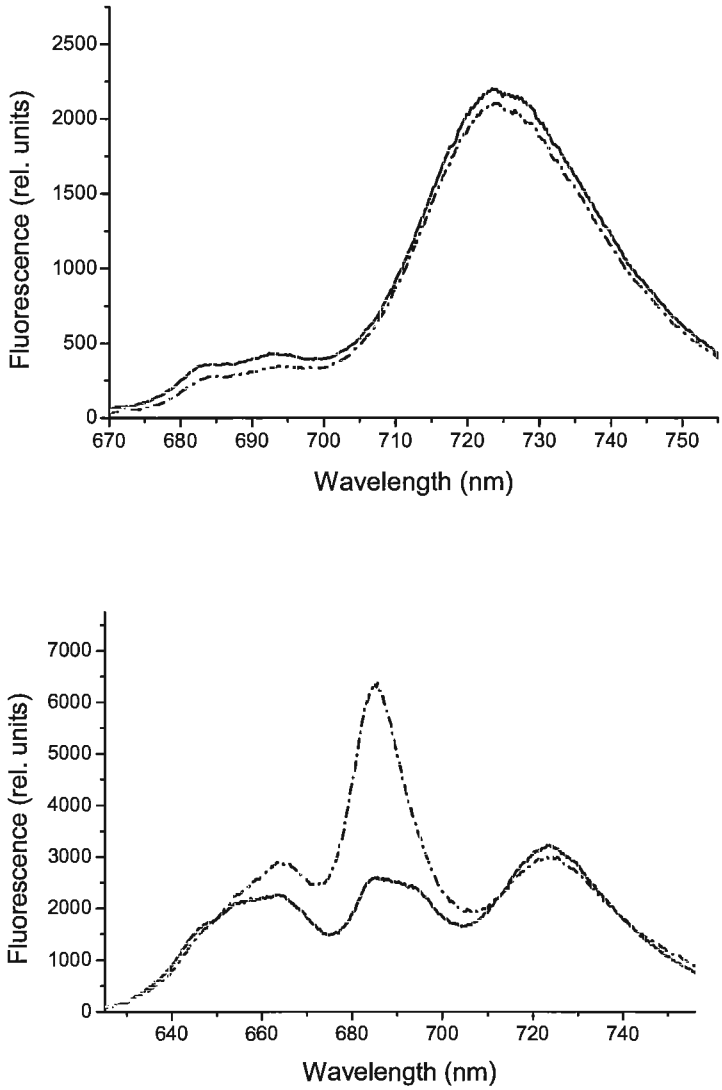

Figure 1.4. 77K fluorescence emission spectra of wild type and the ΔPsbU strain using dark-adapted cells excited at either 435 nm (upper panel) or 600 nm (lower panel). Solid lines are for wild-type cells and the dashed lines are for the ΔPsbU strain. Samples were all at equal Chl concentrations. Spectra were collected from three independent experiments, one representative trial is presented. Spectra were not normalized. Repeat measures of peak amplitudes between independent experiments were within 10%.

revealed large differences between the ΔPsbU mutant and wild type (Figure 1.4, lower panel). The ΔPsbU mutant is characterized by increased emission from allophycocyanin at 665 nm relative to phycocyanin at 650 nm and by a large increase in the 685 nm peak, which has contributions from both PSII Chl *a* and the terminal phycobilin emitters, relative to all other emission peaks. The 695 nm emission peak (red shifted core antenna Chl in CP47) does not increase with the 685 nm peak which suggests that the increase observed at 685 nm results mostly from the terminal phycobilin emitters rather than PSII core antenna Chl. The 77K emission data are thus consistent with a decrease in efficiency of energy transfer from PBS to Chl *a* in the ΔPsbU cells.

Changes in the relative efficiency of energy transfer from the PBS to PSII and to PSI are regulated by the light state transition in cyanobacteria. The increase in emission at 685 nm in the ΔPsbU mutant is somewhat reminiscent of the increases in emission at 685 nm and 695 nm (PSII Chl *a*) relative to 725 nm (PSI Chl *a*) that are characteristic of the transition to light state 1 in cyanobacteria. To investigate possible connections we compared state transitions in the wild type and ΔPsbU mutant. As shown in Figure 1.5 the ΔPsbU cells are state transition competent and undergo transitions of similar magnitude (changes in Fv) to the wild type as assayed by room temperature fluorescence kinetics. Changes in 77K fluorescence emission spectra typical of light state transitions and of similar magnitude to those observed in the wild type are also observed in the ΔPsbU mutant (data not shown). The increase in emission at 685 nm observed in the 77K emission spectra of the ΔPsbU mutant relative to the wild type is thus not indicative of cells with an inhibited state transition that are "stuck" in state 1.

Fluorescence decay kinetics. Picosecond fluorescence decay kinetics were collected to help interpret the differences in emission we observed between the wild type and ΔPsbU mutant with

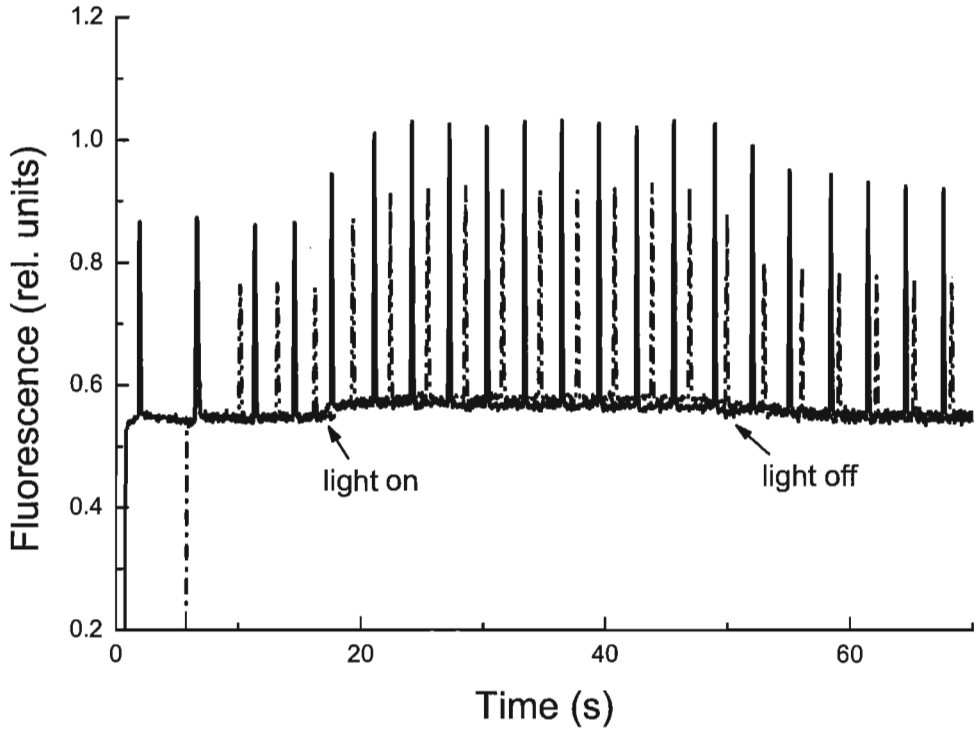

Figure 1.5. Pulse amplitude modulated (PAM) fluorescence kinetic traces for wild type (solid line) and for the ΔPsbU strain (dashed line). Excitation wavelength was 665 nm. Fm was determined with saturating flashes (600 ms) of white light (spikes on traces). Dark-adapted cells (state 2) were exposed to blue light excitation (430 nm excitation, 100 $\mu E\ m^{-2}\ s^{-1}$) to induce a transition to state 1. The blue light was turned on and off as shown by the arrows underneath the traces. Samples were measured at equal Chl concentrations, the trace for the ΔPsbU strain was displaced vertically downwards so that the traces overlapped at the Fo level to facilitate comparison of the blue light induced changes in Fv.

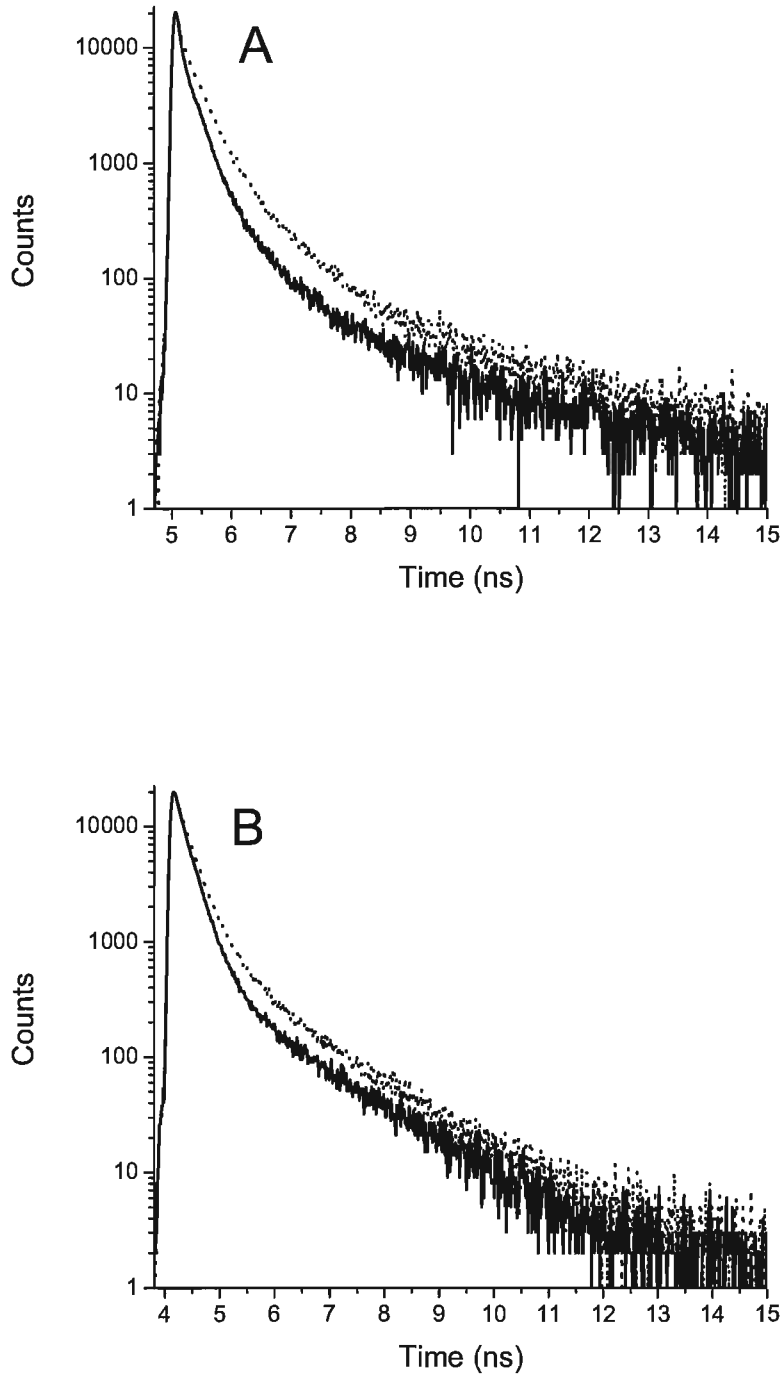

Figure 1.6. Fluorescence decay kinetics of wild type (solid trace) and ΔPsbU strain (dotted trace) for excitation at 407 nm (panel A) and at 650 nm (panel B). The emission wavelength was 680 nm. The traces are for dark-adapted cells at Fo, data were collected to 30,000 counts in the peak channel.

steady-state fluorescence spectroscopy. The fluorescence decay kinetics at Fo for the ΔPsbU strain and wild type are shown in Figure 1.6 for excitation at 407 nm (absorbed by phycocyanin, allophycocyanin and Chl *a*) and for excitation at 650 nm (absorbed predominantly by allophycocyanin). Both excitation wavelengths generated decay kinetics that were slower in the ΔPsbU cells than in the wild type. This suggests that differences between the wild type and mutant may not be restricted to phycobilin emission.

Global lifetime analysis. A global fluorescence decay analysis was done to characterize the individual decay components contributing to the altered fluorescence decay kinetics resulting from loss of PsbU. As described previously (*31*), fluorescence decays were collected at a number of emission wavelengths and fit simultaneously to a sum of exponential decay components. Component lifetimes were assumed invariant across emission wavelength and decay associated spectra (DAS) were constructed by plotting the yield of each decay component as a function of emission wavelength. This approach facilitates the separation of the many components contributing to steady state fluorescence emission and offers more insight into the origins of changes in variable fluorescence. To further facilitate the identification of the origin of the decay components, two different excitation wavelengths were used. Excitation pulses at 407 nm were used to excite Chl a, phycocyanin and allophycocyanin to similar extents whereas the 650 nm excitation was used to more selectively excite allophycocyanin.

The DAS from both wild-type and ΔPsbU cells at Fo are shown in Figure 1.7 for excitation at 650 nm and at 407 nm. The fastest kinetic component had a lifetime of approximately 40 ps and was observed only for excitation at 407 nm. This component was clearly a mixture of at least two components as it had a negative yield (rise component) at short wavelengths and a positive yield (decay component) at longer wavelengths. The short wavelength negative peak at 660 nm

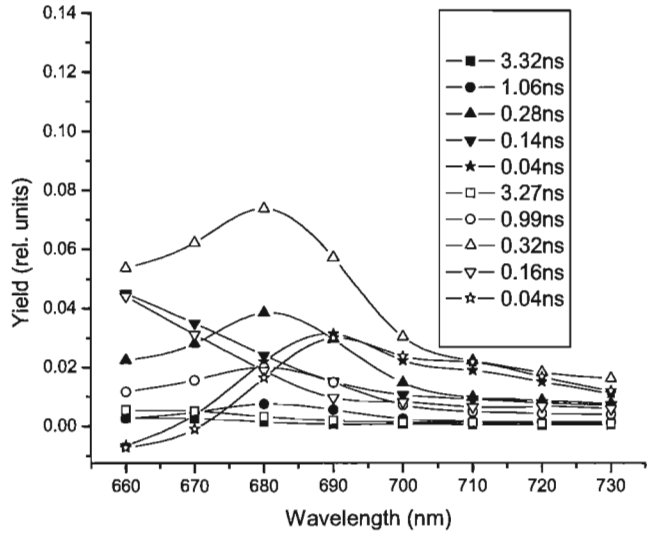

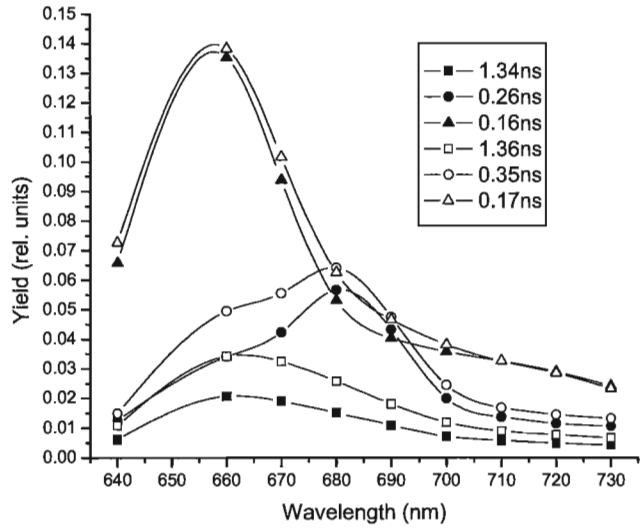

Figure 1.7. Decay associated spectra (DAS) of globally fitted fluorescence decay kinetics from dark-adapted wild type (filled symbols) and ΔPsbU cells (open symbols) at Fo for excitation at 407 nm (upper panel) and for excitation at 650 nm (lower panel). The fluorescence yields (lifetime times amplitude) of each decay component are plotted versus emission wavelength. Five decay components were required for the global fit of the decay data for 407 nm excitation, the χ^2 value was 1.08 for the mutant and 1.09 for the wild type. Three decay components were required for the global fit of the decay data for 650 nm excitation, the χ^2 value was 1.14 for the mutant and 1.13 for the wild type. Cells were measured at equal Chl concentrations and overall fluorescence yields (sum of all decay components) were normalized to the steady-state fluorescence emission yields.

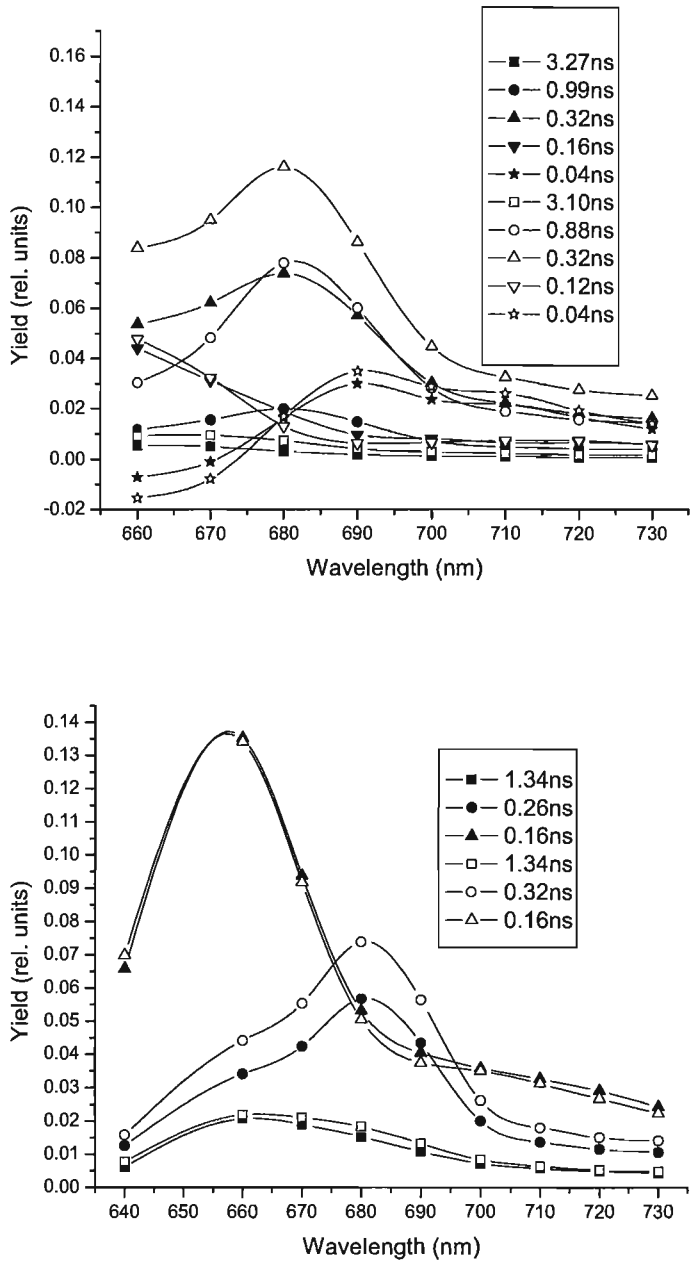

Figure 1.8. Decay associated spectra (DAS) of globally fitted fluorescence decay kinetics from dark-adapted cells. The fluorescence yields (lifetime times amplitude) of each decay component are plotted versus emission wavelength. The upper panel shows the ΔPsbU strain at Fo (filled symbols) and Fm (open symbols) for excitation at 407 nm. Five decay components were required for the global fit of the decay data for 407 nm excitation, the χ^2 value was 1.08 for the Fo data and 1.14 for the Fm data. The lower panel shows wild-type cells at Fo (filled symbols) and Fm (open symbols) for excitation at 650 nm. Three decay components were required for the global fit of the decay data for 650 nm excitation, the χ^2 value was 1.13 for the Fo data and 1.14 for the Fm data. Cells were measured at equal Chl concentrations and overall fluorescence yields (sum of all decay components) were normalized to the steady-state fluorescence emission yields.

likely reflects a rise component in allophycocyanin emission resulting from energy transfer from phycocyanin to allophycocyanin. The longer wavelength peak at 690 nm with a shoulder at 710 nm is typical of PSI decay. The yield of this component did not change when PSII reaction centers were closed by illumination in the presence of DCMU (Figure 1.8) which is also consistent with these assignments. A component with a lifetime of approximately 150 ps peaking at 660 nm was observed for 650 nm excitation and 407 nm excitation in both mutant and wild-type cells. This component was by far the major contributor to decay for 650 nm excitation but had a much smaller relative yield for excitation at 407 nm. The yield of this component was independent of PSII trap closure (Figure 1.8). This and the emission peak at 660 nm clearly localize this component to the PBS. Both phycocyanin and allophycocyanin may contribute to this component at 407 nm excitation, but due to its strong absorption at 650 nm allophycocyanin will dominate the decay at 650 nm excitation. The lifetime of this component may thus reflect excitation energy transfer processes from phycocyanin to allophycocyanin to the terminal long wavelength phycobilin emitters and also possibly from allophycocyanin to Chl *a*. This component makes very similar contributions to wild-type and ΔPsbU cells under all conditions suggesting that these kinetic processes are relatively unaffected by the lack of PsbU.

A decay component with a shoulder at 660 nm and a peak at 680 nm having a lifetime in the 300 ps region was seen for excitation at both 407 nm and 650 nm. Interestingly the spectral shape of this component was independent of excitation wavelength. This component was the largest contributor to the decay for excitation at 407 nm and the second largest for excitation at 650 nm. The yield of this component increased by approximately 30 to 40% when PSII reaction centers were closed by illumination in the presence of DCMU (Figure 1.8). At 407 nm excitation the lifetime of this component was almost invariant across samples. In the wild type

the lifetime was 280 ps at Fo and 310 ps at Fm and in the mutant 325 ps at Fo and 320 ps at Fm. Interestingly, for 650 nm excitation the lifetime of this component appeared to increase upon trap closure and was also somewhat longer in the mutant than the wild-type cells at both Fo and Fm. Lifetimes in the control were 265 ps at Fo and 320 ps at Fm and in the mutant they were 350 ps at Fo and 400 ps at Fm. The most striking feature of this component was the much larger contribution it made to the overall decay at Fo in the mutant than in the control at both excitation wavelengths (Figure 1.7). This was especially apparent at 407 nm, where the yield of this component in the ΔPsbU mutant was twice that of the wild type. For all conditions the relative contribution of the 660 nm emission to the 680 nm emission of this component was larger in the mutant than the wild-type. The spectra of this component suggests emission from PBS core components (allophycocyanin and the terminal phycobilin emitters) and PSII Chl *a*. It is interesting that the shape of the 300 ps decay component spectra is the same for excitation at 407 nm (bilin and Chl *a*) and at 650 nm (predominantly allophycocyanin). This could be consistent with an equilibrium population of PBS core components and PSII Chl *a*. Upon trap closure, the spectral shape remains the same, and changes in the amplitude of this component were more dominant than changes in its lifetime. Photosystem II associated decay components in intact cyanobacteria were previously reported to change yield rather than lifetime upon trap closure (*35*). Our 300 ps decay component may have such an origin and arise from Chl *a* and PBS core components that are tightly coupled energetically and whose lifetimes predominantly reflect the processes within PSII. An alternative possibility, especially for the 650 nm excitation of allophycocyanin is that the component reflects emission from the core of the PBS and the lifetime is related to the relative efficiency of energy transfer to Chl *a* and/or some other quencher.

Two slow decay components with nanosecond lifetimes were distinguished with excitation at 407 nm, the faster one with an approximately 1 ns decay and a clear peak at 680 nm and the slower, a 3.3 ns component peaking at 660 nm. Upon trap closure the yield of the 1 ns component increased greatly in both mutant and wild type (Figure 1.8 shows the mutant data), identifying its origin in closed PSII reaction centers as described previously (*35,36*). The yield of the 3.3 ns component was much smaller and not as sensitive to trap closure. In contrast, at 650 nm excitation a 1.3 ns decay component with a peak at 660 nm and broad shoulder at 680 nm was observed. In both mutant and wild-type cells the 680 nm shoulder increased upon trap closure, but not the 660 nm peak (Figure 1.7 shows the wild type). As direct excitation of allophycocyanin at 650 nm did not generate the 3.3 ns component we assign this longest-lived decay to uncoupled phycocyanin. The 1.3 ns component observed for excitation of allophycocyanin is clearly a mixture of a component associated with closed PSII reaction centers and a long-lived allophycocyanin decay component. The 1.3 ns allophycocyanin decay component made a much more significant contribution to the overall decay at 650 nm than did the 3.3 ns phycocyanin component at 407 nm. Although both of these components were higher in the mutant than in the wild type, the 1.3 ns component will have contributed more significantly to the increased phycobilin emission observed in the steady-state emission spectra of the mutant. However, the most dramatic difference between mutant and wild type was for the 1 ns PSII component observed at 407 nm excitation whose yield was three times higher in the mutant than the wild type. This suggests that a significant number of PSII reaction centers were closed in the mutant cells at Fo.

DISCUSSION

Previous work with a *Synechocystis* sp. PCC 6803 *psbU* deletion mutant indicated that the PsbU protein affected PSII electron transport by moderating the S-state transitions and stabilizing the S_2 state (*18,37*). The *psbU* deletion mutant was also shown to have a reduced rate of oxygen evolution (*17,18*). These results are consistent with the lumenal side location of the PsbU protein and its role in stabilizing the OEC. Our picosecond fluorescence decay data confirm an inhibition of electron transport capacity of PSII in the ΔPsbU mutant and show increases in the contribution of fluorescence decay components associated with closed PSII centers in dark-adapted ΔPsbU cells. Specifically the presence of the 1 ns PSII associated component at Fo clearly indicates that a significant number of PSII centers remain closed in the mutant in the dark and are thus unavailable for photochemistry and will not contribute to oxygen evolution. The lack of PsbU thus affects the efficiency of PSII photochemistry.

In addition our results also indicate an increase in the numbers of partially excitonically decoupled PBS in the ΔPsbU strain. This result was unexpected as the PBS and PsbU are located on opposite sides of the thylakoid membrane. Room temperature PAM and fluorescence emission spectroscopy indicate a significant increase in phycobilin fluorescence in cells without PsbU. The 77K fluorescence emission spectra localize this to allophycocyanin and the terminal phycobilin emitters. This result was confirmed by time-resolved fluorescence decay spectroscopy which showed a large increase in the yield of a 1.3 ns, allophycocyanin associated, decay component in the mutant cells. This component likely reflects allophycocyanin that is uncoupled from the terminal phycobilin emitters in the PBS.

The mutant cells were also characterized by an increase in a 300 ps fluorescence decay component at Fo whose origin is complex. This component increased in amplitude upon PSII trap closure but also showed significant contributions by phycobilin core components. The 300

ps component we observed was likely a mixture of two previously observed fluorescence decay components, one associated with closed PSII centers (500 ps) and the other believed to arise from the terminal phycobilin emitter (200 ps) (*36*). The increase in the 300 ps component upon trap closure and in the ΔPsbU mutant at Fo is consistent with the previously observed increase in contribution of the 500 ps PSII component upon trap closure in intact cyanobacteria. This interpretation is supported by the increased yield of the 1 ns decay component, indicative of closed PSII reaction centers, observed in the mutant cells at Fo. Another possible interpretation, especially for 650 nm excitation, is that this component could reflect decay from phycobilin core components including the terminal phycobilin emitters. A 200 ps component associated with the terminal phycobilin emitters had previously been observed in intact cyanobacteria (*36*). In that study the lifetime was attributed to relatively inefficient energy transfer from the terminal emitter to PSII Chl *a*. In a separate study (*38*), a 500 ps component was attributed to the terminal phycobilin emitters in a PSII-less mutant of *Synechocystis* sp. PCC 6803. That decay was much faster than the 1.5 ns decay associated with emission from the terminal phycobilin emitters in isolated PBS and was attributed to quenching associated with PBS binding to the thylakoid membrane. The increased amplitude of the 300 ps component observed in the ΔPsbU cells in our study may thus reflect an increase in the number of PBS energetically uncoupled from PSII, but still attached to the thylakoid membrane. This interpretation would be consistent with the transient coupling model of PBS and PSII interaction supported by FRAP data (*10,13*) assuming that the terminal emitters decay in the coupled PBS/PSII complex was much shorter than the 300 ps decay component and not observed in our measurements.

Any assessment of the effect that the removal of PsbU has on the energetic coupling of the PBS to PSII is hampered by the lack of consensus on the mechanism of coupling (*8,13*). There is

a PB-loop of the L(CM) domain or hydrophobic linker peptide chain that has been suspected to be involved in either PSII or membrane binding and energy transfer (*8*). Thus it is plausible to infer a disruption in the binding of this linker peptide to PSII and/or the thylakoid membrane when PSII centers do not contain PsbU. However, previous work has shown that the PBS still assembles and functions comparably with wild type in mutants that have the PB-loop deleted from the L(CM) domain (*12*). A "native affinity" has also been demonstrated *in vitro*, whereby isolated PSII complexes and PBS were found to energetically couple without a thylakoid membrane or PB-loop on the PBS (*11*). The native affinity between PSII and the PBS may provide the most likely factor in PSII/PBS energy coupling that is being affected by the removal of PsbU. Energetic coupling from the PBS to PSII and PSI is likely mediated through the phycobilin terminal emitters which are three long wavelength allophycocyanin pigments associated with ApcD, ApcE and ApcF. It is uncertain how these long wavelength emitters couple energetically to the Chl of PSII and PSI, although a number of proposals have been put forward (*8, 39, 40*). It is clear, however, that the energetic coupling of the PBS will be highly dependent on the distance between, and relative orientations of, the terminal PBS emitters and Chl molecules in the PSII core. We propose that the absence of PsbU on the lumenal side of the PSII core may affect a small overall change in PSII core structure which is correlated with a subtle change in the stromal exposed surface of PSII. Modification of the donor side of PSII has previously been shown to influence the acceptor side (*41*). A small change in the shape of the stromal exposed surface of PSII could significantly effect the interaction of the PSII core with the PBS and thus disrupt energy transfer from one or more of these pigments to the core Chl of PSII. We have demonstrated that the PsbU protein influences diverse processes in PSII. Electron transport activity is limited in the absence of PsbU as a proportion of PSII centers

remain closed in dark-adapted cells. In addition, the absence of PsbU impairs energy transfer from the PBS to PSII. PsbU thus serves roles in stabilizing both electron transport and energy transfer in the PBS/PSII assembly in *Synechocystis* sp. PCC *6803*.

REFERENCES

1. Barber, J. (2003) Photosystem II: the engine of life, *Quart. Rev. Biophys. 36*, 71-89.

2. Ferreira, K. N., Iverson, T. M., Maghlaoui, K., Barber, J., and Iwata, S. (2004) Architecture of the photosynthetic oxygen-evolving center, *Science 303*, 1831-1838.

3. Bricker, T. M., and Frankel, L. K. (2002) The structure and function of CP47 and CP43 in photosystem II, *Photosyn. Res. 72*, 131-146.

4. Eaton-Rye, J. J., and Putnam-Evans, C. (2005) The CP47 and CP43 core antenna components, in *Photosystem II: The Water/Plastoquinone Oxido-Reductase of Photosynthesis* (Wydrzynski, T., and Satoh, K., Eds.) Springer, Dordrecht, in press.

5. Ananyev, G. M., Zaltsman, L., Vasko, C., and Dismukes, G. C. (2001) The inorganic biochemistry of photosynthetic oxygen evolution/water oxidation, *Biochim. Biophys. Acta 1503*, 52-68.

6. Kok, B., Forbush, B., and McGloin, M. (1970) Cooperation of charges in photosynthetic O_2 evolution - I. A linear four-step mechanism. *Photobiochem. Photobiol. 11,* 457-475.

7. Debus, R. J. (2000) The polypeptides of photosystem II and their influences on mangano-tyrosyl based oxygen evolution, in *Metal Ions in Biological Systems*, Vol 37 (Sigel, A., and Sigel, H., Eds.) pp 657-711, Marcel Dekker, New York.

8. McConnell, M. D., Koop, R., Vasil'ev, S., and Bruce, D. (2002) Regulation of the distribution of chlorophyll and phycobilin-absorbed excitation energy in cyanobacteria. A structural-based model for the light state transition. *Plant Physiol. 130,* 1201-1212.

9. Bryant, D. A. (1991) Cyanobacterial phycobilisomes: Progress toward complete structural and functional analysis via molecular genetics, in *Cell Culture and Somatic Cell Genetics of Plants, Vol 7B: The Photosynthetic Apparatus: Molecular Biology and Operation* (Bogorad, L., and Vasil, I. L., Eds.) pp 257-300, Academic Press, San Diego.

10. Mullineaux, C. W., Tobin, M. J., and Jones, G. R. (1997) Mobility of photosynthetic complexes in thylakoid membranes, *Nature 390,* 421-424.

11. Kirilovsky, D., and Ohad, I. (1986) Functional assembly *in vitro* of phycobilisomes with isolated photosystem II particles of eukaryotic chloroplasts, *J. Biol. Chem. 261*, 12317-12323.

12. Ajlani, G., and Vernotte, C. (1998) Deletion of the PB-loop in the L(CM) subunit does not affect phycobilisome assembly or energy transfer functions in the cyanobacterium *Synechocytsis* sp. PCC6714, *Eur. J. Biochem. 257*, 154-159.

13. Sarcina, M., Tobin, M. J., and Mullineaux, C. W. (2001) Diffusion of phycobilisomes on the thylakoid membranes of the cyanobacterium *Synechococcus* 7942, *J. Biol. Chem. 276*, 46830-46834.

14. Ashby, M. K., and Mullineaux, C. W. (1999) The role of ApcD and ApcF in energy transfer from phycobilisomes to PS I and PS II in a cyanobacterium, *Photosynth. Res. 61*, 169-179.

15. Nishiyama, Y., Los, D. A., Hayashi, H., and Murata, N. (1997) Thermal protection of the oxygen-evolving machinery by PsbU, an extrinsic protein of photosystem II, in *Synechococcus* species PCC 7002, *Plant Physiol. 115*, 1473-1480.

16. Nishiyama, Y., Los, D. A., and Murata, N. (1999) PsbU, a protein associated with photosystem II, is required for the acquisition of cellular thermotolerance in *Synechococcus* species PCC 7002, *Plant Physiol. 120*, 301-308.

17. Kimura, A., Eaton-Rye, J. J., Morita, E. H., Nishiyama, Y., and Hayashi, H. (2002) Protection of the oxygen-evolving machinery by the extrinsic proteins of photosystem II is essential for development of cellular thermotolerance in *Synechocystis* sp. PCC 6803, *Plant Cell Physiol. 43*, 932-938.

18. Shen, J.-R., Ikeuchi, M., and Inoue, Y. (1997) Analysis of the *psbU* gene encoding the 12-kDa extrinsic protein of photosystem II and studies on its role by deletion mutagenesis in *Synechocystis* sp. PCC 6803, *J. Biol. Chem. 272*, 17821-17826.

19. Summerfield, T. C., Shand, J. A., Bentley, F. K., and Eaton-Rye, J. J. (2005) PsbQ (Sll1638) in *Synechocystis* sp. PCC 6803 is required for photosystem II activity in specific mutants and in nutrient-limiting conditions, *Biochemistry 44*, 805-815.

20. Shen, J.-R., and Inoue, Y. (1993) Binding and functional properties of two new extrinsic components, cytochrome *c*-550 and a 12 kDa protein, in cyanobacterial photosystem II, *Biochemistry 32*, 1825-1832.

21. Eaton-Rye, J. J., Shand, J. A., and Nicoll, W. (2003) pH-dependent photoautotrophic growth of specific photosystem II mutants lacking lumenal extrinsic polypeptides in *Synechocystis* PCC 6803, *FEBS Lett. 543*, 148-153.

22. Clarke, S. M., and Eaton-Rye, J. J. (1999) Mutation of Phe-363 in the photosystem II protein CP47 impairs photoautotrophic growth, alters the chloride requirement, and prevents

photosynthesis in the absence of either PSII-O or PSII-V in *Synechocystis* sp. PCC 6803, *Biochemistry 38*, 2707-2715.

23. Eaton-Rye, J. J. (2004) The construction of gene knockouts in the cyanobacterium *Synechocystis* sp. PCC 6803, in *Methods in Molecular Biology, Vol 274: Photosynthesis Research Protocols* (Carpentier, R., Ed.) pp 309-324, Humana Press, Totowa, New Jersey.

24. Williams, J. G. K. (1988) Construction of specific mutations in the photosystem II photosynthetic reaction center by genetic engineering methods in the cyanobacterium *Synechocystis* 6803, *Meth. Enzymol. 167*, 766-778.

25. Boliver, F. (1978) Contruction and characterization of new cloning vehicles, III. Derivatives of plasmid pBR322 carrying unique *Eco*RI sites for selection of *Eco*RI-generated recombinant DNA molecules, *Gene 4*, 121-126.

26. Prentki, P., Karch, F., Iida, S., and Meyer, J. (1981) The plasmid cloning vector pBR325 contains a 482 base-pair-long inverted duplication, *Gene 14*, 289-299.

27. Rouag, D., and Dominy, P. (1994) State adaptations in the cyanobacterium *Synechococcus* 6301 (PCC) – Dependence on light intensity or spectral composition, *Photosynth. Res. 40*, 107-117.

28. Schreiber, U., Hormann, H., Neubauer, C., and Klughammer, C. (1995) Assessment of photosystem II photochemical quantum yield by chlorophyll quenching analysis, *Aus. J. Plant Physiol. 22*, 209-220.

29. Salehian, O., and Bruce, D. (1992) Distribution of excitation energy in photosynthesis: quantification of fluorescence yields from intact cyanobacteria, *J. Luminescence 51*, 91-98.

30. Vasil'ev, S., Wiebe, S., and Bruce, D. (1998) Non-photochemical quenching of chlorophyll fluorescence in photosynthesis. 5-hydroxy-1,4-napththoquinone in spinach thylakoids as a model for antenna based quenching mechanisms, *Biochim. Biophys. Acta 1363*, 147-156.

31. Vasil'ev, S., and Bruce, D. (1998) Nonphotochemical quenching of excitation energy in photosystem II. A picoscond time-resolved study of the low yield of chlorophyll *a* fluorescence induced by single-turnover flash in isolated spinach thylakoids, *Biochemistry 37*, 11046-11054.

32. Vasil'ev S., and Bruce, D. (2000) Picosecond time-resolved fluorescence studies on excitation energy transfer in a histidine 117 mutant of the D2 protein of photosystem II in *Synechocystis* 6803, *Biochemistry 39*, 14211-14218.

33. MacKinney, G. (1941) Absorption of light by chlorophyll solutions, *J. Biol. Chem. 140,* 315-322.

34. Myers, J., Graham, J.-R and Wang, R.T. (1980) Light-harvesting in *Anacystis nidulans* studied in pigment mutants, *Plant Physiol.* 66, 1144–1149.

35. Mullineaux, C.W. and Holzwarth, A.R. (1993) Effect of photosystem II reaction centre closure on fluorescence decay kinetics in a cyanobacterium, *Biochim. Biophys. Acta 1183*, 345-351.

36. Mullineaux, C.W. and Holzwarth, A.R. (1991) Kinetics of excitation energy transfer in the cyanobacterial phycobiisome-Photosystem II complex, *Biochim. Biophys. Acta 1098*, 68-78.

37. Shen, J.-R., Qian, M., Inoue, Y., and Burnap, R. L. (1998) Functional characterization of *Synechocystis* sp. PCC 6803 Δ*psb*U and Δ*psb*V mutants reveals important roles of cytochrome *c*-550 in cyanobacterial oxygen evolution, *Biochemistry 37*, 1551-1558.

38. Bittersman, E. and Vermaas, W. (1991) Fluorescence lifetime studies of cyanobacterial Photosystem II mutant, *Biochim. Biophys. Acta 1098*, 105-116.

39. Bald, D., Kruip, J. and Rögner M. (1996) Supramolecular architecture of cyanobacterial thylakoid membranes: How is the phycobilisome connected with the photosystems? *Photosynth. Res. 49*, 103-118.

40. Barber, J., Norris, E.P. and da Fonseca, C.A. (2003) Interaction of the allophycocyanin core complex with photosytem II *Photochem. Photobiol. Sci. 2*, 536-541.

41. Johnson, G.N., Rutherford, A.W. and Krieger, A. (1995) A change in the midpoint potential of the quinone Q(A) in photosystem II associated with photoinactivation of oxygen evolution. *Biochim. Biophys. Acta* 1229, 202-207.

Chapter 2: Functional Heterogeneity of Photosystem II in Domain Specific Regions of the Thylakoid Membrane of Spinach (*Spinacia oleracea L.*) *Biochemistry 46*, 3443-3453 (2007)[†]

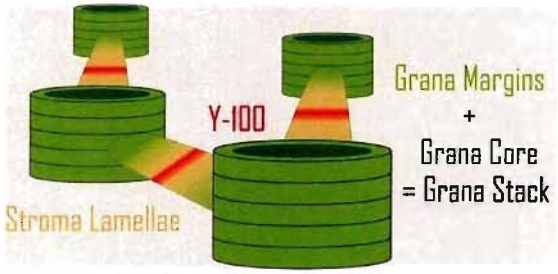

John Veerman[‡], Michael D. McConnell[‡], Sergei Vasil'ev[*,‡], Fikret Mamedov[§], Stenbjörn Styring[§] and Doug Bruce[‡]

Department of Biology, Brock University, St. Catharines, Ontario, L2S 3A1, Canada and Department for photochemistry and molecular science, Molecular Biomimetics, Uppsala University, Box 523, S-751 20, Uppsala, Sweden

[†] This work was supported by a research grant from NSERC to D.B. Work in Sweden was supported from the Swedish Research Council and the Swedish Energy Agency (S.S. and F.M.) We gratefully acknowledge biochemical preparations by and discussions with Prof Per-Åke Albertsson (Lund university), Dr Ravi Danielsson (Lund university) and Dr Rena Gadjieva (Swedish Agricultural University, Uppsala).

[‡] Brock University.

[§] Uppsala University.

* corresponding author, email dbruce@brocku.ca , FAX 905 688-1855, Phone: 905 688-5550 ext 3826

[1]Abbreviations: PS, photosystem; RC, reaction center; Chl, chlorophyll; P680, primary electron donor in photosystem II; Q_A, primary quinone electron acceptor in photosystem II; DAS, decay-associated spectrum; F_0, the minimal fluorescence level associated with photochemically active or "open" reaction centers with an oxidized primary quinone electron acceptor, Q_A, F_M , the maximal level of fluorescence associated with photochemically inactive or "closed" reaction centers with reduced primary quinone electron acceptor, Q_A.

Preface

This chapter was published in the high impact Journal *Biochemistry* in 2007. I wrote the first draft of this article and was heavily involved in revisions and addressing the concerns and critique of both reviewers and the editor of *Biochemistry*.

The thylakoid fractions were produced at the University of Lund in Sweden by Professor Stenbjörn Styring and Dr. Fikret Mamedov. Dr. Mamedov also produced Table 2.1 for the purpose of this study. Dr. Michael McConnell who was a Masters student in our lab before I arrived, collected and analyzed the data presented in Figure 2.2 and the measured absorbance cross sections in Table 2.2. Dr. McConnell also performed a significant amount of work characterizing the thylakoid membrane fractions and was involved in revising the paper for publication. I produced all other figures, tables and illustrations and collected and analyzed the data contained therein.

It should also be noted that Professor Doug Bruce and Dr. Sergei Vasil'ev both guided me through all aspects of this research, from hypothesis formation, data collection, and analysis to writing/revising the article.

ABSTRACT

A mild sonication and phase fractionation method has been used to isolate five regions of the thylakoid membrane in order to characterize the functional lateral heterogeneity of photosynthetic reaction centers and light harvesting complexes. Low temperature fluorescence and absorbance spectra, absorbance cross-section measurements and picosecond time resolved fluorescence decay kinetics were used to determine the relative amounts of photosystem II (PSII) and photosystem I (PSI), the relative PSII antenna size and to characterize the excited state dynamics of PSI and PSII in each fraction. Marked progressive increases in the proportion of PSI complexes were observed in the following sequence: grana core (BS), whole grana (B3), margins (MA), stroma lamellae (T3) and purified stromal fraction (Y100). PSII antenna size was drastically reduced in the margins of the grana stack and stroma lamellae fractions as compared to the grana. Picosecond time-resolved fluorescence decay kinetics of PSII were characterized by three exponential decay components in the grana fractions, and were found to have only two decay components with slower lifetimes in the stroma. Results are discussed in framework of existing models of chloroplast thylakoid membrane lateral heterogeneity and the PSII repair cycle. Kinetic modeling of the PSII fluorescence decay kinetics revealed that PSII populations in the stroma and grana margin fractions possess much slower primary charge separation rates and decreased photosynthetic efficiency when compared to PSII populations in the grana stack.

INTRODUCTION

In the process of oxygenic photosynthesis plants utilize light energy to split water into molecular oxygen, protons and electrons and produce both ATP and NADPH for use in carbon fixation. This process requires photosystem I (PSI) and photosystem II (PSII) operating in tandem.

PSI and PSII core complexes are large supramolecular pigment-protein complexes containing 96 and 35 chlorophyll *a* (Chl *a*) molecules (*1;2*) and (*3;4*), respectively. In higher plants both photosystems are associated with peripheral Chl *a* and Chl *b* - containing antennae complexes, known as light harvesting complex I (LHCI) and light harvesting complex II (LHCII). The PSII associated LHC family includes the Chl binding proteins, CP24, CP26 and CP29. The PSI core complex associates with four LHCI monomers, while two LHCII trimers and three monomers (CP24, CP26 and CP29) are coupled to each PSII core. The association of the auxiliary antennae with the PSI core complex has generated a model of PSI-LHCI with a total of 167 Chl molecules (*5;6*) and a Chl *a/b* ratio of about 9. The PSII-LHCII complex is characterized as possessing about 150 Chl molecules, with a Chl *a/b* ratio of about 2.5 (*7;8*). In addition to these basic structural units, higher plants produce variable amounts of additional LHCII serving to supplement the light harvesting capacity of each photosystem. These additional LHCII complexes can be dynamically reallocated between the two photosystems to optimize cooperation between them in a process denoted as state transitions, see (*9*) for review.

Photosynthetic membranes of chloroplasts consist of the appressed regions (grana stacks) and the unappressed regions (stroma lamellae). Grana stacks contain a preponderance of PSII and the stroma lamellae PSI (*10-12*). PSII populations localized in these two membrane areas are fundamentally different with respect to antenna size and photochemical activity. PSII complexes

in the grana stack represent a highly active population with respect to donor and acceptor side electron transport, while those in the stroma lamellae have been observed to be relatively inactive (*13-15*).

A mild sonication and phase fractionation method has been developed to isolate several grana and stroma fractions (*13;14;16*); these membrane fractions are illustrated with respect to their location in chloroplast thylakoid membranes in **Figure 2.1**. Studies of these fractions have indicated that inactivation of PSII with respect to oxygen evolution and forward electron transfer from Q_A progressively increases with increasing distance from the grana core (*13-15*). Lateral heterogeneity of PSII was explained by damage of highly active PSII complexes in the grana core and their subsequent reallocation to the stroma membrane regions, which are accessible to ribosomes, for repair, see for review (*17*). After repair in the stroma, Q_B binding affinity and the oxygen evolving complex were proposed to be restored during transport back to the grana. By the time PSII complexes reach the margins of the grana stack most are activated and the activation process was proposed to reach completion in the core of the grana stack (*13;14*). The isolation of thylakoid membrane fractions has allowed for the assessment of lateral heterogeneity with respect to Chl *a* and Chl *b* content, PSII/PSI ratio and overall PSII activity as measured by secondary electron transport rates. In addition, the distribution of different forms of PSII, including PSII-LHCII supercomplexes, PSII dimers, PSII monomers, PSII monomers lacking CP43 and D1/D2 reaction centers has been shown to vary greatly across fractions (*18*). The grana core contains most of the supercomplexes and the PSII population in the Y-100 fraction mostly consists of monomers lacking CP43 and D1/D2 reaction centers.

Characterization of primary energy conversion events in PSII, including excitation energy transfer, primary photochemical charge separation, charge stabilization and

recombination in the different thylakoid membrane fractions has not yet been done. The rates of charge separation and stabilization can be obtained from picosecond time resolved fluorescence decay kinetics. However, sophisticated kinetic modeling is required to estimate rates of photochemical processes in such complex pigment aggregates as PSI and PSII. Kinetic modeling, utilizing available structural information and assignment of site energy levels has been applied to estimate rates of photochemical processes from fluorescence decay kinetics of isolated PSI and PSII particles (*2;19-22*). In the case of whole thylakoids many other factors (PSII heterogeneity, heterogeneity of the peripheral antenna, presence of unconnected light-harvesting complexes in the stroma lamellae and mixing of PSI fluorescence with faster PSII decay processes) contribute to the complexity of the fluorescence decay kinetics and determination of the intrinsic charge separation and charge stabilization rates becomes even more complex.. Correct assignment of the observed fluorescence decay components is the first and the most critical step in the interpretation of fluorescence decay components in higher plant thylakoids.

Previously, fluorescence decay components of whole thylakoids have been assigned assuming that homogeneous PSI kinetics are monoexponential and PSII kinetics are biexponential (*23;24*). Two populations of PSII were required to fit data and both populations were inferred to have two decay components with indistinguishable lifetimes of the fast decay components at F_0. The two populations were distinguished by finding a minimal physically reasonable kinetic model capable of describing a set of fluorescence decay kinetics measured at different wavelengths using samples with both closed (F_M) and open reaction centers. At F_M all four lifetimes could be distinguished and, as the relative amount of the two PSII populations was independent of the state of the reaction centers, it was possible to extract kinetic parameters of both PSII populations at F_0 by imposing this constraint on the fit of the F_0 kinetics.

Since then many studies have followed this assignment, particularly in interpretation of kinetic changes due to non-photochemical quenching (*25;26*). Recent studies of isolated PSI and PSII particles have shown, however, that fluorescence decay kinetics of both photosystems are intrinsically more complex (*21;22;27;28*). Thylakoid membrane fractions isolated using the phase fractionation method represent simpler systems than whole thylakoids and are ideally suited for identification of fluorescence decay components. At the same time study of fluorescence decay kinetics in these fractions are critically important for understanding how the photochemical properties of PSII vary *in situ* in different thylakoid membrane regions and thus with different stages of the PSII repair cycle.

In this paper we present time-resolved fluorescence data, and measurements of the functional PSII antenna size of the aforementioned fractions of thylakoid membranes. We make use of independent measurements of relative PSI and PSII content, functional PSII antenna size and global analysis of fluorescence decay kinetics collected with open and closed PSII reaction centers to identify decay components. Our data shows that the functional antenna size of PSII was drastically reduced in the margins of the grana stack and stroma fractions as compared to the grana. We found that fluorescence decay kinetics were relatively fast and three exponential in the grana fractions, while PSII in the stroma was characterized by slower and biexponential decay kinetics. Kinetic modeling of our data revealed essential differences in primary charge separation between PSII localized in the grana and stroma membrane regions. PSII primary charge separation rates and photosynthetic efficiency were depressed in the stroma derived fractions and the grana margins as compared to the grana stack. We discuss our results in the framework of the existing models of chloroplast thylakoid membrane structure and the PSII repair cycle.

MATERIALS AND METHODS

Preparation of thylakoid membrane fractions. All thylakoid membrane fractions were isolated from home grown spinach as described in (*14;15*).

Steady state spectroscopy. Absorption spectra were measured at 10 K using an intensified diode array detector (model 1461 EG&G Princeton Applied Research) and a helium cryostat (Advanced Research Systems, Inc., model DE-202). Samples were resuspended in 50 mM HEPES buffer, pH 7.6, containing 0.1 M sorbitol, 5 mM $MgCl_2$, 5 mM NaCl, and 60% glycerol. Emission spectra were measured at 77 K with the same detector. Chlorophyll concentration of less than 5 μg/ml was used in fluorescence measurements.

PSII absorbance cross-sections. PSII absorption cross-sections were determined by flash saturation curves of variable Chl *a* fluorescence. An optical parametric oscillator (VisIR2, GWU-Lasertechnik) pumped by the third harmonics of a Q-switched Nd:YAG laser (Spectron Laser Systems) was used to provide 6 ns long actinic flashes at a wavelength of 435 nm. The actinic light was delivered via the optical fiber to a 250 μL flow through cuvette where the sample was circulated at the rate of about 1 mL/sec. Chlorophyll concentration of about 5 μg/ml was used in cross-section measurements. Non-actinic 60 μs long measuring light pulses were supplied by blue light emitting diode (450 nm) 100 μs after the pump flash to determine the amplitude of fluorescence. Chlorophyll fluorescence was detected by a photomultiplier tube (Hamamatsu RG967), screened by a ¼ meter monochromator. A small fraction of the actinic flash was directed toward a photodiode so that the energy of each laser pulse could be measured. 20 fluorescence yield and flash energy signals were averaged simultaneously at a flash frequency of 2.5 Hz. Data were fit with the cumulative Poisson single-hit probability distribution (*29*): $\Phi(I) = \Phi_{max}(1 - e^{-I \cdot \sigma})$ where I is the pulse energy, $\Phi(I)$ is the yield of the fluorescence, Φ_{max} is

the maximal yield determined at saturating flash intensity, σ is the effective absorption cross-section.

Absorbance cross sections were also calculated based on the distribution of different types of PSII complexes found in the different fractions of the thylakoid membrane as reported by (*18*). This was performed by representing each subpopulation of PSII with a cumulative Poisson single-hit probability distribution; taking into account the relative proportion and the presumed antennae size of the PSII subpopulation. For each fraction the cumulative Poisson single-hit probability distribution for each constituent subpopulation of PSII were added to produce a simulated curve. The simulation was then fit in the same manner as the experimentally obtained data. The relative antenna sizes of the various subpopulations of PSII identified in (*18*) (PSII-LHCII supercomplexes, PSII dimers, PSII monomers, CP43-less PSII monomers and D1/D2 reaction centers) were calculated based on the following assumptions concerning the number of antenna Chl associated with each "type" of PSII. The D1/D2 reaction centers were assumed to contain the equivalent of 6 Chls, CP43-less centers had 22 Chls, PSII monomers and PSII dimers possessed 35 Chl per reaction center (*30*). While the PSII-LHCII supercomplexes were assumed to possess a variable number of Chl ranging from a minimum of 125 Chl to a maximum of 253 Chl per reaction center. The antennae size of PSII-LHCII was derived via use of CP24 (10 Chl), CP26 (9 Chls) and CP29 (8 Chl) monomeric subunits (*31*); and the LHCII trimers (42 Chl) (*32*) as the building blocks of the PSII auxiliary antennae. It should also be noted that the stroma derived fractions (Margins, T3 and Y100) were assumed to possess PSII-LHCII complexes that were relatively disassembled when compared to the grana derived fractions (BS and B3); while PSII monomers and dimers in the grana derived fractions were assumed to possess some measure of auxillary antennae. This disparity was mandated in order to

determine if the PSII subpopulations were relatively more disassembled in the stroma as compared to the grana. The precise details regarding the implementation of this bias in our calculations can be found in the results section.

Picosecond fluorescence decay kinetics. A single photon timing apparatus utilizing a picosecond pulsed diode laser was used to measure the kinetics of chlorophyll fluorescence decays (*33*). Excitation pulses were delivered at 407 nm by a picosecond diode laser (PicoQuant, PDL 800-B), 54 ps FWHM. Chlorophyll fluorescence was measured by a Hamamatsu R-3809 micro channel plate photomultiplier screened by a double monochromator. A single photon counting PC card (Becker & Hickl, SPC-730) was used for data collection. The instrument response function of the system was 68 ps. To maintain PSII reaction centres in the open (F_0) state samples were circulated with a flow rate of 4 mL/s and low measuring light intensities were used. The F_m state was achieved by addition of DCMU, slowing down the circulation rate and increasing the measuring light intensity. Fluorescence decay data were collected for four detection wavelengths between 680 nm and 730 nm until 20,000 counts in the peak channel were attained. Fluorescence decay curves taken at all wavelengths were fit with the sum of exponential decay functions globally with the model of parallel decaying compartments as described previously (*34;35*).

PSII Kinetic Modeling. Modeling of PSII fluorescence decay kinetics was based on a recently published "coarse grained" model which takes into account supramolecular organization of PSII and LHCII in thylakoid membranes to model the energy migration and charge separation processes in the PSII-LHCII supercomplex (***22***). In this model each pigment-protein subunit in the PSII-LHCII supercomplex is represented by one compartment. The excitation transfer rate between all compartments was assumed to be $(17\ ps)^{-1}$ and charge separation in PSII was

modeled by one reversible radical pair. The antennae size of the PSII population in each fraction was determined from the measured absorbance cross sections and analysis of protein gels, the connectivity between antennae compartments was based on the structural organization of PSII-LHCII complexes. The fitting parameters in the model were the rate constants of charge separation (K_{CS}), its reversal (K_{CS}^{-}) and charge stabilization by secondary electron transfer to Q_A (K_{ST}). This model is approximate, however, it was demonstrated previously that it allows one to draw conclusions about the relative contributions of excitation energy transfer and charge separation to excited state dynamics.(*22*).

RESULTS

Low temperature fluorescence spectra. Low temperature fluorescence emission spectra were measured to assay for relative amounts of PSII and PSI in the thylakoid membrane fractions. The fluorescence peak at ~730 nm (F_{730}) arises from PSI, the fluorescence peak at ~695 nm (F_{695}) from PSII; while the fluorescence peak occurring at ~685 nm (F_{685}) originates in both PSII and LHCII. The F_{695}/F_{730} ratio is a reasonable indicator of the relative PSII/PSI ratio. The F_{695}/F_{730} ratio was high in the grana BS and B3 fractions. It sharply dropped in the margins, and decreased further in stroma fractions (**Figure 2.1**). The trend observed shows the amount of PSII decreasing from grana fractions to stroma fractions, while relative PSI content increases (**Figure 2.1**). This is consistent with existing models of PSII/PSI lateral heterogeneity in chloroplast thylakoid membranes and with EPR measurements performed on similar fractions (**see Table 2.1**) (*15*).

Low temperature absorbance spectra. Low temperature absorption spectra from the B3 and grana core BS regions are very similar to each other and are characterized by a peak in the

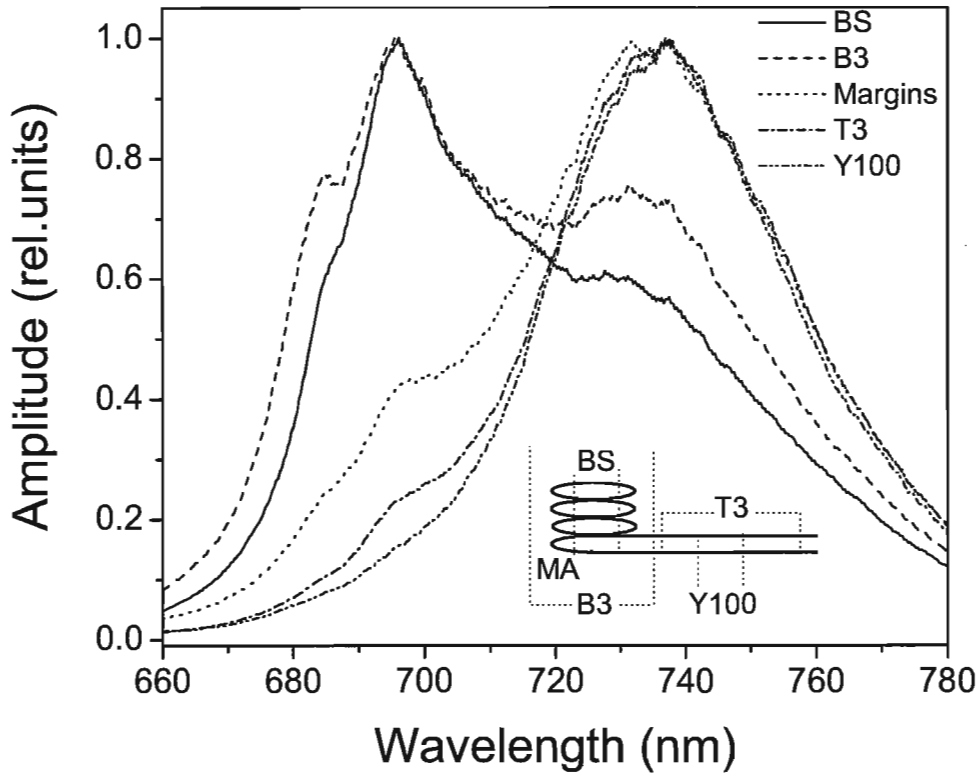

Figure 2.1. 77K fluorescence spectra of chloroplast thylakoid fractions. Spectra were normalized to peak emission. BS, grana core fraction; B3, entire grana stack; margin, grana margins; T3, stroma thylakoid membranes; Y100, purified stroma thylakoid membranes. See materials and methods for details. Diagram illustrating the origin of the specific membrane fractions in relation to the structure of the chloroplast thylakoid membrane is shown in the insert.

Table 2.1. Characterization of the different fractions of the thylakoid membrane.

Fraction	Chl *a/b* (mol/mol)	O_2 evolution [A] [μmol of O_2/ (mg of Chl)$^{-1}h^{-1}$]	Chl/fraction [B], %, ±5	PSII/fraction [B], %, ±5	PSI/PSII [C]	Chl/ $Y_D^{\bullet}$ [D]	Chl/P700$^+$ [D] mol/mol
Grana Core	2.27	271	51	71	0.25 ±0.06	355	1300
Grana	2.60	240	64	81	0.43 ±0.05	408	980
Margins	3.62	94	13	10	1.28 ±0.14	667	508
Stroma	4.40	87	36	19	3.10 ±0.11	971	316
Y-100	7.51	0	5	1	12.75±1.65	2780	222
Thylakoids	3.11	127	100	100	1.13 ±0.05	617	552

[A] – measured with 2 mM ferricyanide and 0.5 mM PpBQ as electron acceptor. [B] – calculated from the counter current distribution that provide the Chl yield in each fraction and from the EPR measurements for the PSII content in the different thylakoid fractions, data from (*18*). [C] – on the basis of EPR measurements, data from (*15*). [D] - on the basis of EPR measurements, data from (*15*). Shows total number of Chl(*a*+*b*) molecules per PSII or PSI center. Note that not all these chlorophylls are connected to PSII or PSI (see discussion in (*15*) for explanation of the calculation of antenna size).

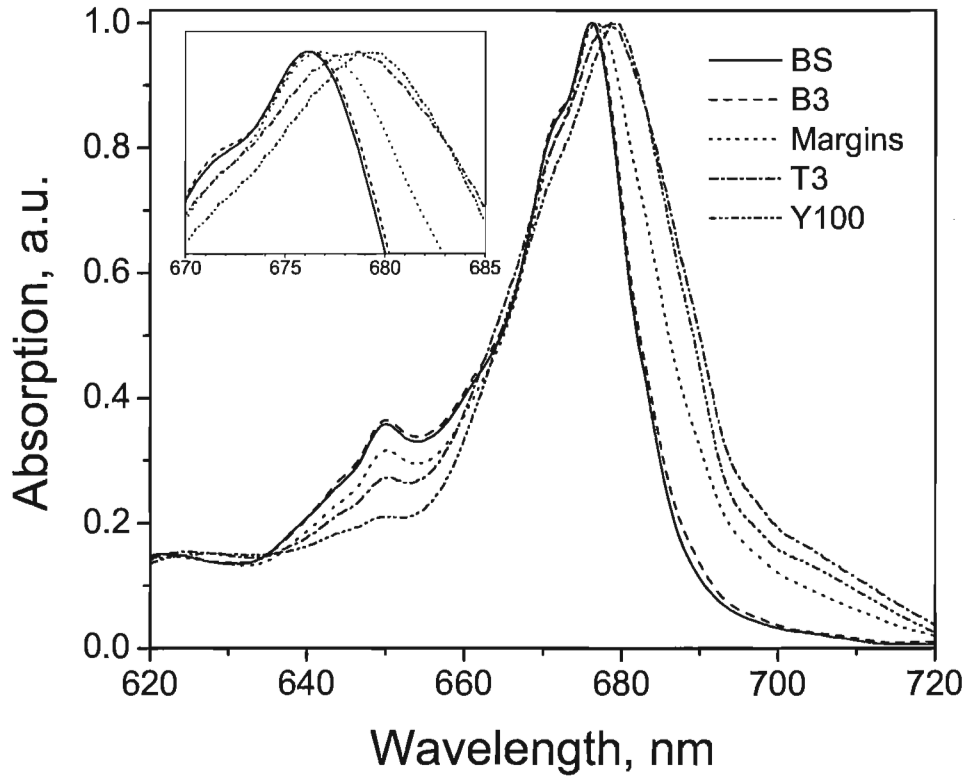

Figure 2.2. 10K absorbance spectra of chloroplast thylakoid fractions. Spectra were normalized to peak absorbance. BS, grana core fraction; B3, entire grana stack; margin, grana margins; T3, stroma thylakoid membranes; Y100, purified stroma thylakoid membranes. Insert shows magnified picture of changes in the maximum absorption peak around 680 nm in the different fractions. See materials and methods for details.

Chl *a* Q_Y region at 676 nm for B3 and BS (**Figure 2.2**) . Both fractions also exhibit a distinct short wavelength shoulder on the Qy band at 671 nm. These two spectra show a relatively large contribution from Chl *b* observed as a distinct peak at 650 nm. Absorption spectra from the T3 and Y100 stroma membrane fractions are characterized by significantly increased contributions of long wavelength Chl *a* forms of PSI to the Qy band. Increase of the abundance of these forms results in a red shift and broadening of the absorption peak in the Chl *a* Q_Y region. The contribution of Chl *b* to the absorption of these fractions (especially in the Y100 fraction) is much lower than in the grana fractions. The spectra from the grana margins are intermediate between the grana and stroma membrane fractions for all of the above described characteristics. The absorption data follows the same trend as the emission data indicating that the amount of PSII and Chl *b* containing LHC complexes decreases from grana fractions to stroma fractions, while relative PSI content increases.

PSII absorbance cross-sections. The absorbance cross-sections of the PSII complexes present in the thylakoid fractions were determined using pump probe fluorescence flash saturation curves as described in Methods. Analysis of the saturation curves showed the absorbance cross section of PSII to be the largest in the whole grana and grana core fractions and sharply decrease in the grana margins and stroma fractions (**Table 2.2**). There was a threefold reduction of the functional antennae size of the PSII complexes from the grana core fraction (BS) to the grana margins, and a five fold decrease from the BS fraction to the Y100 fraction. Since the amplitude of the Chl *b* peak in the absorbance spectra does not decrease proportionally to the decrease of the functional PSII antenna size, a dissociation of LHCII complexes from PSII in the grana margins and stroma fractions is likely responsible for much of the decrease in functional antenna size and is consistent with existing models of PSII repair and measurements of PSII

heterogeneity in chloroplast thylakoid membranes (*18*).

The observed relative difference in PSII antennae size found between the different thylakoid membrane fractions was compared to calculated relative differences in antenna size that were based on a recent proteomic analysis of the thylakoid fractions (*18*). The proteomic analysis showed each isolated thylakoid fraction to have a unique heterogeneous population of PSII centers consisting of PSII-LHCII supercomplexes, PSII dimers, PSII monomers, CP43-less PSII monomers and D1/D2 reaction centers. Our calculation assumed different antenna sizes for each of the different types of PSII centers and two different analyses were done assuming variable sizes for the PSII-LHCII supercomplexes, see **Methods** section for details. Both calculations assumed that PSII dimers and PSII monomers found in the margins, stroma and Y100 fractions were not associated with any LHC's and that any PSII supercomplexes found in the margin fraction were associated with the equivalent of 3 LHCII trimers per PSII-LHCII supercomplex (125 Chls per reaction center). Both calculations also assumed that PSII dimers and PSII monomers in the grana core were associated with 2 LHCII trimers and 1 LHCII trimer respectively (106 Chls per reaction center). The only difference between the two calculations was the assumed size of the PSII-LHCII supercomplex in the grana core. The first calculation assumed that the PSII-LHCII supercomplexes found in the grana core were associated with the equivalent of 5 LHCII trimers per PSII-LHCII supercomplex (169 Chl per reaction center), which is the upper limit for size of an isolated PSII-LHCII supercomplex (*36*). The second calculation assumed that the PSII-LHCII supercomplexes in the core were associated with 9 LHCII trimers (253 Chls per reaction center). This assumption was based on previous studies that indicated a possible PSII antennae size of 250 Chls (*37-39*); provided that all the LHCII present in the grana were utilized by PSII. In the first calculation, the assumptions

used served to maximize the antennae size disparity between the grana fractions as compared to the margins, stroma and Y-100 by using the largest isolated PSII-LHCII antennae size as an upper limit (*37-39*) and the logical boundaries imposed by the PSII population distribution as reported previously in the proteomic data (*18*). Interestingly, in our first calculation, the relative PSII absorbance cross-sections for the margins, stroma and Y-100 fractions were consistently higher than the experimentally determined cross-sections (**Table 2.2**). The much larger antenna size for PSII-LHCII supercomplexes, that represented the only difference between the two calculations, generated relative absorbance cross-sections which were much closer to the experimental results (**Table 2.2**).

Time resolved fluorescence decay kinetics. A global analysis of time resolved fluorescence decay kinetics collected at both F_0 and F_M was undertaken to identify decay components originating from PSII and PSI. To facilitate the identification of the decay components we took advantage of the fact that PSI decay kinetics exhibit negligible changes between F_0 and F_M states. This allowed us to share the amplitudes and lifetimes of PSI components in simultaneous fits of data collected at both F_0 and F_M of the PSII reaction centers. Since the best fits were obtained when the putative PSI components were linked in this manner, the assignment of components to PSII and PSI can be regarded as robust. It should also be noted that the PSI components were not only determined to be static from F_0 to F_M, but these same components have been observed in isolated PSI-200 preparations (*40;41*) and the fast component has been also been observed in isolated PSI cores (*27*). In addition, as will be detailed in the following section, these assigned PSI components gradually emerge as the measurements move from grana to stroma; which is in accordance with our low temperature fluorescence and absorbance measurements as well as a previous study of these fractions (*15*) and other grana and

Table 2.2. PSII absorbance cross sections obtained from flash saturation curves. The fit error is less than 5%. The calculated cross-sections are based on biochemical data for the relative number of PSII supercomplexes, PSII cores, and CP43-less PSII cores found in each fraction in (*18*). See text for details

Fraction	*Measured Cross section*	*Calculated Cross section*[A]	*Calculated Cross section*[B]
BS	1	1	1
B3	0.9	0.91	0.9
Ma	0.31	0.43	0.29
T3	0.27	0.38	0.25
Y100	0.2	0.37	0.24

All cross sections are expressed relative to the grana core fraction. [A] - Cross-sections based on the numbers of LHCII associated with PSII supercomplexes, dimers, and monomers in each of the fractions as determined by proteomic analysis in (*18*). [B] - Cross sections based on the same assumptions as above with the additional assumption that that all of the "free" LHCII trimers that were associated with the grana core fraction were energetically coupled to PSII-LHCII supercomplexes.

stroma preparations (*10-12*). We were particularly interested in characterization of fluorescence decay components originating from open PSII reaction centers as they reflect charge separation and charge stabilization processes.

The decay associated spectra for the grana core fraction BS are shown in **Figure 2.3**. Four components were required for the best possible fit of the data. Lifetimes of the three fastest decay components (τ_1=130 ps, τ_2= 280 ps and τ_3= 530 ps) increased upon closure of PSII reaction centers (data not shown) and all of them had similar spectra. We assigned these components to open PSII reaction centers. The fourth minor component with the lifetime τ_4= 2.4 ns was assumed to originate from a small fraction of closed PSII centers and/or uncoupled LHCII complexes. A similar component was observable in all of the fractions. Global analysis of the BS fraction generated decay associated spectra that lacked any identifiable PSI component, exemplifying the dearth of PSI complexes in the core of the grana stack.

Decay associated spectra of the whole grana (**Figure 2.4**) were quite similar to the grana core; with triphasic (τ_1=120 ps, τ_2= 270 ps and τ_3= 510 ps) PSII kinetics and a minor τ_4= 2.0 ns component. However, the shape of the spectra of the fastest decay component was altered when compared with the BS fraction. In the B3 fraction the 120 ps component showed an elevated amplitude at both 700 nm and particularly at 720 nm. This indicated a contribution from PSI convolved with the fast component of PSII, attesting to a relative increase in the amount of PSI present when compared to the BS fraction. The contribution of PSI fluorescence to the fast decay phase was fairly small and virtually absent at wavelengths shorter than 700 nm. Decay kinetics of both grana fractions were found to be similar to the decay kinetics of BBY particles reported recently (*22*).

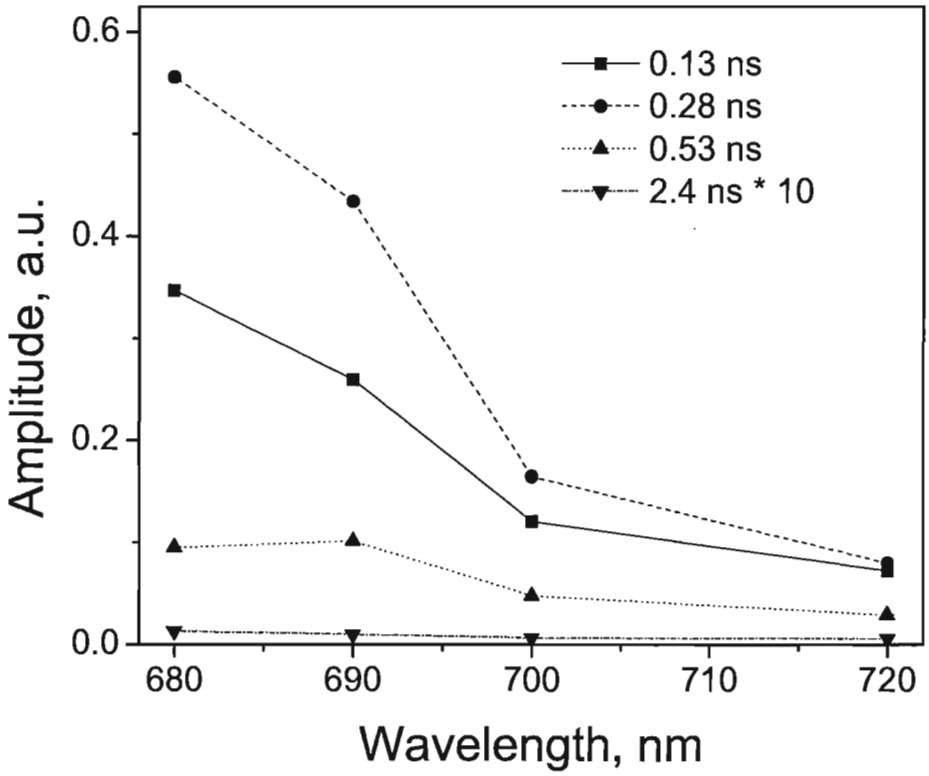

Figure 2.3. Decay-associated fluorescence emission spectra obtained from global analysis of picosecond fluorescent decay kinetics from. the grana core fraction BS. See materials and methods for details.

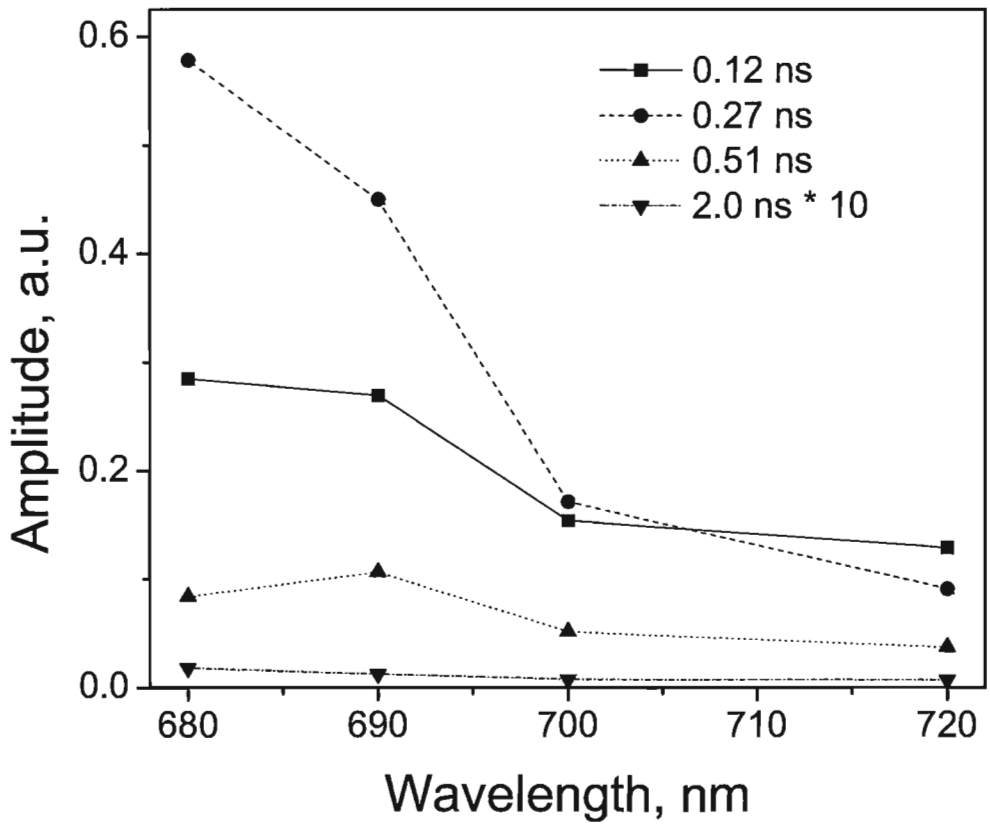

Figure 2.4. Decay-associated fluorescence emission spectra obtained from global analysis of picosecond fluorescent decay kinetics from the grana fraction B3. See Materials and Methods for details.

Fluorescence decay kinetics of the margins of grana stacks were more complex than the kinetics of grana fractions (**Figure 2.5**). Along with four components with lifetimes similar to corresponding components found in the grana fractions an extra component with a lifetime τ_5=60 ps was required to describe the data. The amplitude and lifetime of this component were unaffected by the closure of PSII reaction centers, suggesting an origin in PSI. The red shifted fluorescence emission peak of the 60 ps component was also indicative of PSI emission. A similar component was also observed in the decay kinetics of isolated PSI-200 particles (*40*). Thus, the 60 ps decay component of margins was assigned to PSI. This component was therefore shared and held constant in the global analysis of F_0 and F_M data. As was observed for grana fractions, the lifetimes of three of the decay components (τ_1=120 ps, τ_2= 260 ps and τ_3= 580 ps) increased upon closure of PSII reaction centers (data not shown), indicating their origins in PSII. However, the spectral shape of the τ_1=120 ps component exhibited an even greater bias toward emission at 720 nm as compared to the B3 fraction, indicating that this PSII component is mixed with PSI emission. Considering the emergence of the 60 ps PSI component and the change in shape of the PSII fast component; the relative proportion of PSI complexes clearly increases in margins compared to the whole grana. The two slow components of PSII were also apparent (τ_2=260 ps and τ_3=580 ps), with τ_3=580 ps exhibiting a relatively increased amplitude as compared to the BS and B3 fractions. This indicates that the mean lifetime of PSII decay kinetics in the grana margins was slower than in the other grana fractions. The slow 2.3 ns component also showed a significantly larger amplitude in the margins than in either the BS or B3 fractions. This could be indicative of an increase in the amount of uncoupled antenna.

Five components were also required to fit fluorescence decay kinetics of the stroma T3 fraction, similar to the case of margins (**Figure 2.6**). Based on results from steady state

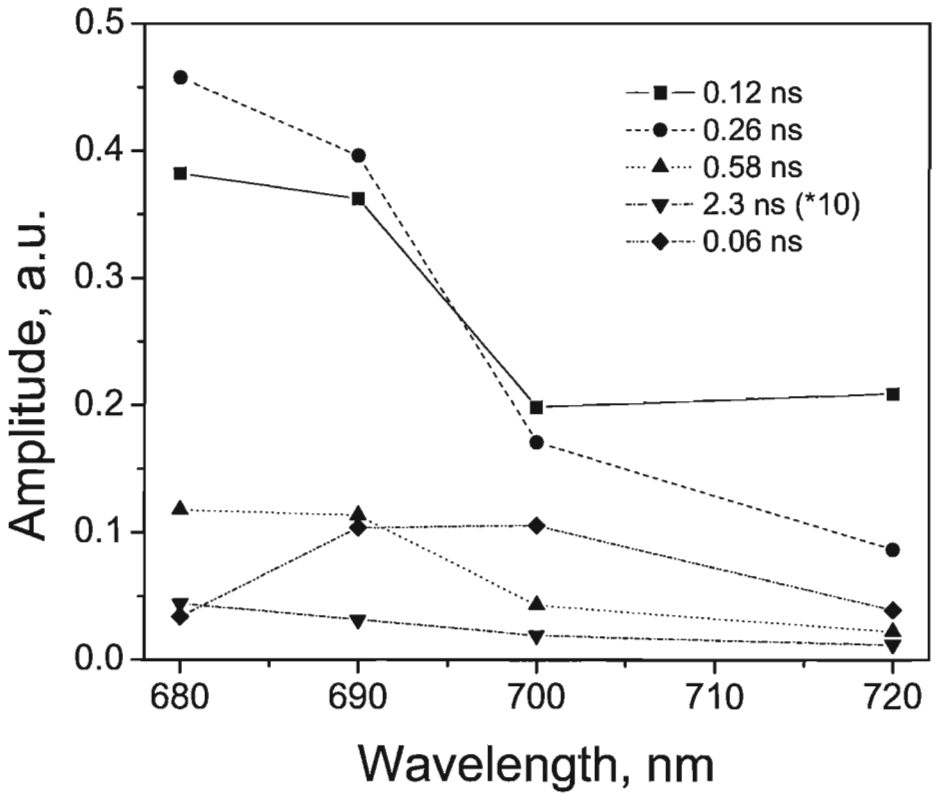

Figure 2.5. Decay-associated fluorescence emission spectra obtained from global analysis of picosecond fluorescent decay kinetics from the grana margin fraction.

spectroscopy **(Figure 2.1)** we expected this fraction to contain more PSI reaction centers. As anticipated, the contribution of PSI to the fluorescence decay was larger, thus allowing us to identify two distinct PSI decay components with lifetimes τ_5=60 ps and τ_1=120 ps. The 120 ps component had a similar lifetime to the PSII fast component from the grana fractions but its spectral shape was clearly indicative of PSI emission. Similar to what was observed for the 60 ps component, the 120 ps component showed no changes upon closure of PSII reaction centers. In our global analysis we, therefore, linked these two PSI components between the F_0 and F_M data sets through both amplitude and lifetime. Both the spectral shapes and relative amplitudes of the 60 ps and 120 ps components that emerged from fit of our data were very similar to the PSI decay components observed in isolated PSI-LHCI particles (*27;40;41*). The contribution of the PSI components confirmed an increased preponderance of PSI in the stroma lamellae as compared to the margins of the grana stack as seen in the fluorescence emission and absorption spectra **(Figures 2.1, 2.2)**. The triphasic PSII decay kinetics observed in the grana fractions and grana margins were not present in the T3 stroma fraction. Only two decay components were found to be sensitive to trap closure and they had lifetimes of 260 ps and 570 ps. Although a small amount of a fast 120 ps PSII component may have been mixed with the trap closure insensitive 120 ps PSI decay component, its relative amplitude, as compared to the two slow PSII decay kinetics, would be much smaller than that observed in the grana fractions. PSII decay kinetics are clearly different and much slower in the T3 stroma membrane fraction than in the grana or grana margin fractions. The contribution of the very slow 2.6 ns component to the fluorescence decay of T3 particles was larger than in grana fractions but similar to grana margins which may be indicative of more energetically uncoupled Chls in these regions.

The Y100 fraction, representing the purified stroma lamellae, showed the same two PSI

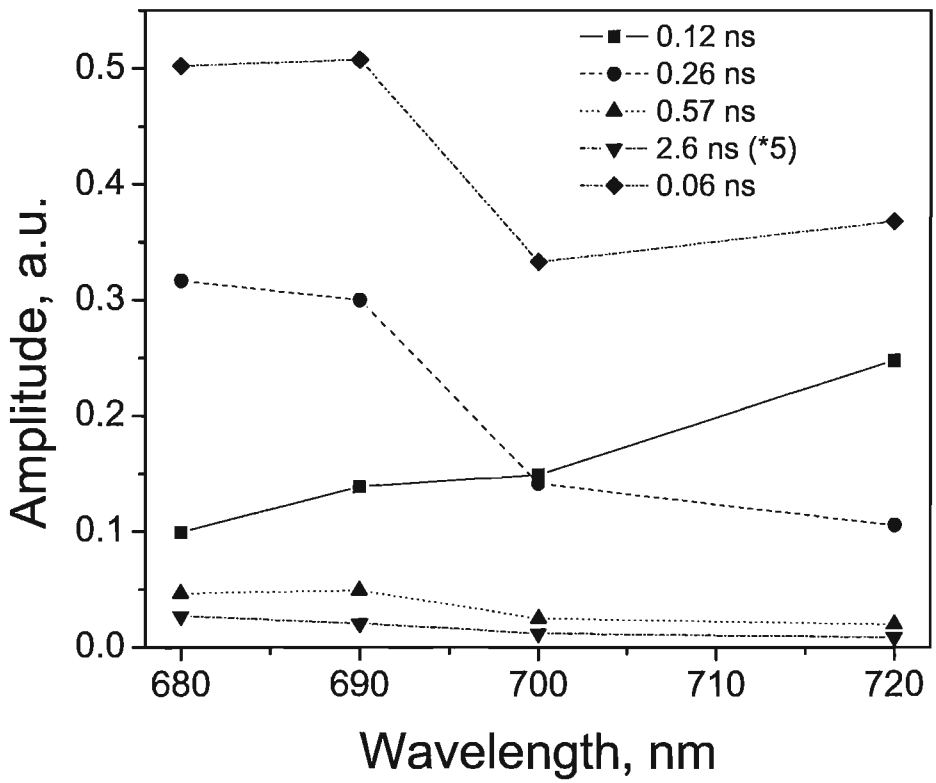

Figure 2.6. Decay-associated fluorescence emission spectra obtained from global analysis of picosecond fluorescent decay kinetics from the stroma thylakoid membrane fraction T3. See materials and methods for details.

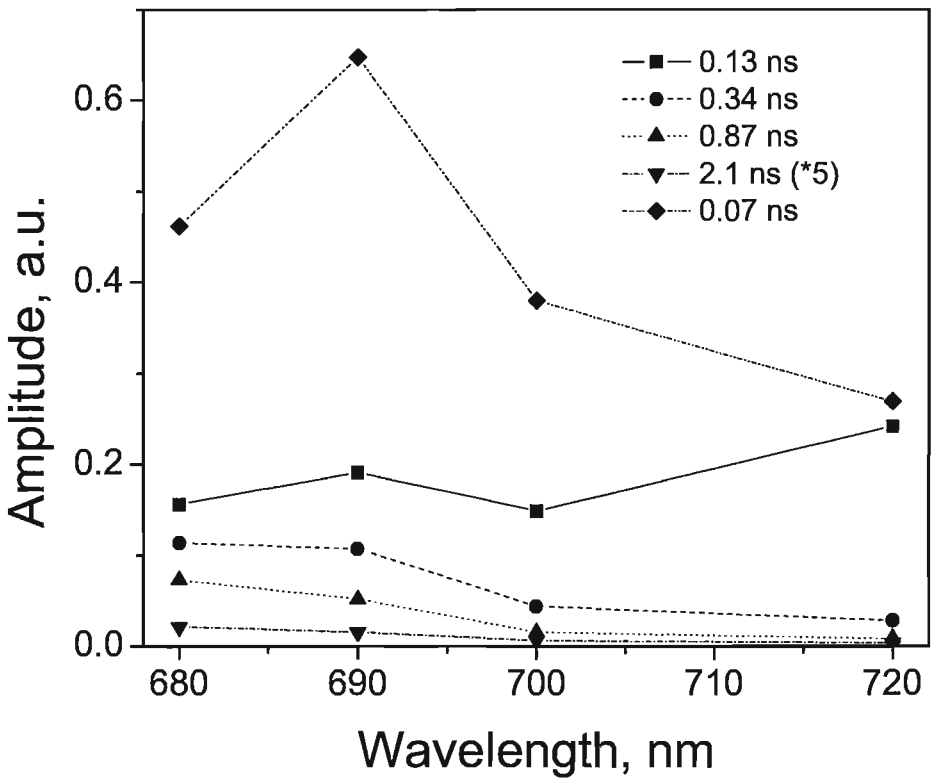

Figure 2.7. Decay-associated fluorescence emission spectra obtained from global analysis of picosecond fluorescent decay kinetics from. the purified stroma fraction Y100. See materials and methods for details.

components as observed in the T3 stroma lamellae (**Figure 2.7**). The spectral shapes, relative amplitudes and lifetimes of these two components are very similar in both fractions and also to those previously determined in isolated PSI-LHCI particles (*27;40;41*). As found for the T3 fraction, the PSII decay kinetics in the Y100 fraction showed no evidence of a fast decay component. The two PSII associated decay components did, however, have even slower lifetimes, 340 ps and 870 ps, The very slow component was of similar amplitude to that observed in the T3 stroma lamellae. The Y100 fraction was thus characterized by significantly slower PSII decay kinetics as compared to the T3 fraction. The Y100 fraction also showed an increased contribution from PSI components, attesting to the increase in proportion of PSI complexes in the Y100 fraction. The analysis of this fraction completed the survey of PSI and PSII in the fractions; confirmed the increase in the PSI population, and revealed a slowing down of PSII kinetics when the sample origin moved from grana to stroma. In addition, the slower biphasic kinetics of PSII complexes in the stroma sharply contrasted with the triphasic kinetics in the grana supporting the idea of fundamentally different PSII populations in the grana as compared to the stroma with respect to charge separation and stabilization.

PSII kinetic modeling. The global analysis of the fluorescence decay kinetics revealed considerable differences in the decay components associated with PSII. Previous studies have shown that the migration time of excitation through the antennae complexes associated with PSII likely contribute to the overall fluorescent decay measured (*22;42;43*). Thus, differences in PSII fluorescence decay kinetics can originate from different auxiliary PSII antenna and/or differences in the rates of charge separation in PSII. Since the measured differences in PSII antennae size were considerable between the grana and stroma derived fractions, a recently

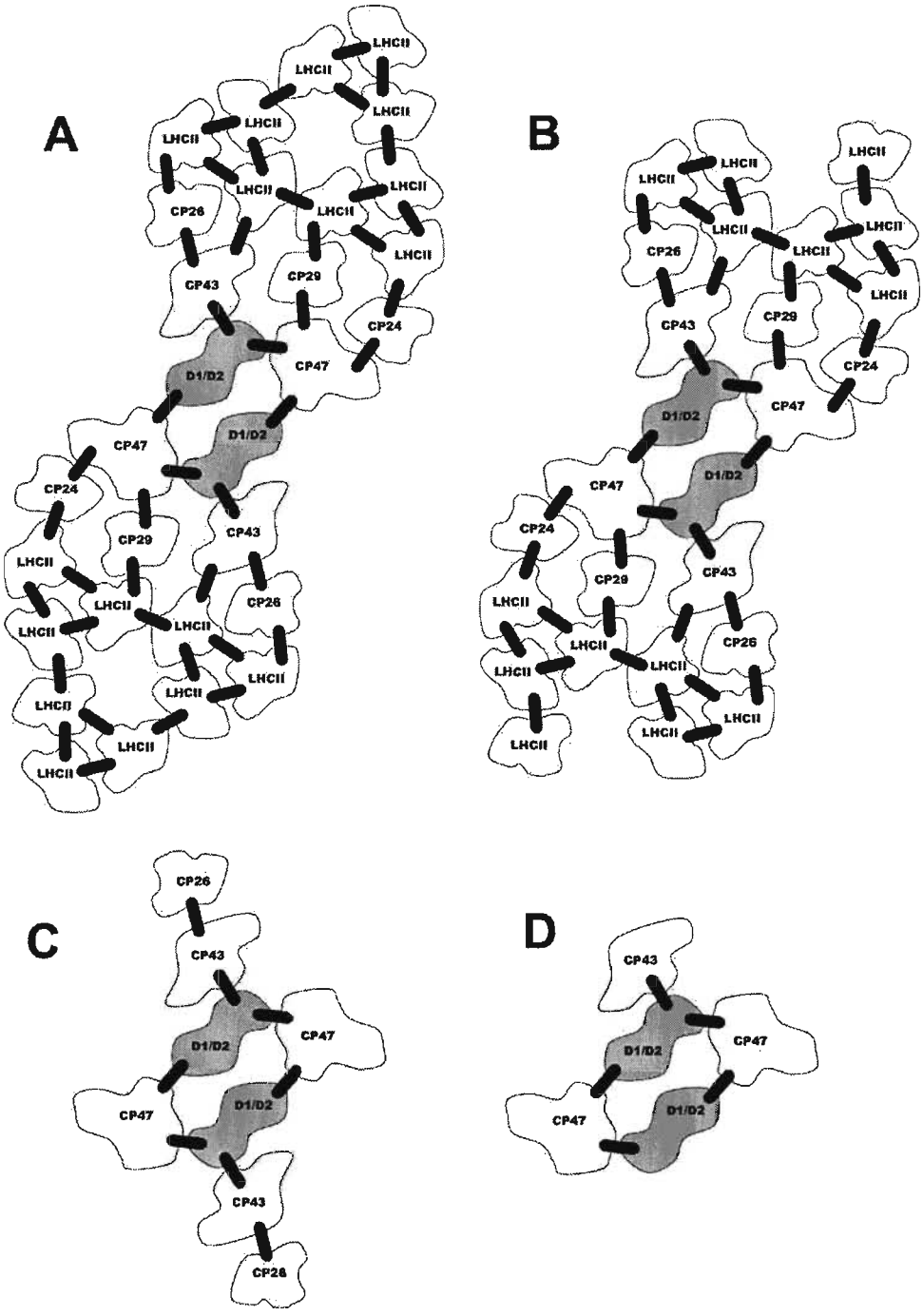

Figure 2.8. Schematic of PSII antennae size and connectivity between antennae compartments in the BS(A), B3(B), Margins(C) and T3/Y100(D) thylakoid fractions used in the kinetic model of PSII. Excitation transfer pathways are represented by the bars connecting compartments. isolated LHCII trimers (*42*).

introduced kinetic model (*22*), which could account for the antennae size differences, was used to model PSII decay kinetics.

The mean number of chlorophylls in the kinetic models for each PSII population was assigned as described above in the "PSII absorbance cross-sections" section. The resulting models are shown in **Figure 2.8**. In modeling of these "coarse-grained" representations of the PSII antennae system we assumed a uniform migration time of $(17\ ps)^{-1}$ between all compartments. This value of inter-compartment transfer time has been shown to describe BBY fluorescence decay kinetics within the context of this model (*22*) and is similar to the experimental value observed for excitation equilibration time in.

The kinetic model used in our study is approximate, we do not expect to determine absolute values for charge separation rates with high accuracy. Nevertheless it is useful to compare results of our analysis of the kinetics with previous studies of isolated RC, PSII cores and BBY particles. The rate of Q_A reduction in our fractions varies from $(243\ ps)^{-1}$ in margins to $(590\ ps)^{-1}$ in Y100. Holzwarth, et.al. (*44*) reported $(350\ ps)^{-1}$ for PSII core complexes. We found the same value in the grana core fraction, **Table 2.3**. The free energy difference between the RC excited state and the radical pair is 1036 cm^{-1} for grana core fraction. Broess et al. (*22*) reported 2380 cm^{-1} for BBY preparations while in another study free energy difference between RC excited state and second radical pair was 930 cm^{-1} for PSII cores (*44*). Our estimation of the rate of charge separation in the grana core $(2.5\ ps)^{-1}$ is between the rate determined in (*22*) for BBY preparations $(1.25\ ps)^{-1}$ and the rate of charge separation determined by Holzwarth et al. (*44*) $(5.5\ ps)^{-1}$ for PSII cores and isolated reactions centers. We have observed that when the size of antenna is close to the size of PSII antenna in the grana stack, the model becomes transfer to the trap limited, kinetics become insensitive to increase of K_{CS} and alternative fits with higher K_{CS}

Table 2.3. Photochemical rate constants and Q_A reduction efficiency in each fraction as determined via kinetic modeling.

Fraction	K_{CS}, ns^{-1}	ΔG, cm^{-1} [A]	K_{ST}, ns^{-1}	*Efficiency of charge stabilization, (%)* [B]
BS	403	1036	2.82	92.8
B3	143	894	4.11	90.4
Ma	33.8	690	3.46	73.2
T3	13.1	807	3.06	65.6
Y100	7.7	597	1.7	49.6

[A] - Free energy difference between the excited state of the RC and the radical pair was calculated from the forward and backward rates of electron transfer. [B] - To characterize changes in efficiency of the reaction centers independently of the antenna size the number of pigments in the BS fraction was used for calculation in all fractions.

are possible. Thus, our analysis of the grana core fraction representing active PSII revealed reasonable charge separation rates comparable with previous studies.

The rate constants for charge separation obtained by fitting fluorescence decay kinetics with the model are shown in **Table 2.3**. The results show a stark decrease in the rate of primary charge separation (K_{CS}) and photosynthetic yield characterizing the differences observed when moving from grana to stroma. The free energy difference
between the excited state of RC and the radical pair also shows a similar trend while charge stabilization (K_{ST}) shows a modest relative increase in the Margins, T3 and B3 fractions as compared to BS. This increase in K_{ST} may be attributable to alternate forms of electron transfer and will be dealt with in the discussion section in more detail.

The modeling results indicate that vast differences in PSII charge separation and by extension photosynthetic efficiency exist between the grana and stroma derived fractions. These results suggest that the grana core represents the only compartment in the thylakoid membrane with a highly functional PSII population, with the grana margins containing relatively inactive PSII while the stroma and Y-100 fractions contain PSII populations that are severely limited with respect to charge separation. If the relative antennae size of each PSII population is considered, the margins of the grana stack and stroma lamellae represent areas where the PSII population would provide a negligible contribution to overall photochemistry in the chloroplast.

DISCUSSION

Our low temperature steady state absorbance and fluorescence emission spectra are consistent with previous work describing the heterogeneous distribution of PSII and PSI within the thylakoid membrane (*11;14;45*). We found, as expected, a substantial increase in PSI

associated long wavelength absorbance and emission peaks and decrease in PSII associated short wavelength absorbance and emission peaks in the T3 and Y100 stroma membrane regions as compared to the B3 and BS grana fractions . Absorbance and fluorescence spectra of the grana margins appeared to be intermediate in character between the spectra of grana and stroma membrane regions. These results are consistent with previous characterizations of the isolated fractions by room temperature fluorescence induction, EPR spectroscopy and pigment analysis (*13;14*)

We addressed the question of activity differences between PSII centers originating in different thylakoid regions by measuring the functional absorbance cross-sections and picosecond fluorescence decay kinetics of the fractions. Our single turnover flash saturation measurements determine the functional absorbance cross-section of PSII centers that are competent to undergo charge separation, reduce Q_A and generate variable fluorescence. Our results show the PSII population in the whole grana and grana core fractions to have the largest absorbance cross-sections. This is an expected result due to the clear association of PSII with LHCII in the grana (*7;9;46;47*). In contrast, PSII cross-sections in the grana margins and stroma thylakoid membranes (T3 fraction) were considerably smaller. The decrease in functional antennae size in both margins and stroma regions was more than threefold compared to the grana core consistent with a large scale dissociation of LHCII from PSII in the grana margins and in the stroma membrane regions. These results are consistent with recent models for PSII repair processes which propose the stripping off of LHCII as photodamaged PSII complexes leave the grana stacks for repair in the stroma membrane regions (*48*). However, when we attempted to model the decrease in antenna size of PSII between the grana core and margins and stroma membrane fractions based on recent proteomics data for the membrane fractions (*18*); it could

not match the experimental result unless we assumed that the PSII-LHCII supercomplexes had a much larger antenna size (253 Chls per reaction center) than the largest isolated PSII-LHCII supercomplexes would be predicted to have (169 Chl per reaction center). A significant amount of "free" LHCII, existing as both trimers and monomers, is ubiquitous in non-denaturing gels of grana thylakoids (*47;48*), and a recent proteomic study of the different thylakoid membrane fractions also showed a significant amount of "free" LHCII in the grana core fraction as well as in the margin and stroma fractions (*18*). Early studies calculated an effective antenna size for PSII in the grana of approximately 253 Chls per reaction center based on the assumption that all of the LHCII present was energetically coupled to all of the PSII centers (*37-39*). Our absorbance cross section data is thus strong evidence that the "free" LHCII monomers and trimers observed in proteomic studies are functionally energetically connected to PSII in the grana cores, but not in the margins or stroma membrane regions.

The measured absorbance cross section of PSII in the Y100 fraction of the stroma lamellae was significantly smaller than for PSII in the margins or overall stroma membrane regions. This result was not predicted from the calculated absorbance cross-sections based on the heterogeneity of PSII observed in the stroma and Y100 fractions (*18*). Until recently, the most highly disassembled type of PSII that could be observed using proteomics methods in the stroma lamellae had been identified as CP43-less PSII monomers (*47;48*). Recent work has shown that D1/D2 reaction centers are also found in stroma lamellae and Y100 fractions (*18*). The preponderance of disassembled PSII's (CP43-less PSII cores and PSII reaction centers) found in the Y100 fraction (*18*) is consistent with the idea that disassembly of the PSII core for purpose of repair may occur in the Y100 fraction. It has been previously shown that PSII repair specifically requires the removal of CP43 to allow access to the D1 protein subunit for removal and

replacement (*47*); the physical reasons for this can be readily observed by considering the crystal structure of the PSII complex (*3;4*). Although additional patterns of PSII disassembly may occur during the repair cycle in order to facilitate the replacement of D2, psbH ,CP-47, CP-43 and even the entire PSII complex via degradation and *de novo* synthesis; the majority of PSII repair involves D1 replacement (*47;49*). The smaller than expected cross-section of PSII found in the Y-100 fraction may arise from some form of additional excitation energy quenching in this fraction.

The PSII population in the core of the grana stack was characterized by triphasic fluorescence decay kinetics with lifetimes, relative amplitudes and spectral shapes very similar to those of isolated BBY particles (*22*). There were no detectable PSI decay kinetics in this fraction. The grana margins exhibited noticeably slower PSII kinetics (larger contribution of slower decay components) as compared to the grana core and whole grana fractions. Slower PSII decay kinetics can result from increases in the antenna size as exemplified by recent model studies of PSII-LHCII (*22*). However, the PSII population in the margins had a much smaller antenna size than the PSII from the grana core so the slower decay kinetics must reflect changes in charge separation and/or stabilization in the PSII reaction center. Our data thus indicate a decline in the primary electron transport capability of PSII in the grana margins; a finding corroborated by a previous study showing that both donor and acceptor side electron transport in PSII is impaired in the margins of the grana stack (*14*). In the stroma derived fractions, the PSII-associated fast decay component is missing entirely and the remaining slow biphasic decay kinetics of PSII signify a drastic change in function, indicating a significant alteration of primary photochemistry. The slow biphasic decay we observe may be a characteristic of an over-riding mechanism responsible for inactivation of PSII in the stroma lamellae as part of the PSII repair process.

Such an inactivation has been proposed to be due to disassembly of the manganese cluster (*13;14*); with eventual near total loss of the cluster in the Y100 fraction. Supporting this idea was the fact that the Y100 fraction exhibited even slower PSII decay kinetics than the stroma lamellae.

The differences observed in the kinetic modeling were pronounced; the difference between grana and stroma derived PSII populations K_{CS} was approximately 30 times, while a previous study on whole thylakoids determined the difference to be about 2.5 times (*23*). This disparity illustrates the utility of isolating fractions from each compartment; as the domination of the whole thylakoid PSII population by PSII originating in the grana core (**Table 3**) and the heterogeneity of PSII in whole thylakoids complicate the assignment of PSII components. In the case of the Y100 fraction, which only represents 1% of the total PSII population; observation of this compartment would be nearly impossible in whole thylakoids. In our measurements, the grana margins were the most complicated, due to the emergence of PSI components and the heterogeneity of the PSII population (*18*). As such, it should be noted that the modeling of the grana margins and to some extent the whole grana; which includes a considerable margin fraction, should be examined with some reservation. However, the rate constants and efficiency of the grana margins remain reasonable as previous studies show the compartment as containing a PSII population with intermediate electron transfer facility (*13;14*). In the case of the stroma derived fractions, PSII assignment of decay components appears critical since the proportion of PSII decreases and the emergence of a possible PSII/PSI composite component in the 100 ps range. However, we did model this possibility in the Y100 fraction; a reasonable assignment of 20% of identified PSI components to PSII in our modeling yielded a K_{CS} of 23 and efficiency of 62%; while assigning all fast decay to PSII in the Y100 fraction yielded a K_{CS} of only 41 and an

efficiency of 74%. Considering this, our assignment of a low amplitude fast component to PSI in the margins, although reasonable, had a nominal effect on the modeling results. As stated in the results section, the K_{ST} was elevated in the B3, margins and T3 as compared to the BS fraction. This increase in stabilization rate may represent the loss of excitation through unconventional channels, as the margins represent the beginning of PSII assembly and inactivation in the repair cycle (*13;14*).

In summary, our data shows that PSII centers capable of generating variable fluorescence are only functionally connected to peripheral antenna within the core of the grana stacks and primary electron transport is highly modified in PSII centers found in the stroma membrane regions. Specifically, decreased primary charge separation, decreased free energy difference between the excited state of the RC and the radical pair, and decreased overall photosynthetic efficiency characterize the PSII population in the grana margins and stroma lamellae. The heterogeneity in PSII absorbance cross-sections and primary PSII activity of the thylakoid membrane fractions we observed supports existing models of compartmentalized PSII repair in chloroplast thylakoid membranes (*14;47;48*).

References

1. Schubert, W.-D., Klukas, O., Krauß, N., Saenger, W., Fromme, P., and Witt, H.-T. (1997) Photosystem I of Synechococcus elongatus at 4 angstrom resolution: Comprehensive structure analysis *J. Mol. Biol. 272*, 741-769.

2. Jordan, P., Fromme, P., Witt, H.-T., Klukas, O., Saenger, W., and Krauß, N. (2001) Three-dimensional structure of cyanobacterial photosystem I at 2.5 Å resolution *Nature 411*, 909-917.

3. Ferreira, K. N., Iverson, T. M., Maghlaoui, K., Barber, J., and Iwata, S. (2004) Architecture of the photosynthetic oxygen-evolving center *Science 303*, 1831-1838.

4. Kern, J., Loll, B., Zouni, A., Saenger, W., Irrgang, K. D., and Biesiadka, J. (2005) Cyanobacterial Photosystem II at 3.2 angstrom resolution - the plastoquinone binding pockets *Photosynth. Res. 84*, 153-159.

5. Ben Shem, A., Frolow, F., and Nelson, N. (2003) Crystal structure of plant photosystem I *Nature 426*, 630-635.

6. Jolley, C., Ben Shem, A., Nelson, N., and Fromme, P. (2005) Structure of plant photosystem I revealed by theoretical modeling *Journal of Biological Chemistry 280*, 33627-33636.

7. Nield, J., Orlova, E. V., Morris, E. P., Gowen, B., van Heel, M., and Barber, J. (2000) 3D map of the plant photosystem II supercomplex obtained by cryoelectron microscopy and single particle analysis *Nature struct. biol. 7*, 44-47.

8. Barber, J. (2002) Photosystem II: a multisubunit membrane protein that oxidises water *Current Opinion in Structural Biology 12*, 523-530.

9. Dekker, J. P. and Boekema, E. J. (2005) Supramolecular organization of thylakoid membrane proteins in green plants *Biochimica et Biophysica Acta-Bioenergetics 1706*, 12-39.

10. Anderson, J. M. (2002) Changing concepts about the distribution of Photosystems I and II between grana-appressed and stroma-exposed thylakoid membranes *Photosynth. Res. 73*, 157-164.

11. Andersson, B. and Anderson, J. M. (1980) Lateral Heterogeneity in the Distribution of Chlorophyll-Protein Complexes of the Thylakoid Membranes of Spinach-Chloroplasts *Biochim. Biophys. Acta 593*, 427-440.

12. Melis, A. and Anderson, J. M. (1983) Structural and functional organization of the photosystems in spinach chloroplasts. Antenna size, relative electron-transport capacity, and chlorophyll composition *Biochim. Biophys. Acta 724*, 473-484.

13. Mamedov, F. and Styring, S. (2003) Logistics in the life cycle of Photosystem II - lateral movement in the thylakoid membrane and activation of electron transfer *Physiol. Plant. 119*, 328-336.

14. Mamedov, F., Stefansson, H., Albertsson, P. A., and Styring, S. (2000) Photosystem II in different parts of the thylakoid membrane: A functional comparison between different domains *Biochemistry 39*, 10478-10486.

15. Danielsson, R., Albertsson, P. A., Mamedov, F., and Styring, S. (2004) Quantification, of photosystem I and II in different parts of the thylakoid membrane from spinach *Biochimica et Biophysica Acta-Bioenergetics 1608*, 53-61.

16. Albertsson, P.-Å., Andréasson, E., Stefansson, H., and Wollenberger, L. (1986) Fractionation of thylakoid membrane *Methods Enzymol 228*, 469-482.

17. Kanervo, E., Suorsa, M., and Aro, E. M. (2005) Functional flexibility and acclimation of the thylakoid membrane *Photochemical & Photobiological Sciences 4*, 1072-1080.

18. Danielsson, R., Suorsa, M., Paakkarinen, V., Albertsson, P. A., Styring, S., Aro, E. M., and Mamedov, F. (2006) Dimeric and monomeric organization of photosystem II - Distribution of five distinct complexes in the different domains of the thylakoid membrane *Journal of Biological Chemistry 281*, 14241-14249.

19. Byrdin, M., Jordan, P., Krauss, N., Fromme, P., Stehlik, D., and Schlodder, E. (2002) Light harvesting in photosystem I: Modeling based on the 2.5-angstrom structure of photosystem I from Synechococcus elongatus *Biophys. J. 83*, 433-457.

20. Sener, M. K., Jolley, C., Ben Shem, A., Fromme, P., Nelson, N., Croce, R., and Schulten, K. (2005) Comparison of the light-harvesting networks of plant and cyanobacterial photosystem I *Biophys. J. 89*, 1630-1642.

21. Miloslavina, Y., Szczepaniak, M., Muller, M. G., Sander, J., Nowaczyk, M., Rogner, M., and Holzwarth, A. R. (2006) Charge separation kinetics in intact photosystem II core particles is trap-limited. A picosecond fluorescence study *Biochemistry 45*, 2436-2442.

22. Broess, K., Trinkunas, G., van der Weij - de Witt, C., Dekker, J. P., van Hoek, A., and van Amerongen, H. (2006) Excitation energy transfer and charge separation in photosystem II membranes *Biophys. J. doi:10.1529/biophysj.106.085068.*

23. Roelofs, T. A., Lee, C.-H., and Holzwarth, A. R. (1992) Global target analysis of picosecond chlorophyll fluorescence kinetics from pea chloroplasts *Biophys. J. 61*, 1147-1163.

24. Holzwarth, A. R. and Roelofs, T. A. (1992) Recent advances in the understanding of chlorophyll excited- state dynamics in thylakoid membranes and isolated reaction center complexes *J. Photochem. Photobiol. B-Biol. 15*, 45-62.

25. Wagner, B., Goss, R., Richter, M., Wild, A., and Holzwarth, A. R. (1996) Picosecond time-resolved study on the nature of high-energy-state quenching in isolated pea thylakoids - Different localization of zeaxanthin dependent and independent quenching mechanisms *J. Photochem. Photobiol. B-Biol. 36*, 339-350.

26. Richter, M., Goss, R., Wagner, B., and Holzwarth, A. R. (1999) Characterization of the fast and slow reversible components of non-photochemical quenching in isolated pea thylakoids by picosecond time-resolved chlorophyll fluorescence analysis *Biochemistry 38*, 12718-12726.

27. Croce, R., Dorra, D., Holzwarth, A. R., and Jennings, R. C. (2000) Fluorescence decay and spectral evolution in intact photosystem I of higher plants *Biochemistry 39*, 6341-6348.

28. Vasil'ev, S., Lee, C.-I., Brudvig, G. W., and Bruce, D. (2002) Structure-based kinetic modeling of excited-state transfer and trapping in His-tagged PSII core complexes from *Synechocystis. Biochemistry 41*, 12236-12243.

29. Mauzerall, D. and Greenbaum, N. L. (1989) The absolute size of a photosynthetic unit *Biochim. Biophys. Acta 974*, 119-140.

30. Loll, B., Kern, J., Saenger, W., Zouni, A., and Biesiadka, J. (2005) Towards complete cofactor arrangement in the 3.0 angstrom resolution structure of photosystem II *Nature 438*, 1040-1044.

31. Sandona, D., Croce, R., Pagano, A., Crimi, M., and Bassi, R. (1998) Higher plants light harvesting proteins. Structure and function as revealed by mutation analysis of either protein or chromophore moieties *Biochimica et Biophysica Acta-Bioenergetics 1365*, 207-214.

32. Liu, Z. F., Yan, H. C., Wang, K. B., Kuang, T. Y., Zhang, J. P., Gui, L. L., An, X. M., and Chang, W. R. (2004) Crystal structure of spinach major light-harvesting complex at 2.72 angstrom resolution *Nature 428*, 287-292.

33. Bruce, D. and Miners, J. (1993) Use of a pulsed laser diode to measure picosecond fluorescence lifetimes *Photochem Photobiol 58*, 464-468.

34. Vasil'ev, S., Wiebe, S., and Bruce, D. (1998) Non-photochemical quenching of chlorophyll fluorescence in photosynthesis. 5-hydroxy-1,4-naphthoquinone in spinach thylakoids as a model for antenna based quenching mechanisms *Biochim. Biophys. Acta 1363*, 147-156.

35. Vasil'ev, S. and Bruce, D. (1998) Nonphotochemical quenching of excitation energy in photosystem II. A picosecond time-resolved study of the low yield of chlorophyll *a* fluorescence induced by single-turnover flash in isolated spinach thylakoids *Biochemistry 37*, 11046-11054.

36. Boekema, E. J., van Roon, H., Calkoen, F., Bassi, R., and Dekker, J. P. (1999) Multiple types of association of photosystem II and its light-harvesting antenna in partially solubilized photosystem II membranes *Biochemistry 38*, 2233-2239.

37. Boekema, E. J., Hankamer, B., Bald, D., Kruip, J., Nield, J., Boonstra, A. F., Barber, J., and Rogner, M. (1995) Supramolecular Structure of the Photosystem-Ii Complex from Green Plants and Cyanobacteria *Proceedings of the National Academy of Sciences of the United States of America 92*, 175-179.

38. Lam, E., Baltimore, B., Ortiz, W., Chollar, S., Melis, A., and Malkin, R. (1983) Characterization of A Resolved Oxygen-Evolving Photosystem-Ii Preparation from Spinach Thylakoids *Biochim. Biophys. Acta 724*, 201-211.

39. Peter, G. F. and Thornber, J. P. (1991) Biochemical-Composition and Organization of Higher-Plant Photosystem-Ii Light-Harvesting Pigment-Proteins *Journal of Biological Chemistry 266*, 16745-16754.

40. Ihalainen, J. A., Jensen, P. E., Haldrup, A., van Stokkum, I. H. M., van Grondelle, R., Scheller, H. V., and Dekker, J. P. (2002) Pigment organization and energy transfer dynamics in isolated, photosystem I (PSI) complexes from Arabidopsis thaliana depleted of the PSI-G, PSI-K, PSI-L, or PSI-N subunit *Biophys. J. 83*, 2190-2201.

41. Melkozernov, A. N., Kargul, J., Lin, S., Barber, J., and Blankenship, R. E. (2004) Energy coupling in the PSI-LHCI supercomplex from the green alga Chlamydomonas reinhardtii *Journal of Physical Chemistry B 108*, 10547-10555.

42. Barzda, V., Gulbinas, V., Kananavicius, R., Cervinskas, V., van Amerongen, H., van Grondelle, R., and Valkunas, L. (2001) Singlet-singlet annihilation kinetics in aggregates and trimers of LHCII *Biophys. J. 80*, 2409-2421.

43. van Amerongen, H. and Dekker, J. P. (2003) Light-Harvesting in Photosystem II in *Light-Harvesting Antennas in Photosynthesis* (Green, B. R. and Parson, W. W., Eds.) pp 219-251, Kluwer Academic Publishers., Dordrecht.

44. Holzwarth, A. R., Muller, M. G., Reus, M., Nowaczyk, M., Sander, J., and Rogner, M. (2006) Kinetics and mechanism of electron transfer in intact photosystem II and in the isolated reaction center: Pheophytin is the primary electron acceptor *Proceedings of the National Academy of Sciences of the United States of America 103*, 6895-6900.

45. Albertsson, P. A. (2001) A quantitative model of the domain structure of the photosynthetic membrane *Trends in Plant Science 6*, 349-354.

46. Kerfeld, C. A., Sawaya, M. R., Brahmandam, V., Cascio, D., Ho, K. K., Trevithick-Sutton, C. C., Krogmann, D. W., and Yeates, T. O. (2003) The crystal structure of a cyanobacterial water-soluble carotenoid binding protein *Structure 11*, 55-65.

47. Aro, E. M., Suorsa, M., Rokka, A., Allahverdiyeva, Y., Paakkarinen, V., Saleem, A., Battchikova, N., and Rintamaki, E. (2005) Dynamics of photosystem II: a proteomic approach to thylakoid protein complexes *Journal of Experimental Botany 56*, 347-356.

48. Baena-Gonzalez, E., Barbato, R., and Aro, E. M. (1999) Role of phosphorylation in the repair cycle and oligomeric structure of photosystem II *Planta 208*, 196-204.

49. Rokka, A., Suorsa, M., Saleem, A., Battchikova, N., and Aro, E. M. (2005) Synthesis and assembly of thylakoid protein complexes: multiple assembly steps of photosystem II *Biochemical Journal 388*, 159-168.

Chapter 3: Photoprotection in the lichen, *Parmelia sulcata*. The origins of desiccation induced fluorescence quenching. *Plant Physiology* *145*, 997-1005 (2007)

John Veerman, Sergej Vasil'ev, Gavin D. Paton, Justin Ramanauskas, and Doug Bruce

Department of Biological Sciences, Brock University, 500 Glenridge Ave., St. Catharines, Ontario, L2S 3A1 Canada

This work was supported by grants from the Natural Sciences and Engineering Research Council of Canada to DB.

Corresponding author: Doug Bruce, Department of Biological Sciences, Brock University, 500 Glenridge Ave., St. Catharines, Ontario, L2S 3A1 Canada. Tel: (905) 688 5550 ex 3826, Fax: (905) 688 1855, e-mail: dbruce@brocku.ca

Preface

This chapter was published in the high impact Journal *Plant Physiology* in 2007. I wrote the first draft of this article and was heavily involved in revisions and addressing the concerns and critique of both reviewers and the editor of *Plant Physiology*.

Gavin Paton working in our lab as an undergraduate student did extensive work characterizing the desiccation response and collecting samples. Justin Ramanauskas working in our lab as an undergraduate student produced Figure 1.2. I produced all other figures, tables and illustrations and collected and analyzed the data contained therein.

It should also be noted that Professor Doug Bruce and Dr. Sergei Vasil'ev both guided me through all aspects of this research, from hypothesis formation, data collection, and analysis to writing/revising the article.

ABSTRACT

Lichens, a symbiotic relationship between a fungus (mycobiont) and a photosynthetic green algae or cyanobacteria (photobiont), belong to an elite group of survivalist organisms termed resurrection species. When lichens are desiccated they are photosynthetically inactive, but upon re-hydration they can perform photosynthesis within seconds. Desiccation is correlated with both a loss of variable chlorophyll *a* (Chl *a*) fluorescence and a decrease in overall fluorescence yield. The fluorescence quenching likely reflects photoprotection mechanisms which may be based on desiccation induced changes in lichen structure that limit light exposure to the photobiont (sunshade effect) and/or active quenching of excitation energy absorbed by the photosynthetic apparatus. To separate and quantify these possible mechanisms we have investigated the origins of fluorescence quenching in desiccated lichens with steady state, low temperature and time-resolved Chl fluorescence spectroscopy. We found the most dramatic target of quenching to be photosystem II (PSII), which produces negligible levels of fluorescence in desiccated lichens. We show that fluorescence decay in desiccated lichens was dominated by a short lifetime, long wavelength component energetically coupled to PSII. Remaining fluorescence was primarily from PSI and although diminished in amplitude, PSI decay kinetics were unaffected by desiccation. The long wavelength quenching species was responsible for most (about 80%) of the fluorescence quenching observed in desiccated lichens, the rest of the quenching was attributed to the sunshade effect induced by structural changes in the lichen thallus.

Lichens are made up of two main components: the mycobiont, or fungal portion, and the photobiont, which may be algae or cyanobacteria. The mycobiont affords protection for the photobiont which supplies energy to the mycobiont in the form of reduced carbons. Lichens can contain several different photobionts, these may be different types of green algae, cyanobacteria, or a mixture of the two (Green et al., 2002). It has, however, been observed that the green algae *Trebouxia* is the most abundant photobiont, and it is found in approximately 75% of lichenized relationships (Green et al., 2002). *Trebouxia* species have been found living outside a mycobiont, however this is rarely seen.

Lichens are poikilohydric, and can survive severe bouts of desiccation, which has profound effects on most physiological factors. This is manifested by a reduction in growth rates and reduced photosynthesis (Scheidegger et al., 1995; Bukhov, 2004). Lichens are often found growing on exposed rocks or trees, where they may face high levels of irradiation while in the desiccated state (Gauslaa and Solhaug, 1999). This is particularly problematic as it has high potential to be damaging to the photosynthetic apparatus of the photobiont under conditions where metabolic activities, including repair mechanisms, are shut down (Gauslaa and Solhaug, 1999). However, lichens are found in almost every ecological niche and thrive in extreme environments. They clearly possess the ability to survive dehydrated conditions while protecting the photosynthetic apparatus from light damage and can regain photosynthetic competency immediately upon hydration.

With water as its electron donor, photosystem II (PSII) is an obvious target of desiccation induced damage. PSII often suffers from light induced damage (Aro et al., 1993; Melis, 1999; Ohnishi et al., 2005) and even a low level of PSII activity would be hazardous when water is unavailable. PSII damage under desiccated conditions would also inhibit the recovery of lichens

upon rehydration as PSII repair requires large amounts of protein synthesis (Allakhverdiev et al., 2005) . As a result, lichens must render PSII largely inactive and/or minimize the amount of solar radiation reaching it to maximize their endurance while desiccated and their recovery upon rehydration.

PSII activity is often assessed *in vivo* by the measurement of variable Chl *a* fluorescence, which originates from active PSII reaction centers. The minimal level of fluorescence (F_0) is associated with "open" reaction centers that have an oxidized primary quinone electron acceptor (Q_A). "Closed" reaction centers, where Q_A is reduced, exhibit a maximal yield of fluorescence (F_M). Exposure of PSII to saturating light induces an increase in fluorescence from F_0 to the F_M level which is often used as a measure of PSII activity. The difference between F_M and F_0 (F_M - F_0) is called variable fluorescence (F_V).

In lichens, the desiccated state is characterized by a shutdown of photosystem II (PSII), manifested by the lack of F_V. Desiccated lichens emit a level of fluorescence much lower than F_0 of hydrated lichens. Upon exposure to water, an immediate increase in fluorescence, back to F_0, is observed, followed by a resumption of normal PSII activity as indicated by a return of F_V upon exposure to saturating light flashes (Heber et al., 2000; Green et al., 2002). This ability to resume photosynthesis almost immediately after hydration of desiccated lichens is an adaptation to their particular cycles of wetting and dehydration. These cycles have been found to occur on a daily basis in some species (Gauslaa et al., 2001). The ability to withstand exposure to light while desiccated is extremely important for these organisms.

The decrease in fluorescence emission observed in desiccated lichens is likely associated with their phototolerance and could be caused by multiple mechanisms. One mechanism occurs primarily in the fungal thallus and involves structural changes which induce

changes in light-scattering and "shading" properties. During desiccation the algae aggregate and change shape to limit exposure to light, while at the same time the lichen thallus curls to minimize the available surface area and reduce light absorbance (Scheidegger et al., 1995; de los Rios et al., 2007). The thallus also offers some protection against photodamage through the use of light absorbing pigments (Gauslaa and Solhaug, 1999; Holder et al., 2000). All of these mechanisms decrease the exposure of the photosynthetic apparatus of the photobiont to light and can be grouped as "sunshade" mechanisms.

Protection from photodamage also exists within the photobiont. Many photobionts contain the carotenoid zeaxanthin which is involved in non-photochemical quenching (Demmig-Adams and Adams, 1990; Farber et al., 1997). The existence of a zeaxanthin dependent quenching pathway in green algal containing lichens has been documented, however there is also an additional desiccation induced fluorescence quenching which is independent of zeaxanthin (Heber et al., 2001; Heber and Shuvalov, 2005; Heber et al., 2006).

Previous studies have characterized the desiccated state of lichens using steady-state spectroscopy and pulse amplitude modulated (PAM) Chl a fluorescence measurements. While these methods provide information about the relative decrease in measured fluorescence and the spectral properties of the quenched and unquenched states, they are not able to separate decreases in emission induced by changes in the structural organization and/or light scattering properties of the thallus from mechanisms of fluorescence quenching within the photosynthetic apparatus.

Based on the observation of an enhanced 720 nm fluorescence emission feature in desiccated lichens, it was previously suggested that a red-shifted form of chlorophyll acts as a putative long wavelength quencher (Heber and Shuvalov, 2005). However, long wavelength

emission can originate from a number of sources and there was no direct evidence that this particular long wavelength feature originated from a quenching species. In addition, any quantitative analysis of the contribution of various emitting species to overall emission in the hydrated and desiccated state is complicated by the pronounced changes in light-scattering properties and structural organization of the thallus.

In the present study we investigate the mechanism of fluorescence quenching in desiccated lichens using a combination of time-resolved and steady-state fluorescence spectroscopy at room and low temperatures. This approach allowed us to separate and quantify the contributions of mechanisms which serve to minimize the absorption of light by the photobiont (sunshades) from mechanisms involving the dissipation of absorbed energy by the photosynthetic apparatus of the photobiont (quenchers).

RESULTS AND DISCUSSION

PAM measurements.

A representative PAM trace of hydration is shown in **Figure 3.1**. As observed previously for other species of lichens (Bukhov, 2004; Heber et al., 2006), the room temperature fluorescence yield of desiccated *P. sulcata* (F_D) was low and there was no induction of maximal fluorescence (F_M) with saturating multiturnover flashes of light. Hydration induced a marked increase in the dark-adapted fluorescence level followed quickly by the appearance of variable fluorescence in response to saturating light flashes. Variable fluorescence appeared within a few seconds of the addition of water. Most of the hydration induced changes were complete in 10 to 15 minutes. Typically the fluorescence in desiccated lichens (F_D) was about 5 times lower than

F_0 in hydrated lichens. As discussed previously this change may arise from anatomical changes of the thallus, including changes in its light scattering properties as well as changes in excited state quenching within the photosynthetic apparatus of the photobiont.

Steady-state room temperature fluorescence spectroscopy.

Room temperature fluorescence emission spectra of *P. sulcata* are shown in **Figure 3.2**. Fluorescence spectra of desiccated samples showed an apparent PSII peak at 685 nm and a broad (720-750 nm) long wavelength emission peaking at 740 nm. Interestingly, the relative contribution of the 685 nm peak increases dramatically from its start as a relatively low amplitude shoulder in the desiccated sample to becoming the dominant peak in fully hydrated lichens. In addition, overall emission from both regions increases greatly in the sample during hydration. Similar results were reported by (Heber and Shuvalov, 2005) who identified a 720 nm emission peak in *P. sulcata* under desiccated conditions. The wavelength discrepancy may be related to the enhanced spectral response in the red region characteristic of the CCD detector used in our study.

Steady state 77 K emission spectra.

Low temperature fluorescence emission spectra allow for the observation of Chl forms associated with PSII and PSI and were determined for desiccated and hydrated samples (**Figure 3.3**). The 77 K emission spectrum of the hydrated lichen sample was similar to spectra of most green algae and shows characteristic contributions from two shoulders at 685 nm and 695 nm (PSII associated) and a peak at 720 nm (PSI associated). In desiccated lichens the overall fluorescence yield at 77 K was approximately ten times lower than in hydrated lichens and the

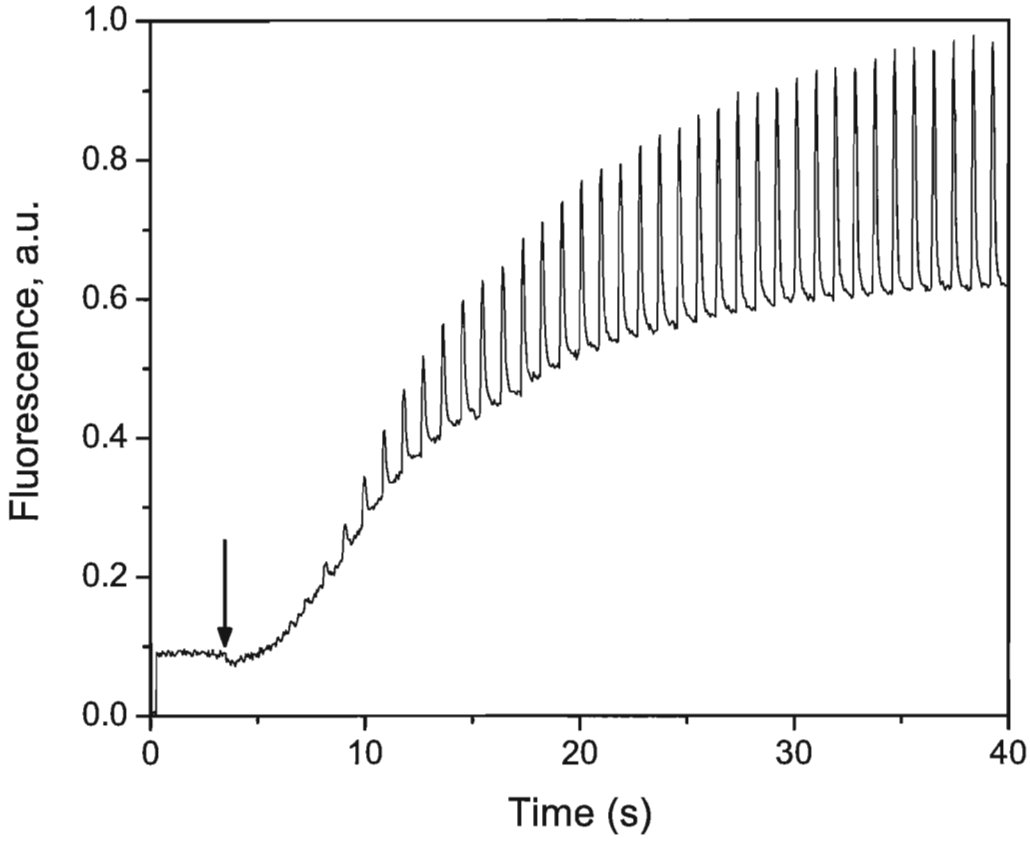

Figure 3.1. Pulse amplitude modulated (PAM) Chl *a* fluorescence kinetic trace following the hydration of a desiccated sample of *P. sulcata.* Time of addition of water is indicated by the arrow. Multiturnover saturating light flashes (50 ms duration) were delivered to the sample at a frequency of 1 Hz starting at time zero on the trace.

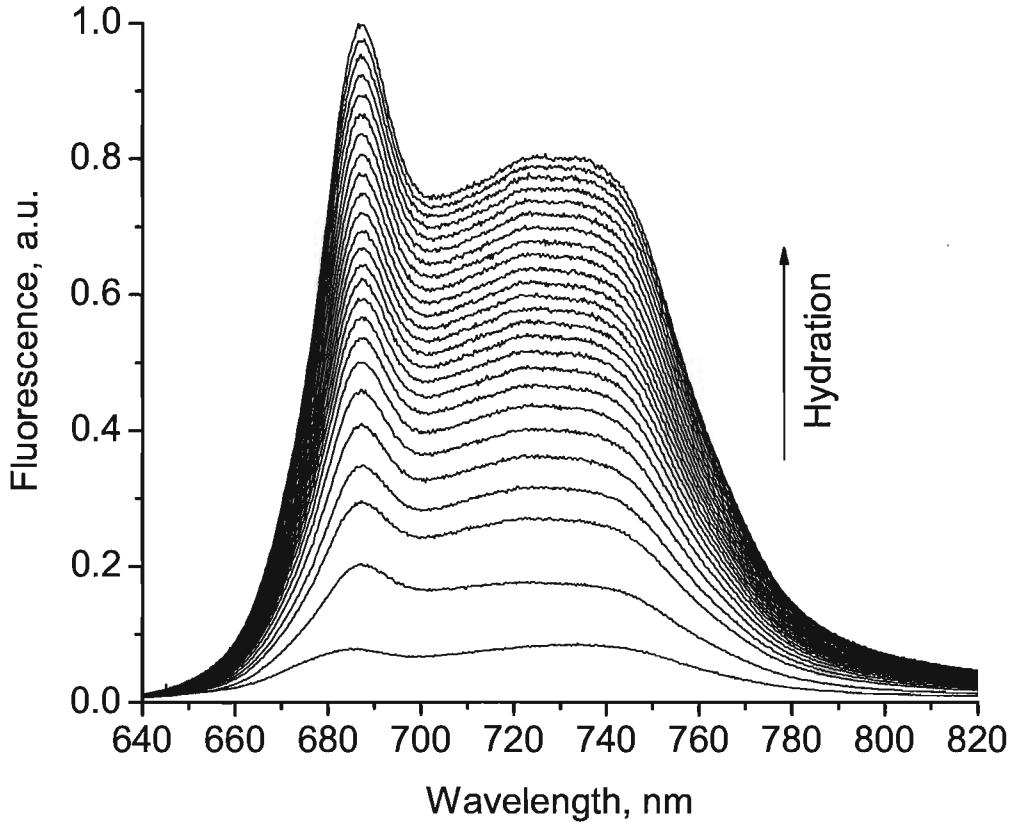

Figure 3.2. Room temperature fluorescence emission spectra measured during the hydration of desiccated *P. Sulcata*. Spectra were recorded every 15 seconds over a six minute hydration period. The excitation wavelength was 435 nm.

spectra in Figure 3 have been normalized to facilitate comparison. In desiccated lichens the contributions from PSII at 685 and 695 nm were barely discernable and the spectrum is dominated by the PSI emission at 720 nm. The longer wavelength band, peaking at 740 nm, observed at room temperature appeared largely absent from the 77 K spectra of both hydrated and desiccated samples. However, the PSI emission peak in the desiccated sample appears slightly red shifted which may indicate increased fluorescence under desiccated conditions from longer wavelength (> 720 nm) forms, as was observed for the room temperature fluorescence data. The apparently minor contribution of the long wavelength pigments to the low temperature emission spectra would be consistent with a quenching role.

Room temperature time-resolved fluorescence decay kinetics.

To obtain a better understanding of the origin of fluorescence bands observed in the steady state spectra of the lichens, we measured the picosecond fluorescence decay kinetics of desiccated and hydrated *P. sulcata* (**Figure 3.4**). Hydrated lichens show decay kinetics that are typical of green algae and higher plants at both the F_0 and F_M states. The overall decay at F_0 is much faster than at F_M reflecting efficient photochemical trapping in open PSII reaction centers. F_M decay is dominated by slow PSII components, contributed to by charge recombination in the absence of photochemistry, that are characteristic of closed reaction centers. The fluorescence kinetics are very different in desiccated lichens, and the decay at F_D is dominated by much faster decay components than are observed in hydrated samples at either F_M or F_0. This rapid decay demonstrates that a significant fraction of quenching in desiccated lichens arises from excited state lifetime shortening of pigments energetically coupled to PSII. Interestingly, the relative contribution and lifetime of a low amplitude slow decay component to the decay kinetics at both

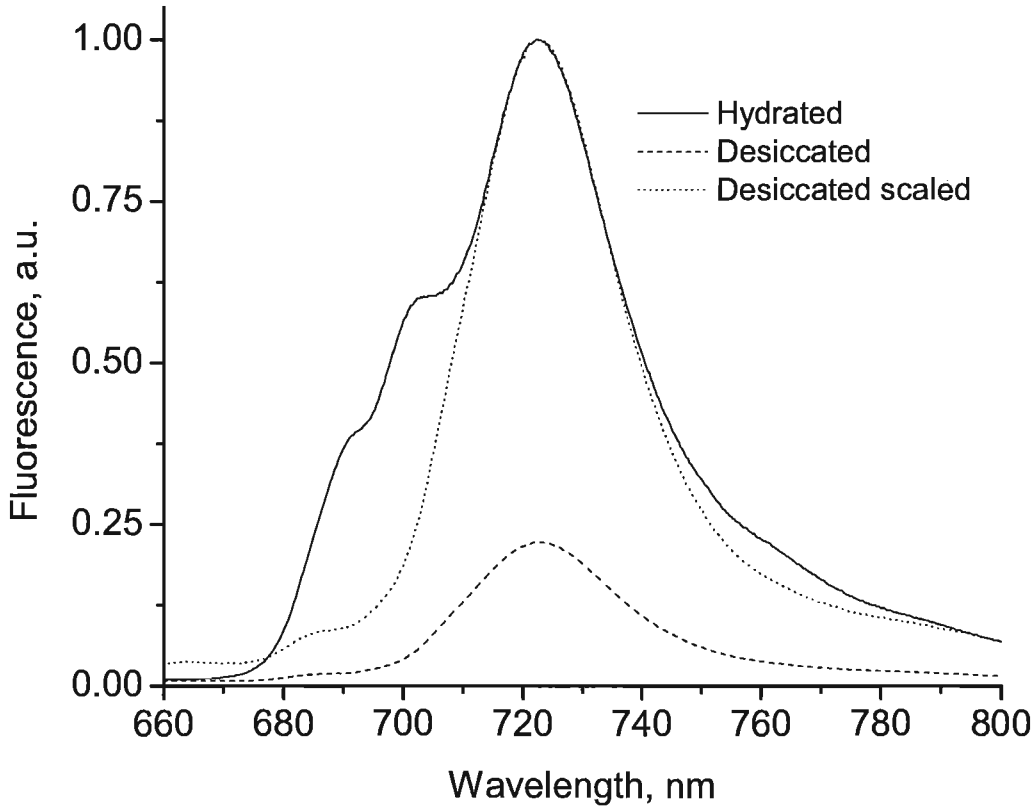

Figure 3.3. Low temperature fluorescence emission spectra of hydrated and desiccated *P. sulcata*. The spectra have been normalized to peak emission for comparison, the fluorescence yield of the desiccated sample was approximately ten times lower than the hydrated sample.

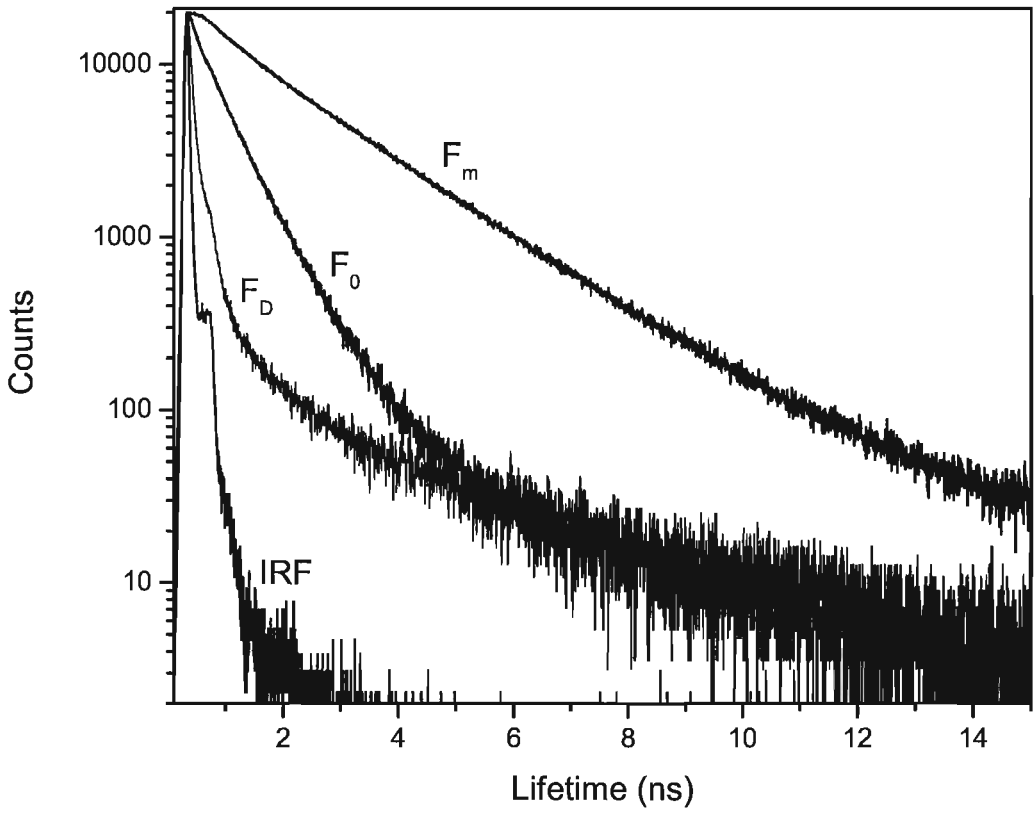

Figure 3.4. Fluorescence decay kinetics of desiccated *P. sulcata* (F_D), hydrated samples with open reaction centers (F_0) and hydrated samples with closed reaction centers (F_M) and instrument response function (IRF). Detection wavelength was 680 nm.

F_D and F_0 is the same, indicating that it originates from a small pool of pigments unaffected by quencher.

To determine the origin of components contributing to the fluorescence decay, kinetic measurements were taken at 11 emission wavelengths covering the range from 660 nm to 760 nm. The data collected at all detection wavelengths were analyzed with a model of parallel decaying compartments in order to determine the spectra of decay components and further explore the origins of desiccation induced quenching. The resulting decay associated spectra (DAS) are shown in **Figure 3.5**. Four decay components were required to describe the fluorescence decay kinetics at F_D and F_M and five at F_0 (**Figure 3.5**). Of the five components contributing to decay at F_0, the spectral shape (peaks at 720 nm and 700 nm) and lifetimes of the two fast decay components (τ_1 = 40 ps and τ_2 = 90 ps) were indicative of PSI emission. We assigned the next two slower components (τ_1 = 300 ps and τ_2 = 640 ps), which had emission peaks in the 685 nm to 690 nm region, to PSII. The last slow decay component τ_5 = 2.1 ns with very low amplitude and peak in the 685 nm to 690 nm region was assigned to a small fraction of closed PSII reaction centers and/or uncoupled antenna.

The components contributing to the decay of fluorescence at F_0 (**Figure 3.5**) had DAS in the short-wavelength range (660-700 nm) which were similar to those previously studied in the free growing green algae, *Trebouxia* which also included decay components with lifetimes of 80 ps, 300 ps, 600 ps and 2 ns (Wendler and Holzwarth, 1987). We resolved an additional short component (τ_5 = 40 ps) in the present study and assigned it to PSI. Fast decay components with similar lifetimes have been reported in recent studies of various PSI preparations from higher plants (Croce et al., 2000; Ihalainen et al., 2002; Melkozernov et al., 2004) and PSI rich

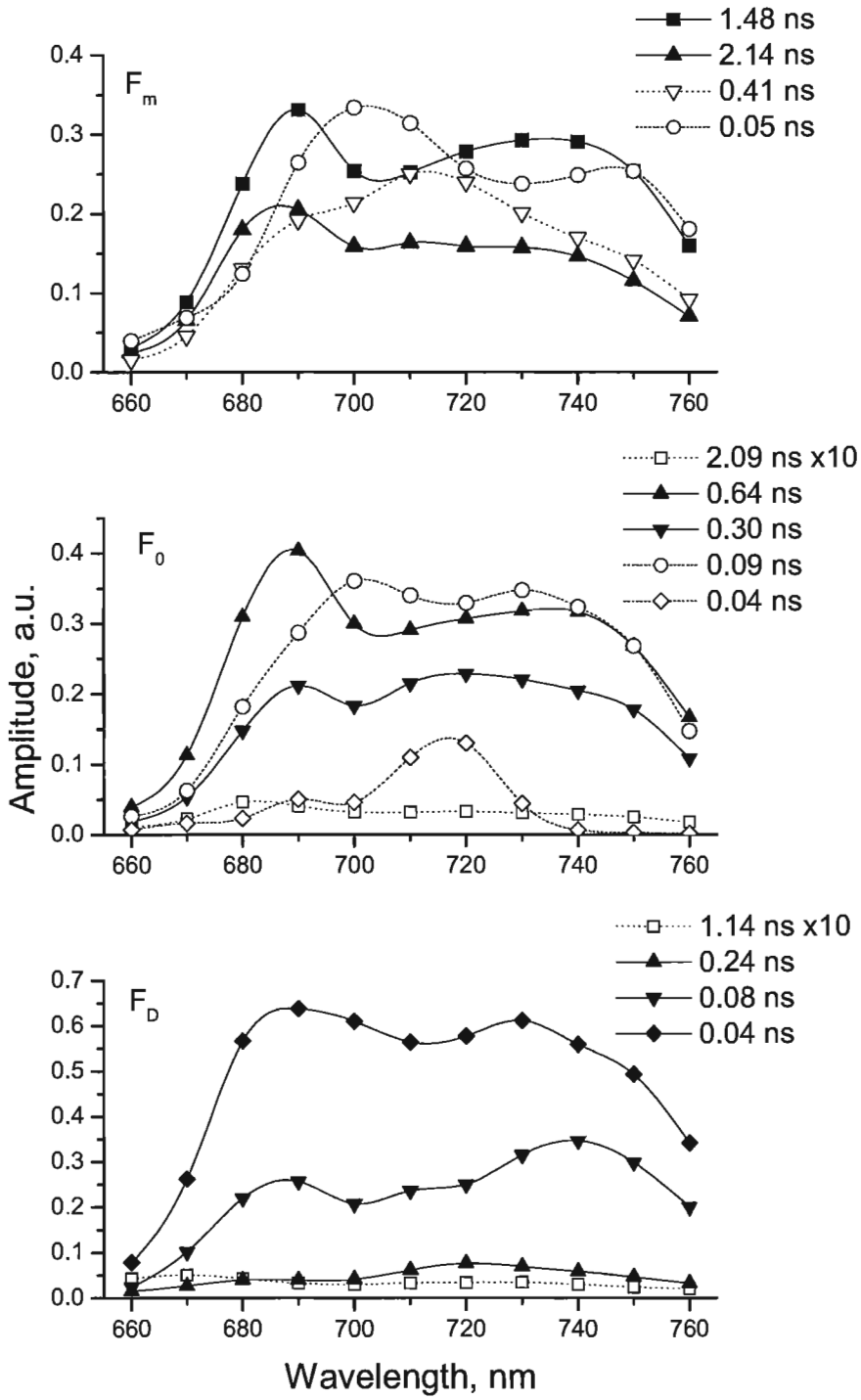

Figure 3.5. Decay-associated fluorescence emission spectra obtained from global analysis of 407 nm laser induced picosecond fluorescent decay kinetics from the lichen *P. sulcata* under desiccated conditions (F_D), hydrated conditions with open centers (F_0) and closed centers (F_m).

thylakoid membrane compartments (Veerman et al., 2007). Two distinct PSI decay components are thought to originate from the peripheral and inner PSI antenna correspondingly (Croce et al., 2000; Melkozernov et al., 2004). It is noteworthy that in all of these previous studies the amplitude of the 40 ps component was larger than the 80 ps component, indicating a larger size of the inner PSI antenna; while in *P. sulcata* it is the another way round. This observation may indicate a different organization of the peripheral PSI antenna in this organism. There are also significant differences in the spectral shapes of the 40 ps and 90 ps components which may be indicative of a mixture of PSII and PSI contributions in the 90 ps component.

Interestingly, although the DAS of the PSII components were similar to previously reported DAS in the range of 660-700 nm, they appeared to have unusual long wavelength contributions. It is well established that PSII emission in many organisms, including higher plants and cyanobacteria, has only one peak at 685 nm at room temperature. In the present study we observed a pronounced long wavelength emission peaking at 740 nm that had the same decay kinetics as fluorescence at 685 nm in both of the PSII decay components. This observation suggests that a novel long-wavelength pigment species is energetically coupled to PSII pigments. If this is the case then DAS components with the same spectral signatures are expected to also be observed in hydrated samples in the F_M state and in the desiccated samples (F_D) as well.

Four components were required to fit the fluorescence decay kinetics of *P. sulcata* at F_M. Only one PSI associated component was observed with a lifetime of 50 ps and an emission peak at 700 nm. This component is likely a mixture of the two decay components we observed at F_0. As expected, the closure of PSII reaction centers resulted in a pronounced slow down of PSII associated decay components. We observed two decay components with lifetimes of 1.48 ns and 2.1 ns that had DAS which appeared to be the same as the 300 ps and 600 ps components

observed in the F_0 state. The appearance of peaks in both the characteristic PSII region of about 685 nm and in the long wavelength region from 720 nm to 740 nm strongly supports the idea that a long wavelength emitter is energetically coupled to PSII. We found that an additional 410 ps component was required to fit the data. The origin of this component is not quite clear. It resembles DAS of PSII components, but its long-wavelength emission peak is shifted to 710 nm. It is known that PSII has complex decay kinetics at F_M. For example, in a previous study of the algae *Scenedesmus obliquus* PSII decay kinetics were described by three components: 380, 1300 and 2100 ps (Roelofs and Holzwarth, 1990) which are quite similar to our 400, 1480 and 2100 ps lifetimes. Therefore it is reasonable to suggest that 410 ps component at least partially arises from PSII as well. Origins of the enhanced emission of this component at 710 nm are not clear at present.

The DAS of desiccated *P. sulcata* are dominated by two short lifetime components at 40 ps and 80 ps. Both components exhibited shapes reminiscent of PSII components observed at both F_0 and F_M. However, the spectra were broadened as compared to PSII components most likely due to convolution with PSI components which would have similar lifetimes. The consistent spectral shape of the PSII DAS components observed at all three measured states indicates that the long wavelength pigment pool is energetically coupled to PSII regardless of the physiological state of the reaction centers. A 240 ps component of low amplitude was also observed in the desiccated sample with peaks at 685 nm and 720 nm. This component is somewhat similar to the 300 ps PSII component observed in the F_0 DAS and may reflect a small fraction of relatively unquenched PSII. The relatively large contribution of the 720 nm peak to this component suggests some contribution from PSI, however the 240 ps lifetime is longer than

expected. There was also a very low amount of a long lived component (1.1 ns lifetime) with significant short and long wavelength contributions which may arise from uncoupled antennae.

Low Temperature Fluorescence Decay Kinetics.

Low temperature fluorescence decay kinetics were measured to facilitate the identification of the quenching species. At room temperature the broad absorption and emission spectra of antenna chromophores make it possible for a quencher of relatively high energy to still efficiently quench emission from a broad range of emitters. However, at low temperatures only a long wavelength quencher would be able to decrease the fluorescence lifetime of low energy pigments.

Assignment of DAS components at low temperature is complicated due to pronounced decay components arising from unidirectional energy transfer from higher energy to lower energy pigments that are mostly irreversible at 77 K. This is clearly observed in the short wavelength spectral region (680-730 nm) of the measured DAS in *P. sulcata* (**Figure 3.6**). The general trend in this spectral region is that shorter wavelength components have shorter lifetimes and the fastest lifetime component (20 ps) exhibits the shortest wavelength peak at 680 nm. Such behavior is expected for systems where several long-wavelength forms are coupled to the bulk short wavelength pool. Similar features have been observed in PSII, PSI and LHCII of many other photosynthetic organisms where long wavelength pigment pools are not quenched and have long lifetimes at low temperature (Mullineaux et al., 1993; Palsson et al., 1995; Komura et al., 2006). However, the longer wavelength Chl forms of *P. sulcata* do not follow this trend. Interestingly, the amplitudes of the two shortest lifetime components (20 and 120 ps) increase again at wavelengths >730 nm and these components exhibit a large peak at 740 nm. Lifetime analysis showed that most of the steady-state fluorescence yield at 77 K originates from the two

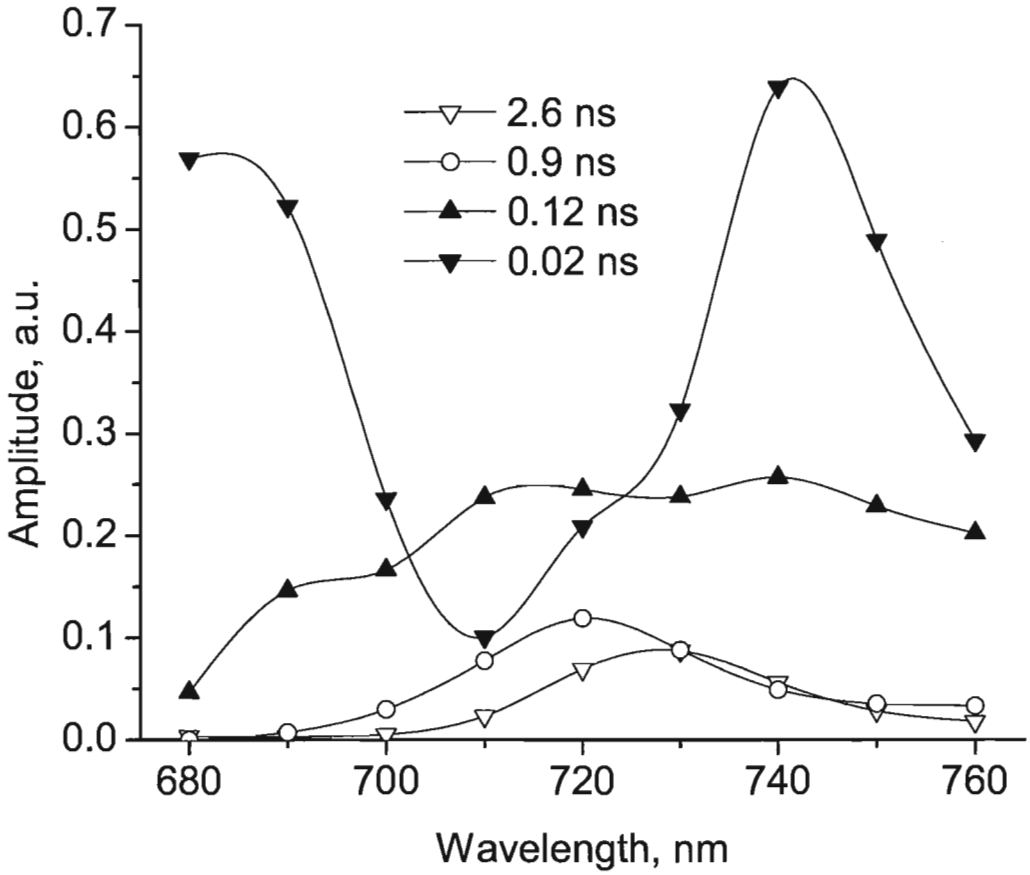

Figure 3.6. 77 K decay-associated fluorescence emission spectra obtained from global analysis of 407 nm laser induced picosecond fluorescent decay kinetics from the lichen *P. sulcata* under desiccated conditions.

slow (0.9 and 2.6 ns) components, associated with the long wavelength forms of PSI while the longest wavelength species have very short lifetimes, similar to those observed at room temperature. These results indicate that PSI is unquenched in desiccated lichens and support the assignment of a PSII associated low energy quencher as responsible for the long wavelength emission observed.

CONCLUSIONS

Photoprotection in dessicated lichens, "sunscreen" or excited state decay?

The ability of lichens to survive severe desiccation while exposed to solar radiation is correlated with a large decrease in the yield of steady state Chl *a* fluorescence emission. Photoprotection associated with a decreased yield of fluorescence could arise from the action of a "sunscreen" type mechanism that decreases the amount of light absorbed by the photobiont and/or an excitation energy quenching mechanism that safely dissipates energy absorbed by the photosynthetic apparatus as heat.

There are changes in the morphology of the thallus of lichens upon desiccation that increase light scattering and decrease the transmission of light to the photobiont. This "sunscreen" mechanism must contribute, at least to part, to the decrease in fluorescence characteristic of desiccated lichens. But how much, and is there another quenching mechanism? Based on the observation of a relative increase in the contribution of long-wavelength emission in fluorescence spectra of desiccated lichens it was previously suggested that low energy Chl forms may act as a quencher of PSII (Heber and Shuvalov, 2005). Reliable identification of a quencher must be based on the lifetime of its excited state: an efficient quencher will have a short lifetime and be capable of fast energy dissipation. Increases in the contribution of long

wavelength emission to steady-state spectra are not necessarily related to quenching. For example, long wavelength species with peaks near 700 nm were observed previously in the fluorescence of aggregated LHC II at low temperature and were suggested to be involved in non-photochemical quenching of excitation energy in higher plants. (Horton et al., 1991; Ruban and Horton, 1992). However, this postulate was later discarded because the decay lifetime of the 700 nm species was found to be only slightly shorter (3.3 ns) than the lifetime of the bulk LHC II species (4 ns) (Mullineaux et al., 1993). To date there has been no direct proof of an excitation energy quenching mechanism in desiccated lichens.

Our steady state emission spectroscopy confirmed the relative increase in long wavelength Chl *a* fluorescence in desiccated lichens. We observed a somewhat broader emission than previously reported with a peak at 740 nm. In addition, our room temperature fluorescence decay kinetics revealed the presence of novel short lifetime components in desiccated lichens that were associated with both PSII emission and long wavelength emission. This is clear evidence for excited state energy quenching. Our data showed that long wavelength emission was also present in hydrated lichens at both F_0 and F_m where its fluorescence lifetimes were identical to those of PSII. This important result indicates a tight energetic coupling between the long wavelength emitters and PSII antenna. In desiccated lichens we observe de-excitation of the bulk PSII pool with a rate constant of 25 ns^{-1}. This rate is almost 8 times faster than the rate constant for exciton trapping in active PSII species at Fo (3 ns^{-1}) (Roelofs et al., 1992). It is clear that an excitation energy quenching mechanism is efficiently down-regulating PSII in desiccated lichens.

How much do the two mechanisms, "sunscreen" and excitation energy quenching, contribute to the measured decrease in fluorescence yield in desiccated lichens? Fluorescence

yield changes measured by the analysis of steady state fluorescence emission spectra or with a pulse amplitude modulated (PAM) Chl *a* fluorometer will be affected by contributions from both of these mechanisms. In contrast, yield changes determined from an analysis of changes in the excited state decay lifetimes will only be influenced by excitation energy quenching. Comparing these two techniques allowed us to determine that most of the decrease in fluorescence emission was a result of excitation energy quenching within the photobiont. In all of our samples, less than 25 % of the observed fluorescence decrease in desiccated lifetimes arose from the "sunscreen" effect of desiccated thallus.

Identification of the quenching species.

Even though the room temperature decay data showed fast decay components at long wavelengths, it is not clear that the lowest energy emitters are indeed the origin of quenching. Due to the large overlap between the relatively broad absorbance and emission spectra of PSII antenna pigments at room temperature, a quencher of intermediate or relatively high energy could also be responsible for the quenching observed at 685 nm and 740 nm in desiccated lichens. However, our low temperature fluorescence decay measurements showed that the fluorescence lifetime of the longest wavelength emitters remained short at 77 K, clearly showing the long wavelength emitting species as being actively involved in quenching. This is in contrast to "unquenched" PSII in higher plants, algae or cyanobacteria where the longest wavelength emission at 77 K (695 nm) exhibits the longest decay lifetime (3.5 ns) (Komura et al., 2006). In desiccated lichens we observed no long lived PSII component at 695 nm at 77 K: more evidence that the quencher is coupled to PSII.

The decay lifetime of the long wavelength (740 nm) quenching species at room temperature in desiccated lichens (40 ps) was much faster than the lifetime of the major decay component of PSII with open reaction centers (300 ps) indicating that the quencher can efficiently compete for excitation with open PSII reaction centers. Thus, the long wavelength quencher closely coupled to PSII identified in the present study is clearly capable of providing efficient down regulation of PSII in desiccated lichens and fast restoration of PSII upon rehydration.

The composition and structure of the long wavelength quencher is unknown. Tight energetic coupling to PSII reaction centers implies that the red-shifted emission originate from a pigment pool located in the vicinity of PSII. This could be either a group of pigments within the PSII core or a novel antenna pigment-protein complex specific to lichen photobionts. The key to the quencher is the desiccation induced shortening of its excited state lifetime. The mechanism by which this occurs is still unknown, but it could, in principle be quite simple, e.g. analogous to the mechanism proposed for non-photochemical quenching in CP24 and CP29 proteins by (Crofts and Yerkes, 1994). Formation of new energy levels is known to introduce thermal pathways of energy deactivation of chlorophylls (Beddard et al., 1976). Desiccation-induced conformational change in the hypothetical long-wavelength antenna pigment-protein complex could allow certain chlorophyll to interact at a short enough range with neighboring chlorophylls or carotenoids to form exciton-coupled bands and thus form an efficient quencher.

MATERIALS AND METHODS

Sample preparation.

Parmelia sulcata was utilized for all measurements. Samples were collected on the campus at Brock University primarily off the tree species *Robinia pseudoacacia* (Black Locust). Lichen samples were taken from the north facing side of the trees at a height between 0.9 and 1.8 m from the ground in an effort to control for any variables associated with spatial orientation.

Steady-state and PAM spectroscopy.

Room temperature fluorescence measurements were all obtained with the use of a standard pulse amplitude modulated fluorometer (PAM), (H. Walz, Effeltrich, Germany). The pulsed measuring beam had a peak wavelength of 660 nm. Unless stated otherwise, F_M was determined by using 500 ms saturation pulses of white actinic light at an intensity of 4200 $\mu mol/m^2/s$. Re-hydration of desiccated samples was achieved by placing the sample on a section of filter paper and adding distilled water to the filter paper.

Fluorescence emission spectra were measured at 77 K with Triax-320 imaging spectrograph and back illuminated deep depleted nitrogen cooled CCD array (Jobin Yvon). Lichen samples assayed by this method were sandwiched between a glass slide and a purpose built sample holder. The lichens were hydrated while on the sample holder and then immersed in liquid nitrogen in the case of the 77K measurements. The excitation wavelength was 435 nm.

Picosecond fluorescence decay kinetics.

A single photon timing apparatus utilizing a picosecond pulsed diode laser was used to measure the kinetics of chlorophyll fluorescence decays (Vasil'ev et al., 2002). Excitation pulses were delivered at 407 nm by a picosecond diode laser (PicoQuant, PDL 800-B), 54 ps FWHM. Chlorophyll fluorescence was measured by a Hamamatsu R-3809 micro channel plate

photomultiplier screened by a double monochromator. A single photon counting PC card (Becker & Hickl, SPC-730) was used for data collection. The instrument response function of the system had a width at half height of 68 ps. To maintain PSII reaction centres in the open (F_0) state samples were held in a rotating sample wheel (140 mm diameter, 500 rpm) and low measuring light intensities were used. *P. sulcata* lobes cut from a variety of colonies and desiccated in the dark for 24 hours were loaded into a groove near the periphery of the disk and held in place with a 140 mm petri dish cover. Averaged data was thus collected from a large number of samples (typically 50 lobes). The F_M state was achieved by treating samples for 45 min with DCMU (samples exposed to a 10 μM solution of DCMU in water), slowing down the rotation rate to 0.1 rpm, and increasing the measuring light intensity. For all samples, fluorescence decay data were collected for 11 detection wavelengths between 660 nm and 760 nm until 20,000 counts in the peak channel were attained. After lifetime data was collected from the desiccated samples, distilled water was added to the lichens while they were still held in the sample wheel. The lichens were allowed to hydrate fully for one hour in the dark before subsequent measurement at F_0 and at F_M. F_0 and F_M were considered to be obtained when further decreases or increases, respectively, of excitation laser intensity did not affect the decay kinetics. Fluorescence decay curves taken at all wavelengths were fit with the sum of exponential decay functions globally with the model of parallel decaying compartments as described previously (Vasil'ev et al., 1998; Vasil'ev and Bruce, 1998).

Literature Cited

Allakhverdiev SI, Nishiyama Y, Takahashi S, Miyairi S, Suzuki I, Murata N (2005) Systematic analysis of the relation of electron transport and ATP synthesis to the photodamage and repair of photosystem II in Synechocystis. Plant Physiol 137: 263-273

Aro EM, Virgin I, Andersson B (1993) Photoinhibition of Photosystem II. Inactivation, protein damage and turnover. Biochim Biophys Acta 1143: 113-134

Beddard GS, Carlin SE, Porter G (1976) Concentration Quenching of Chlorophyll Fluorescence in Bilayer Lipid Vesicles and Liposomes. Chem Phys Lett 43: 27-32

Bukhov NG (2004) Dynamic light regulation of photosynthesis. Russian Journal of Plant Physiology 51: 742-753

Croce R, Dorra D, Holzwarth AR, Jennings RC (2000) Fluorescence decay and spectral evolution in intact photosystem I of higher plants. Biochemistry 39: 6341-6348

Crofts A, Yerkes C (1994) A molecular mechanism for qE-quenching. FEBS Lett 352: 265-270

de los Rios A, Wierzchos J, Ascaso C (2007) Study of lichens with different state of hydration by the combination of low temperature scanning electron and confocal laser scanning microscopies. International Microbiology 2: 251-257

Demmig-Adams B, Adams WW (1990) The carotenoid zeaxantin and 'high-energy-state quenching' of chlorophyll fluorescence. Photosynth Res 25: 187-197

Farber A, Young AJ, Ruban AV, Horton P, Jahns P (1997) Dynamics of xanthophyll-cycle activity in different antenna subcomplexes in the photosynthetic membranes of higher plants - The relationship between zeaxanthin conversion and nonphotochemical fluorescence quenching. Plant Physiol 115: 1609-1618

Gauslaa Y, Ohlson M, Solhaug KA, Bilger W, Nybakken L (2001) Aspect-dependent high-irradiance damage in two transplanted foliose forest lichens, Lobaria pulmonaria and Parmelia sulcata. Canadian Journal of Forest Research-Revue Canadienne de Recherche Forestiere 31: 1639-1649

Gauslaa Y, Solhaug KA (1999) High-light damage in air-dry thalli of the old forest lichen Lobaria pulmonaria - interactions of irradiance, exposure duration and high temperature. J Exp Bot 50: 697-705

Green TGA, Schlensog M, Sancho LG, Winkler JB, Broom FD, Schroeter B (2002) The photobiont determines the pattern of photosynthetic activity within a single lichen thallus containing cyanobacterial and green algal sectors (photosymbiodeme). Oecologia 130: 191-198

Heber U, Bilger W, Bligny R, Lange OL (2000) Phototolerance of lichens, mosses and higher plants in an alpine environment: analysis of photoreactions. Planta 211: 770-780

Heber U, Bilger W, Shuvalov VA (2006) Thermal energy dissipation in reaction centres and in the antenna of photosystem II protects desiccated poikilohydric mosses against photo-oxidation. Journal of Experimental Botany 57: 2993-3006

Heber U, Bukhov NG, Shuvalov VA, Kobayashi Y, Lange OL (2001) Protection of the photosynthetic apparatus against damage by excessive illumination in homoiohydric leaves and poikilohydric mosses and lichens. J Exp Bot 52: 1999-2006

Heber U, Shuvalov VA (2005) Photochemical reactions of chlorophyll in dehydrated Photosystem II: two chlorophyll forms (680 and 700 nm). Photosynth Res 84: 85-91

Holder J, Wynn-Williams D, Rull Perez F, Edwards H (2000) Raman spectroscopy of pigments and oxalates in situ within epilithic lichens: Acarospora from the Antarctic and Mediterranean. New Phytol 145: 271-280

Horton P, Ruban AV, Rees D, Pascal AA, Noctor G, Young AJ (1991) Control of the light-harvesting function of chloroplast membranes by aggregation of the chlorophyll-protein complex. FEBS Lett 292: 1-4

Ihalainen JA, Jensen PE, Haldrup A, van Stokkum IHM, van Grondelle R, Scheller HV, Dekker JP (2002) Pigment organization and energy transfer dynamics in isolated, photosystem I (PSI) complexes from Arabidopsis thaliana depleted of the PSI-G, PSI-K, PSI-L, or PSI-N subunit. Biophys J 83: 2190-2201

Komura M, Shibata Y, Itoh S (2006) A new fluorescence band F689 in photosystem II revealed by picosecond analysis at 4-77 K: Function of two terminal energy sinks F689 and F695 in PSII. Biochimica et Biophysica Acta-Bioenergetics 1757: 1657-1668

Melis A (1999) Photosystem-II damage and repair cycle in chloroplasts: what modulates the rate of photodamage in vivo? Trends in Plant Science 4: 130-135

Melkozernov AN, Kargul J, Lin S, Barber J, Blankenship RE (2004) Energy coupling in the PSI-LHCI supercomplex from the green alga Chlamydomonas reinhardtii. J Phys Chem B 108: 10547-10555

Mullineaux CW, Pascal AA, Horton P, Holzwarth AR (1993) Excitation-energy quenching in aggregates of the LHC II chlorophyll-protein complex: a time-resolved fluorescence study. Biochim Biophys Acta 1141: 23-28

Ohnishi N, Allakhverdiev SI, Takahashi S, Higashi S, Watanabe M, Nishiyama Y, Murata N (2005) Two-step mechanism of photodamage to photosystem II: Step 1 occurs at the oxygen-evolving complex and step 2 occurs at the photochemical reaction center. Biochemistry 44: 8494-8499

Palsson LO, Tjus SE, Andersson B, Gillbro T (1995) Energy-Transfer in Photosystem-I - Time-Resolved Fluorescence of the Native Photosystem-I Complex and Its Core Complex. Chem Phys 194: 291-302

Roelofs TA, Holzwarth AR (1990) In Search of A Putative Long-Lived Relaxed Radical Pair State in Closed Photosystem-Ii - Kinetic Modeling of Picosecond Fluorescence Data. Biophys J 57: 1141-1153

Roelofs TA, Lee C-H, Holzwarth AR (1992) Global target analysis of picosecond chlorophyll fluorescence kinetics from pea chloroplasts - a new approach to the characterization of the primary processes in photosystem II alpha-units and beta-units. Biophys J 61: 1147-1163

Ruban AV, Horton P (1992) Mechanism of delta pH-dependent dissipation of absorbed excitation energy by photosynthetic membranes. I. Spectroscopic analysis of isolated light-harvesting complexes. Biochim Biophys Acta 1102: 30-38

Scheidegger C, Schroeter B, Frey B (1995) Structural and Functional Processes During Water-Vapor Uptake and Desiccation in Selected Lichens with Green Algal Photobionts. Planta 197: 399-409

Vasil'ev S, Bruce D (1998) Nonphotochemical quenching of excitation energy in photosystem II. A picosecond time-resolved study of the low yield of chlorophyll *a* fluorescence induced by single-turnover flash in isolated spinach thylakoids. Biochemistry 37: 11046-11054

Vasil'ev S, Lee C-I, Brudvig GW, Bruce D (2002) Structure-based kinetic modeling of excited-state transfer and trapping in His-tagged PSII core complexes from *Synechocystis*. Biochemistry 41: 12236-12243

Vasil'ev S, Wiebe S, Bruce D (1998) Non-photochemical quenching of chlorophyll fluorescence in photosynthesis. 5-hydroxy-1,4-naphthoquinone in spinach thylakoids as a model for antenna based quenching mechanisms. Biochim Biophys Acta 1363: 147-156

Veerman J, McConnell MD, Vasil'ev S, Mamedov F, Styring S (2007) Functional heterogeneity of photosystem II in domain specific regions of the thylakoid membrane of spinach (*Spinacea oleracea L.*). Biochemistry in press:

Wendler J, Holzwarth AR (1987) State Transitions in the Green-Alga Scenedesmus-Obliquus Probed by Time-Resolved Chlorophyll Fluorescence Spectroscopy and Global Data-Analysis. Biophys J 52: 717-728

Chapter 4: The Q130E substitution of the D1 protein protects PSII from photodamage by altering the electron transfer kinetics of primary photochemistry

John Veerman[‡], Julian J. Eaton-Rye[§], Sergei Vasil'ev[‡], and Doug Bruce[‡]*

[‡]Department of Biological Sciences, Brock University, St. Catharines, Ontario, L2S 3A1, Canada. [§]Department of Biochemistry, University of Otago, P.O. Box 56, Dunedin, New Zealand.

Preface

The point mutations for this chapter were generated at the University of Otago in New Zealand, by Professor Julian Eaton-Rye. I performed initial work with the MD simulation working under the creator Dr. Sergei Vasil'ev, later Dr. Vasil'ev with Abdullah Mahboob used a revised model that included protonation states to produce the shift reported for the Q130E mutant. I produced all figures, tables and illustrations, and collected and analyzed the data contained therein.

It should also be noted that Professor Doug Bruce and Dr. Sergei Vasil'ev both guided me through all aspects of this research, from hypothesis formation, data collection, and analysis to writing/revising.

I wrote this chapter in publication format with the intention of submitting the work for publication in the near term.

ABSTRACT

Various point mutations targeting the ligands of chromophores in the CP47 and D1 protein subunits were assayed for changes in PSII spectral properties and function. It was found that the H114Q mutant exhibited a blue-shifted 695nm fluorescence peak at low temperature, while various other point mutants including the 'linker' chlorophyll ligated H466Q and H469Q did not exhibit a shift in the 695nm peak. The Q130E mutant possessed a red-shifted Pheophytin Q_Y transition absorbance band as well as increased charge stabilization and non-radiative charge recombination rates. The increased rate of non-radiative charge recombination likely serves to protect PSII and is consistent with previous observations of 130E containing D1 type 2 PSII centers resisting photoinhibition. Interestingly, higher plants use the 130E configuration and the fluorescence kinetics observed for the Q130E mutant approach those of higher plant PSII complexes at Fo. These results indicate that this single mutation is partially or perhaps even completely responsible for the previously observed attenuation of PSII photodamage in D1 type 2 substituted centers. An MD simulation of PSII was utilized and was able to reasonably predict the red-shift in the Q130E mutant Pheophytin Qy transition.

INTRODUCTION

The varying light levels encountered by photosynthetic organisms and propensity for PSII to incur damage during operation (*1-3*) has resulted in the emergence of various mechanisms by which energy flow into the photosynthetic apparatus is regulated. In higher plants, complex mechanisms involving quenching of excitation energy are utilized, to ensure that PSII activity and excitation remain balanced (*4*). In cyanobacteria, a number of excitation energy related regulatory mechanisms are also present, such as blue light induced quenching (*5*), state transitions (*6*) and PBS quenching (*7*). However, in contrast to higher plants, cyanobacteria, such as *Synechococcus* PCC 7942, directly regulate PSII activity by alternating from one type of D1 protein to another, depending on light conditions (*8*).

The two main varieties of D1 are known as type 1(D1:1) and type 2(D1:2), and are encoded by three genes, *psbAI* encoding D1:1 while *psbAII* and *psbAIII* encode D1:2; the two isoforms are quite similar as the disparity in sequence identity amounts to 10% (*9*). Under high light conditions and/or elevated UV-B exposure D1:2 is expressed and replaces D1:1 in the PSII population (*10;11*). However, D1 replacement is transient under high levels of visible light while excessive exposure to UV-B light results in the replacement of D1 for the duration of the exposure (*11*). Other forms of stress such as low temperature or anoxia also induce D1 replacement (*12*). PSII populations containing D1:2 are resistant to photoinhibition, exhibit increased variable fluorescence, elevated oxygen evolution rates and appear ideal for high light conditions (*10;13*). Of the two forms of D1, D1:2 more closely resembles the amino acid sequence of the D1 protein subunit present in higher plants (*9;11*).

Of the differences between D1:1 and D1:2, a particular mutation has been implicated as a crucial factor regarding the differences observed with respect to primary photochemistry (*12;14*);

this mutation also represents a key similarity between D1:2 and higher plant D1. The mutation is the Q130E substitution present in D1:2, the amino acid position ligates the D1 pheophytin (D1:Ph) in the RC of PSII (*15*). The ligation takes the form of a hydrogen bond between the residue and D1:Ph, and the Q130E substitution is thought to cause a weakening of this bond (*16*). Such modification of the hydrogen bond has been implicated in the alteration of spectral properties of the D1:Ph as well as causing the midpoint potential of D1:Ph to shift to a value closer to that observed in higher plants (*16-18*). These changes, particularly the shift in midpoint potential, cause the Q130E mutant to exhibit a higher quantum yield of primary charge separation (*19;20*). The mutation also confers resistance to photoinhibition and has been observed to increase the rate of direct charge recombination from $P680^+Q_A^-$ (*14*).

The spectral properties of the cofactors and pigments present in PSII remains an area of intense interest in the field because of the associated functional implications with respect to primary photochemistry (*21*). Q_Y transitions in particular are important for energy transfer from pigment to pigment; and together with the orientation and location of each pigment determine the efficiency with which excitons are funneled to the reaction center (*22;23*). Previous research has implicated the chlorophyll ligated to the H114 residue in CP47 as exhibiting the most red-shifted Q_Y transition of any antennae chlorophyll in PSII as evidenced by a blue shift in the spectra of H114Q mutant PSII complexes (*24*). This chlorophyll is located in the periphery of the PSII complex and is likely of unremarkable contribution to the overall yield of PSII relative to the other chlorophylls present (*22*). However, other studies based on hole burning data have implicated the 'linker' Chl *a* molecules which serve to excitonically link CP47 to the reaction center as the source of the red shifted features observed in CP47 at low temperature (*25*). The source of the red shifted spectral features originating from CP47 remains important to identify

because this information could potentially shed light on the spectral shifts of other chromophores in PSII by providing a verifiable example of such a shift and absolute energy level(Q_Y transition) of this specific chlorophyll. If the relationship between spectral shift and local protein environment can be delineated then the spectra distribution of all the chlorophylls in PSII and in other pigment protein complexes might be derived using computer simulations.

In the present study, Q130E mutant *Synechocystis* PCC 6803 was assayed for changes in PSII absorbance and fluorescence decay kinetics. We found that the Q130E mutant exhibited a red shift in the Q_Y absorbance band and global analysis of time resolved fluorescence kinetics revealed faster PSII kinetics in whole cells were consistent with increased rates of non-radiative charge recombination of the primary radical pair. In addition, the H114 ligated chlorophyll was confirmed as the most red-shifted chlorophyll in PSII.

MATERIALS AND METHODS

Growth of Synechocystis sp. PCC 6803 strains. Cultures were maintained on BG-11 plates containing 5 mM glucose and 20 μM atrazine and, when required, chloramphenicol and/or kanamycin was present at a concentration of 30 μg/mL and 50 μg/mL respectively; this was the case in both solid and liquid BG-11 media. The solid media was supplemented with 10 mM TES-NaOH (pH 8.2) and 0.3% sodium thiosulfate and liquid cultures were grown photoautotrophically unless otherwise noted. Cells were grown under a continuous illumination of 30 $\mu E\ m^{-2}\ s^{-1}$ and the temperature in the growth chamber was 30^0C. The *Synechocystis* sp. PCC 6803 strain used in this study was the glucose-tolerant strain from Williams (*26*) and this is referred to throughout as wild type.

Steady state spectroscopy. Absorption spectra were measured at 10 K using a back illuminated deep depleted nitrogen cooled CCD array (Jobin Yvon) and a helium cryostat

(Advanced Research Systems, Inc., model DE-202). Samples were re-suspended in 50 mM HEPES buffer, pH 7.6, containing 0.1 M sorbitol, 5 mM $MgCl_2$, 5 mM NaCl, and 60% glycerol. Emission spectra were measured at 77 K with Fluorescence emission spectra were measured at 77 K with Triax-320 imaging spectrograph and the same detector. Chlorophyll concentration of less than 5 μg/ml was used in fluorescence measurements.

Molecular Dynamic Simulation of PSII. The MD simulation of PSII was performed as described in (*27*), with the AMBER-8 package (University of California, San Francisco, CA) of the NAMD program (*28*). While quantum calculations were performed using the GAUSSIAN-98 (Gaussian, Wallingford, CT) package and *ab initio* Q_Y transitions were calculated using the single excitation configuration interaction method (CIS). The molecular visualization program VMD(*29*) was also utilized.

The simulation consisted of the PSII complex without the O, U and V subunits existing in a lipid bilayer with PSII associated lipids and water molecules also present. Point mutations were inserted into the simulation by editing PDB files so as to replace the atoms differing between the amino acids in question, performing energy minimization on the substituted amino acid, and then on the entire system and finally raising the temperature to 300K over a time period of 200ps. The system was equilibrated for 500ps and then four sets of single point excited state calculations were performed for each mutation at an interval of 500ps. Each set consisted of 240 single point excited state energy calculations at an interval of 5ps. The system used for the excited state energy calculations included acetamide and acetic acid which were used to represent Gln and Glu residues respectively. The acetic acid group was protonated as Poisson-Boltzmann calculations on the D1-Glu 130 mutant indicated that this was the case for the residue when present in the local protein environment of the PSII reaction center.

Fluorescence decay kinetics. Fluorescence decay kinetics were measured with dark-adapted whole cell cultures at a Chl *a* concentration of 10 μg/mL using the single photon timing apparatus previously described (*30-32*). The 650 nm picosecond pulsed diode laser (Picoquant, Berlin, Germany) used for excitation was operated at 10 MHz. For each measurement a 200 mL sample was circulated at a flow rate of ~4 mL s^{-1}. The detector was a Hamamatsu R3809 microchannel plate (Hamamatsu, Japan). Decay data was collected in 4096 channels over 50 ns with a Becker & Hickl SPC-630 single photon timing card (Berlin, Germany) in a Pentium PC. Decay data was collected at Fo from dark-adapted samples and Fm from preilluminated samples in the presence of DCMU as described in (*32*).

Global lifetime analysis. Global lifetime analyses of fluorescence decays at multiple emission wavelengths were done as described previously (*32*). The detection wavelength range was 660-720 nm taken at 10 nm increments. All programs used for data manipulation and global analysis were written by Sergei Vasil'ev.

RESULTS

Low temperature fluorescence emission spectra. In order to confirm the results of a previous study (*24*) that showed a blue-shift in the characteristic PSII 695nm fluorescence peak, a low temperature fluorescence emission spectrum of the H114Q cells was collected. The results are displayed in both Figure 4.1 and 4.2 which show the shoulder/peak at 695nm in the wild-type emission spectrum had been blue-shifted in the H114Q mutant cells by ~3nm. This shift suggests that the chlorophyll ligated to this histidine in CP47 is the source of the 695nm fluorescence peak observed at 77 degrees Kelvin.

Low Temperature absorbance spectra. Since the Q130E mutation had been previously shown to red-shift the Q_Y absorbance band of the D1:Ph (*15*), the effect of the mutation on the

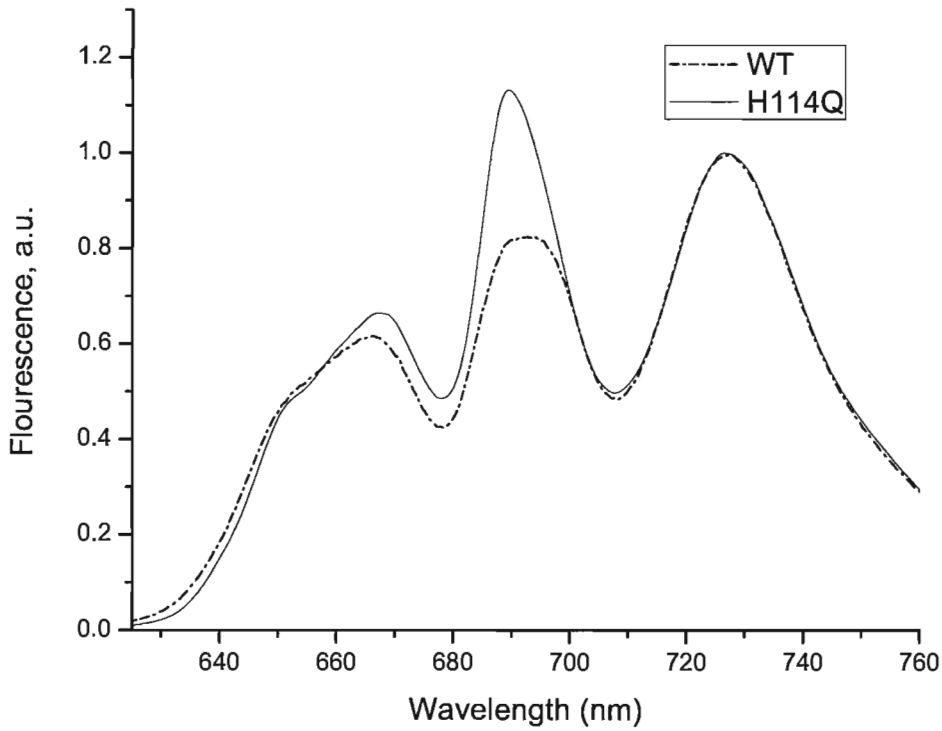

Figure 4.1 Low temperature fluorescence emission spectra of wild-type (WT) and H114Q *Synechocystis sp.* PCC 6803 cells using an excitation wavelength of 590nm.

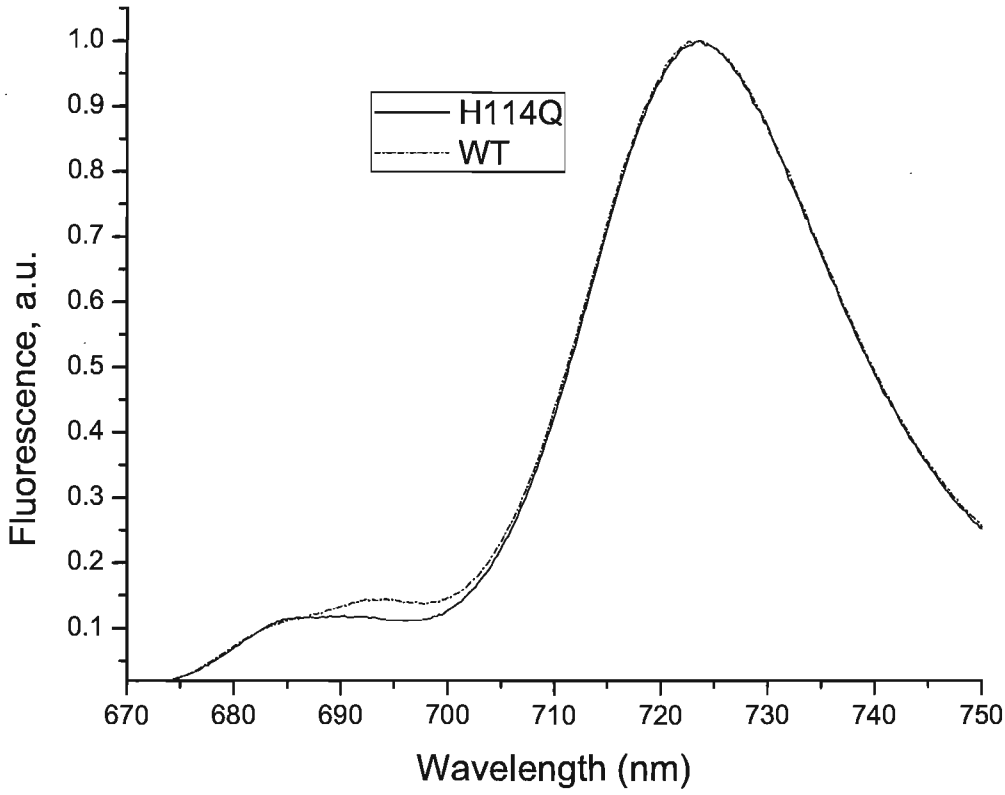

Figure 4.2 Low temperature fluorescence emission spectra of wild-type (WT) and H114Q *Synechocystis sp.* PCC 6803 cells using an excitation wavelength of 435nm.

Q_Y band was assessed by obtaining 10K absorbance spectra of isolated thylakoid membranes. The results shown in Figure 4.3 show a distinct change in shape in the spectra, as the shoulder observed at 671nm becomes more prominent and the peak at 679nm was red-shifted by ~0.6nm. These results are consistent with a change in the Q_Y absorbance band of the D1:Ph, specifically the aforementioned red-shift. However, the red-shift reported in the previous study was from 685.6nm to 686.9nm for the D1:Ph (*15*). This 1.3nm shift represents the shift for the pheophytin only and is insufficient to explain the ~0.6nm shift in the absorbance peak of isolated thylakoid membranes, which include both PSII and PSI associated chlorophylls. The shape of the shoulder at 671nm also indicates there has been a loss of absorbance between the 671nm shoulder and the 679nm peak. The difference spectra shown in Figure 4.4 corroborates these qualitative observations as the roughly Gaussian shaped negative component at ~675nm and positive component at ~685nm indicate at least a 2nm red-shift of D1:Ph present in the Q130E mutant. This was an interesting finding as the D2:Ph has been previously implicated as possessing a Q_Y absorbance band centering at 670nm and the D1:Ph exhibiting a Q_Y absorbance band at 681nm (*33*); thus ~680nm is a plausible assignment for D1:Ph. In addition, the relative area displaced as shown in the difference spectra corresponds to a ratio of approximately 179 chlorophyll pigment molecules per D1:Ph and suggests a PSII:PSI ratio of ~0.66; which is within established parameters for cyanobacteria cells (*34*).

Molecular Dynamic Simulation of PSII. The Q130E point mutation affords an opportunity to model subtle changes in the properties of D1:Ph which result in gross alterations of PSII spectral properties/photochemical function. In order to facilitate such modeling a molecular dynamic(MD) simulation of PSII (*27*), was utilized in conjunction with *ab initio* calculation of the Q_Y transition (see methods). The Q130E ligated Ph was red shifted by 2.18

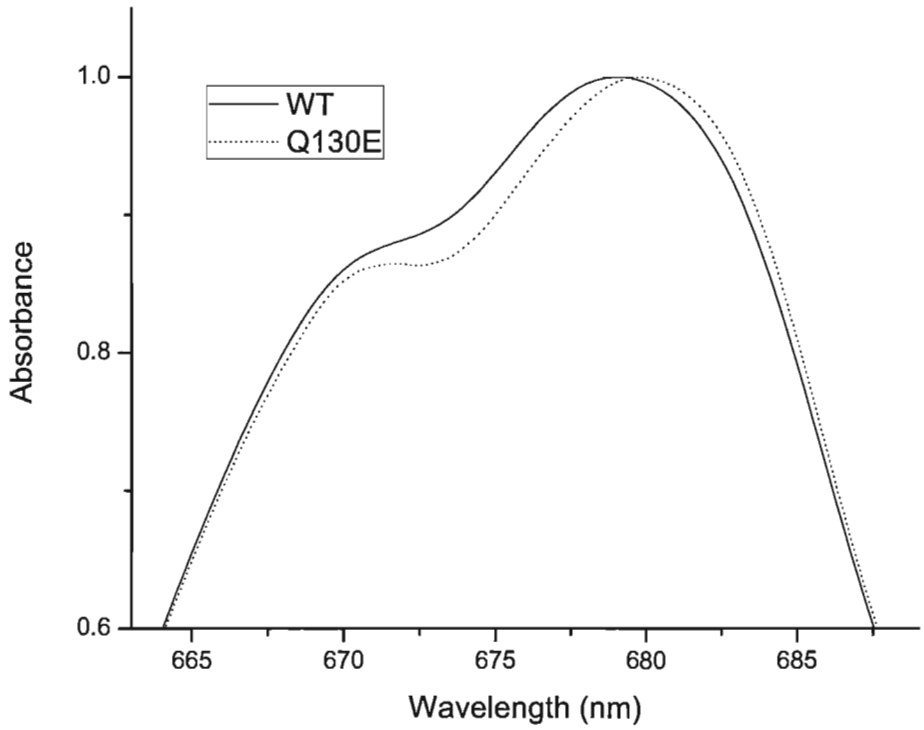

Figure 4.3 10K absorbance spectra of wild-type and Q130E *Synechocystis sp.* PCC 6803 isolated thylakoid membranes.

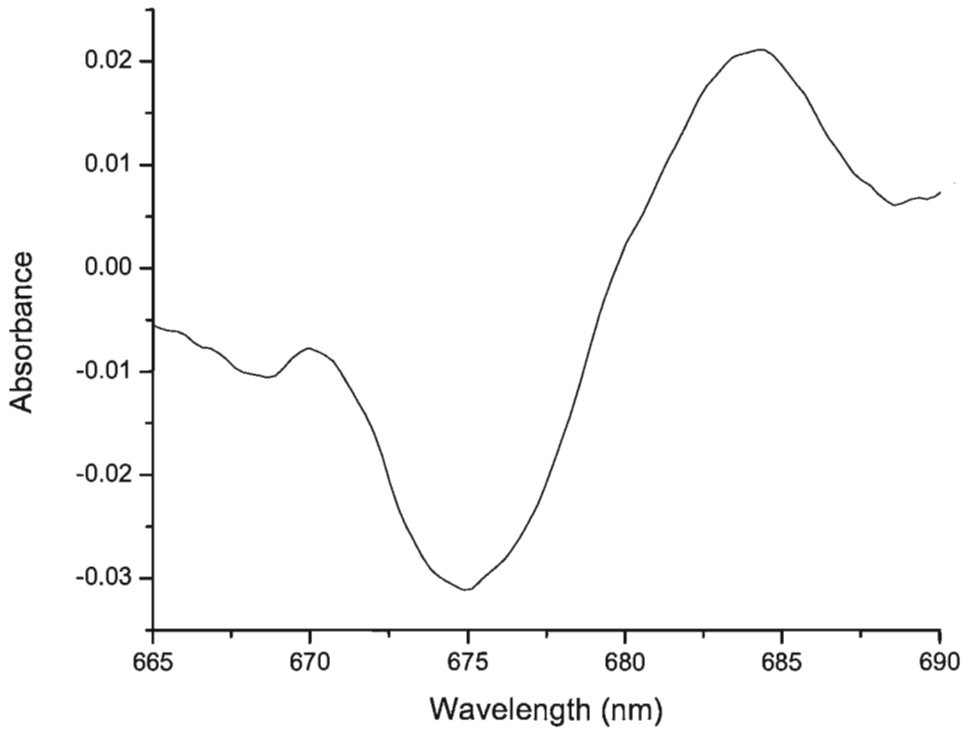

Figure 4.4 Difference spectra obtained by subtracting Q130E 10K thylakoid membrane absorbance spectra from WT.

nm, which was consistent with the values reported previously in the literature (*15*) as well as that reported in the present study.

Fluorescence decay kinetics. The status of the Q130E mutant as a key factor affecting PSII photochemistry through altering the potential associated with the ligated pheophytin (*16-19;35;36*) rendered the mutant highly interesting with respect to PSII kinetics. For this reason, time resolved fluorescence measurements were carried out on the Q130E mutant.

The results displayed in Figure 4.5 and Figure 4.6 both show that the Q130E mutant displays faster decay kinetics than the wild-type cells. This data, considered in isolation, suggests that the yield of primary photochemistry was substantially elevated in Q130E mutant cells.

Global lifetime analysis. In order to confirm PSII as the origin of the faster kinetics observed and to attempt to resolve the photochemical process inside PSII that were altered by the Q130E substitution, global analysis of the fluorescence decay kinetics was performed. The results are displayed in Figure 4.7 and 4.8, under both F_o and F_m conditions a ~200ps component which we had previously identified as a PSII fluorescence decay component present in intact *Synechocystis* PCC 6803 cells (*37;38*) was observed. Similarly, under F_o conditions a second characteristic PSII component associated with intact *Synechocystis* PCC 6803 cells was also present in the form of a 473ps component for the wild-type and 762ps component for the Q130E mutant. This component was of a lower relative amplitude as compared to the ~200ps component and of a longer lifetime in the Q130E mutant. This component can be reasonably ascribed to PSII(*38;39*), specifically to PSII charge recombination. The longer lifetime and lower amplitude of this component in the Q130E mutant cells indicated that radiative charge recombination in the Q130E mutant is of a lower rate and population. Since the apparent quantum yield of PSII was higher in the Q130E mutant, the lower population of charge

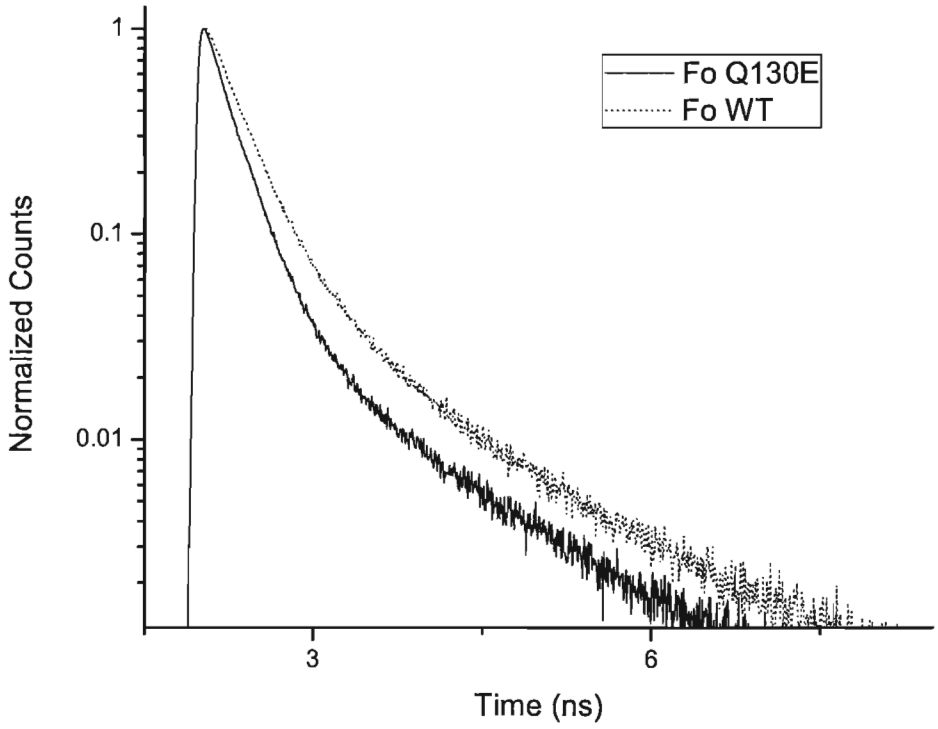

Figure 4.5 Fluorescence decay kinetics of wild-type and Q130E *Synechocystis sp.* PCC 6803 cells at F_o. Detection wavelength was 680 nm and excitation was 650nm.

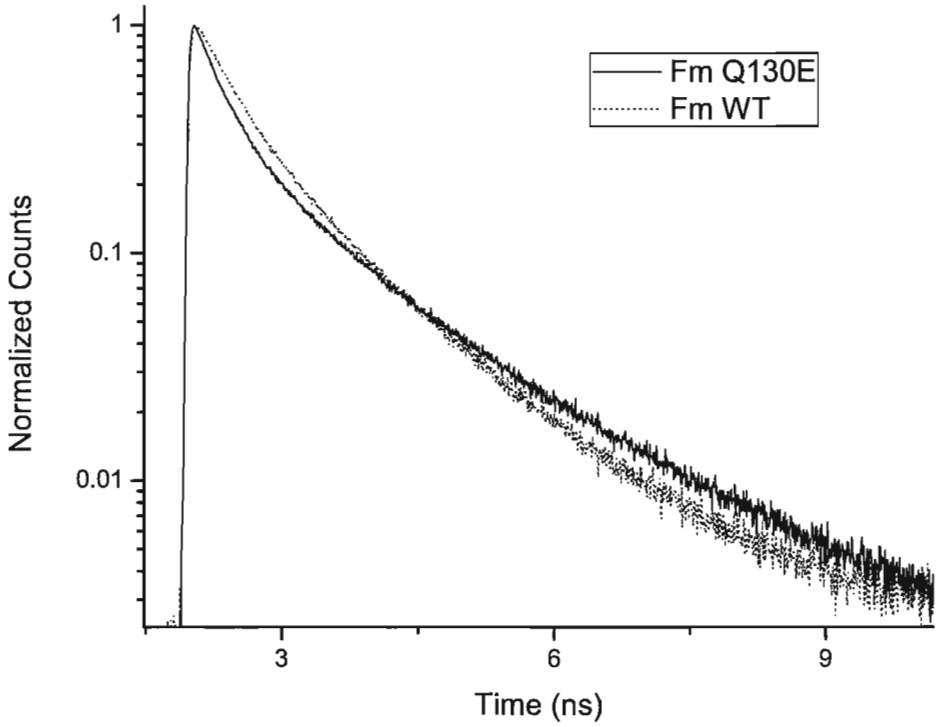

Figure 4.6 Fluorescence decay kinetics of wild-type and Q130E *Synechocystis sp.* PCC 6803 cells at F_m. Detection wavelength was 680 nm and excitation was 650nm.

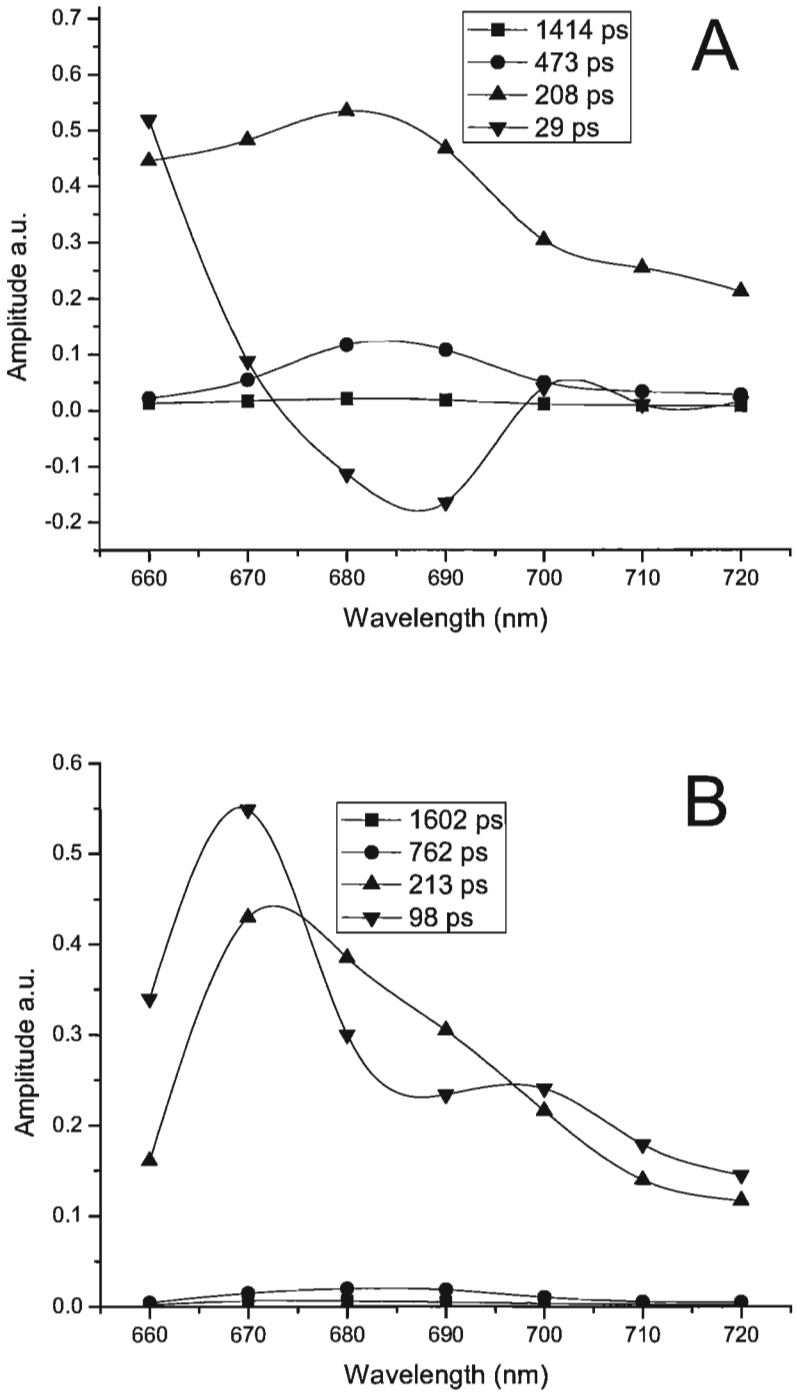

Figure 4.7 Decay-associated fluorescence emission spectra obtained from global analysis of 650 nm laser induced picosecond fluorescent decay kinetics from wild-type (A) and Q130E (B) *Synechocystis sp.* PCC 6803 cells at F_o.

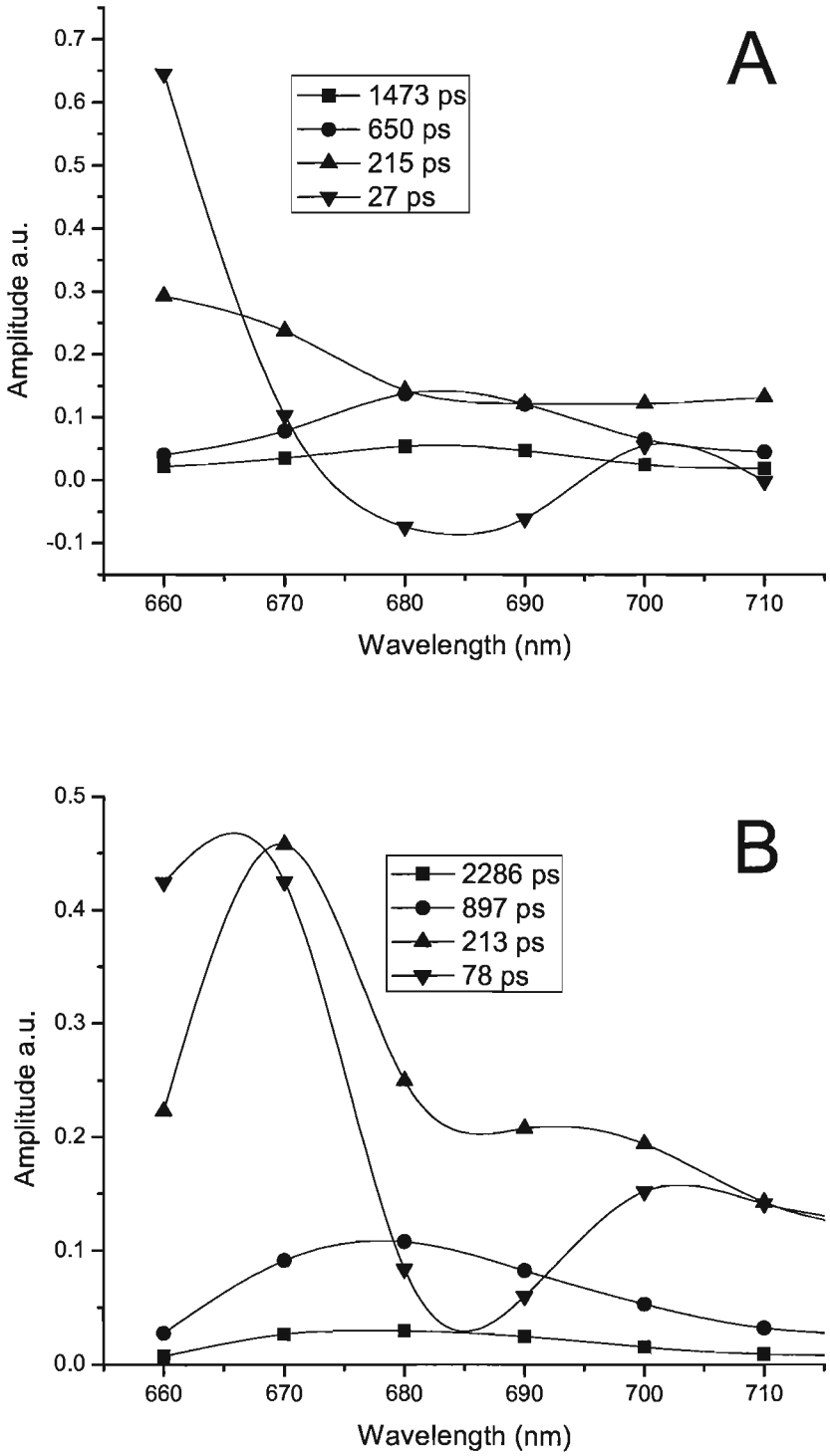

Figure 4.8 Decay-associated fluorescence emission spectra obtained from global analysis of 650 nm laser induced picosecond fluorescent decay kinetics from wild-type (A) and Q130E (B) *Synechocystis sp.* PCC 6803 cells at F_m.

recombination was likely due to increased rates of charge stabilization or increased non-radiative internal conversion (*12*), possibly both. Certainly the non-radiative internal conversion could be a result of non-radiative charge recombination. Interestingly, the apparent decreased rate of radiative charge recombination indicates that both forms of recombination occur along the same pathway. Although the total rate of charge recombination might be higher, the rate for radiative appears lower and yields a longer lifetime in this analysis because only radiative recombination is measured. Longer lifetime components, 1414ps in WT cells and 1602ps in the Q130E mutant were also present but with nominal amplitudes. These components likely included both decoupled PBS and closed PSII centers.

The ~30ps component in the WT cells at both F_o and F_m can be attributed to PBS components due to the rise component at ~685nm and also includes PSI components as evidenced by the peak observed at ~700nm. In the WT this component exhibits a negative peak at 680nm; suggesting a rise component attributable to exciton transfer from AP to the AP_E and perhaps also transfer from the AP_E to Chl a populations. However, in the Q130E mutant cells the fastest component was of a longer lifetime exhibiting 78ps and 98ps lifetimes at F_o and F_m respectively and also was of a different shape. Interestingly, the shape of the component is relatively unaffected by trap closure in the WT cells, while the Q130E mutant cells exhibits a noticeable shape change roughly consistent with the loss of a Guassian shaped peak at ~685nm at F_m. This suggests that a novel PSII component at ~90ps is present in the Q130E mutant when the PSII centers are open. Interestingly, higher plant PSII exhibits a ~100ps component as well as the aforementioned ~200ps and ~600ps PSII components observed in the PSII rich thylakoid fractions studied in Chapter 2 of this thesis and also in previous studies (*40*). It appears that the Q130E mutation changes the kinetics of the open PSII centers to resemble the kinetics observed

in higher plants (Figure 4.9); as the ~100ps component observed in both the PSII rich BS thylakoid fraction from Chapter 2 of this thesis and BBY preparations (*40*) appears to emerge in the Q130E mutant.

The results under F_m conditions were similar as the 650ps component for the wild-type was again of a larger amplitude relative to the ~200ps component than the 897ps component of the Q130E mutant. The trend was akin to the difference between the wild-type 1473ps component and Q130E 2286ps component; which likely represent charge recombination related components in closed PSII centers. Interestingly, the longer lifetimes of these components in the Q130E mutant reflect the aforementioned decreased recombination rates but the lower amplitude cannot be explained via charge stabilization. PSII complexes do not appreciably undergo charge stabilization under F_m conditions, particularly in this case, when DCMU is used to block the electron transport chain at the Q_B binding pocket. The lower amplitude of these components suggests that the radical pair in the Q130E mutant is more likely to be internally converted via non-radiative internal conversion. Again, as was the case under F_o conditions, the data would be consistent with non-radiative charge recombination and would presumably contribute to the resistance of D1:2 substituted PSII to photoinhibition.

DISCUSSION

The observed blue-shift of the 695nm peak in the H114Q mutant was in agreement with that reported for a PSI-less and APC-less cell line possessing the same mutation (*24*). However, previous research in the field based on hole burning data had indicated that the 'linker' chlorophylls were the source of this fluorescence peak (*25*). This assertion included the idea of a lower energy charge separated state of P680, specifically in the ~730nm range, and thus indicates that the so called 'trap' chlorophyll(s) emitting at 695nm is not a trap at all but a primary site of

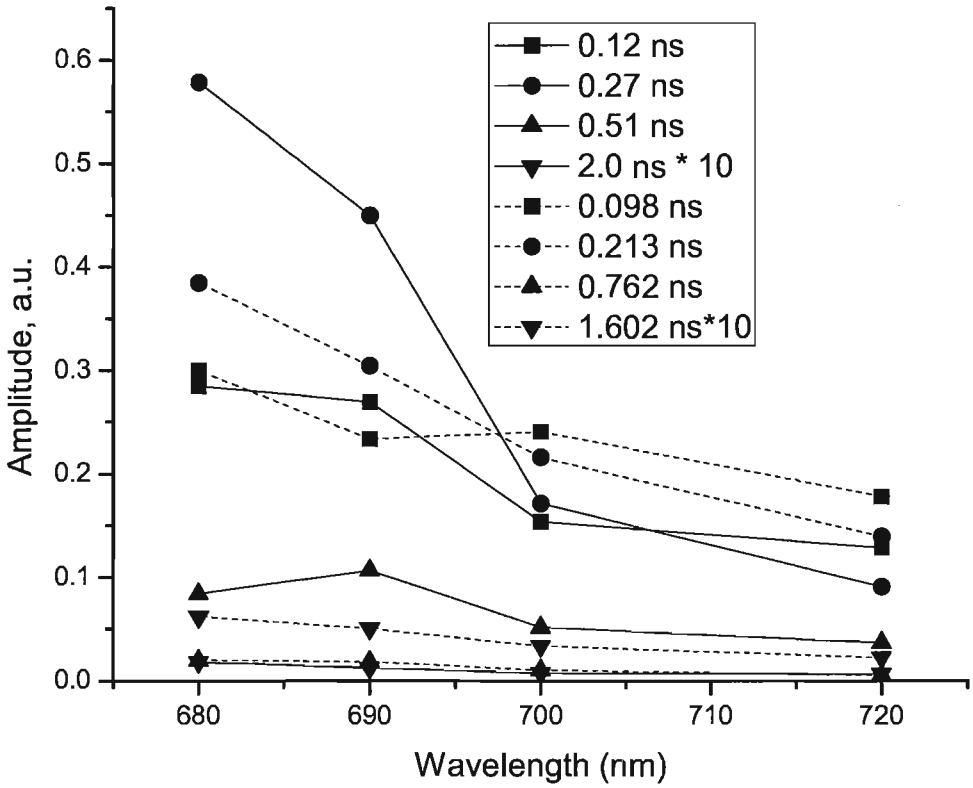

Figure 4.9 Decay-associated fluorescence emission spectra obtained from global analysis of 650 nm laser induced picosecond fluorescent decay kinetics from Q130E *Synechocystis sp.* PCC 6803 cells at F_o (Dashed Lines) and 407 nm laser induced picosecond fluorescent decay kinetics from the BS thylakoid fraction from Chapter 2 (Solid Lines).

energy transfer. At low temperature, PSII centers would be essentially in a closed state and thus energy transfer would be effectively slowed down at the RC allowing for the high yield of the 695nm peak. This model, as presented in the literature (*25;41*) is both plausible and consistent when considered with the assumptions associated with the argument. However, the data obtained in this study remains difficult to reconcile with this model of PSII exciton transfer. The mutation is a single substitution and PSII light harvesting function in the H114Q mutant appears relatively unaffected with the exception of the shift observed in the 695nm fluorescence peak at 77K. It is generally known that the introduction of point mutations is capable of impairing PSII assembly and assembly is indeed marginally impaired in the H114Q mutant (*24*). However, a total of five other point mutations to chlorophyll ligands (H100Q, H455Q, H466Q, H469Q and H198Q) were assayed for the presence of fluorescence shifts in the 695nm peak; without any discernable differences identified (data not shown). Thus, from the data presented in the present study it appears unlikely that differences in assembly caused the observed shift in the 695nm peak in the H114Q mutant. It should also be noted that the data implicating the H114 ligated chlorophyll as the most red shifted in the complex might have useful applications in computer simulations of PSII(*22;42*) as the distribution of excited state energy levels has important implications when modeling exciton transfer.

Previous studies have identified the Q130E mutation as perhaps the most important difference between PSII type 1 and type 2 reaction centers in cyanobacteria in regards to primary photochemistry (*8;10;15*). The present study corroborates these ideas as this single mutation significantly alters PSII photochemistry. In particular, the kinetics of open PSII reaction centers begin to resemble those of higher plant centers; illustrating the significance of the mutation in relation to PSII kinetics. If using prevailing models of PSII primary photochemistry

(*23;43;44*) as a basis for the analysis, charge recombination rates appear to be decreasing in addition to a marked reduction in the population of the charge separated state in the Q130E mutant. However, as stated in the results section, non-radiative recombination of the primary radical pair is also capable of explaining these results. It has been previously reported that the shift in E_m of the Ph could conceivably increase the rate of non-radiative charge recombination (*12*); which might be accomplished by both increasing the rate of charge recombination overall and/or decreasing the probability of triplet state formation upon charge recombination. This pathway would aid in explaining the apparent resistance of the Q130E substituted PSII complexes to photodamage as P680+ would be effectively quenched by such recombination. This is important because a major mechanism of PSII damage is caused by inactivation of the manganese cluster of the OEC; effectively blocking donor side electron transport and causing an increase in highly oxidizing P680+ in the PSII population. The non-radiative recombination would also change the intrinsic ratio of singlet to triplet states that occur as a result of recombination itself, thereby further decreasing the rate of damage. It should also be noted that the differences in charge recombination were much more pronounced at F_o as compared to F_m. Since charge stabilization does not occur at an appreciable level at F_m the results suggest an increased rate of charge stabilization in the Q130E mutant; although it is also possible that the presence of charges in the electron transport chain under F_m conditions alter the kinetics differentially in the Q130E mutant as compared to wild-type cells.

The MD simulation of PSII was of utility in the present experiment as the simulation did show a red shift in the Q_Y transition of the ligated pigments in the Q130E mutant. This simulation represents a remarkably comprehensive model with membrane, water molecules and the PSII complex present and the electrostatic environment inside the protein was assayed for

protonation states in the immediate vicinity of the mutation. Since the point mutation was located deep within the protein the Poisson–Boltzmann based method for titrating the proimal amino acids was used to render the Q_Y transition calculation both more accurate and representative (*45*). Looking to the future, the protonation states of various amino acids and their effect on the pigments in PSII may yield additional insights into the importance of various conserved residues and related motifs. It is also conceivable that amino acids which are located at a distance exceeding that which would directly affect cofactors or pigments might cause a 'chain' of changed protonation states that do influence the local protein environment. However, at the present time the computing power required to achieve this remains prohibitively high.

The use of protonation state calculations represents a single step in the incremental improvement that is a key element when utilizing such a simulation, with the ultimate goal being to reproduce results from a variety of sources. Provided the shifts in the Q_Y transitions observed can be reproduced through spectroscopy, the next logical step would be to model the effect on light harvesting efficiency particularly in the case of the Q130E mutant. Such a method would include the aforementioned protonation state calculations and use the empirical equation known as "Dutton's Ruler" as reported in the literature previously (*27*).

References

1. Veerman, J., McConnell, M. D., Vasil'ev, S., Mamedov, F., Styring, S., and Bruce, D. (2007) *Biochemistry 46*, 3443-3453.

2. Murata, N., Takahashi, S., Nishiyama, Y., and Allakhverdiev, S. I. (2007) *Biochimica et Biophysica Acta-Bioenergetics 1767*, 414-421.

3. Aro, E. M., Suorsa, M., Rokka, A., Allahverdiyeva, Y., Paakkarinen, V., Saleem, A., Battchikova, N., and Rintamaki, E. (2005) *Journal of Experimental Botany 56*, 347-356.

4. Campbell, D., Clarke, A. K., Gustafsson, P., and Oquist, G. (1996) *Plant Science 115*, 183-190.

5. Scott, M., McCollum, C., Vasil'ev, S., Crozier, C., Espie, G. S., Krol, M., Huner, N. P. A., and Bruce, D. (2006) *Biochemistry 45*, 8952-8958.

6. McConnell, M. D., Koop, R., Vasil'ev, S., and Bruce, D. (2002) *Plant Physiology 130*, 1201-1212.

7. Karapetyan, N. V. (2007) *Biochemistry-Moscow 72*, 1127-1135.

8. Tichy, M., Lupinkova, L., Sicora, C., Vass, I., Kuvikova, S., Prasil, O., and Komenda, J. (2003) *Biochimica et Biophysica Acta-Bioenergetics 1605*, 55-66.

9. Sicora, C. I., Brown, C. M., Cheregi, O., Vass, I., and Campbell, D. A. (2008) *Biochimica et Biophysica Acta-Bioenergetics 1777*, 130-139.

10. Campbell, D., Bruce, D., Carpenter, C., Gustafsson, P., and Oquist, G. (1996) *Photosynthesis Research 47*, 131-144.

11. Campbell, D., Eriksson, M. J., Oquist, G., Gustafsson, P., and Clarke, A. K. (1998) *Proceedings of the National Academy of Sciences of the United States of America 95*, 364-369.

12. Mulo, P., Sicora, C., and Aro, E. M. (2009) *Cellular and Molecular Life Sciences 66*, 3697-3710.

13. Komenda, J. (2000) *Biochimica et Biophysica Acta-Bioenergetics 1457*, 243-252.

14. Cser, K. and Vass, I. (2007) *Biochimica et Biophysica Acta-Bioenergetics 1767*, 233-243.

15. Stewart, D. H., Nixon, P. J., Diner, B. A., and Brudvig, G. W. (2000) *Biochemistry 39*, 14583-14594.

16. Dorlet, P., Xiong, L., Sayre, R. T., and Un, S. (2001) *Journal of Biological Chemistry 276*, 22313-22316.

17. Giorgi, L. B., Nixon, P. J., Merry, S. A. P., Joseph, D. M., Durrant, J. R., Rivas, J. D., Barber, J., Porter, G., and Klug, D. R. (1996) *Journal of Biological Chemistry 271*, 2093-2101.

18. Stewart, D. H., Nixon, P. J., Diner, B. A., and Brudvig, G. W. (2000) *Biochemistry 39*, 14583-14594.

19. Merry, S. A. P., Nixon, P. J., Barter, L. M. C., Schilstra, M., Porter, G., Barber, J., Durrant, J. R., and Klug, D. R. (1998) *Biochemistry 37*, 17439-17447.

20. Rappaport, F., Guergova-Kuras, M., Nixon, P. J., Diner, B. A., and Lavergne, J. (2002) *Biochemistry 41*, 8518-8527.

21. Raszewski, G. and Renger, T. (2008) *Journal of the American Chemical Society 130*, 4431-4446.

22. Vassiliev, S., Lee, C. I., Brudvig, G. W., and Bruce, D. (2002) *Biochemistry 41*, 12236-12243.

23. Vassiliev, S. and Bruce, D. (2008) *Photosynthesis Research 97*, 75-89.

24. Shen, G. Z. and Vermaas, W. F. J. (1994) *Biochemistry 33*, 7379-7388.

25. Hughes, J. L., Prince, B. J., Krausz, E., Smith, P. J., Pace, R. J., and Riesen, H. (2004) *Journal of Physical Chemistry B 108*, 10428-10439.

26. Williams, J. G. K. (1988) *Methods in Enzymology 167*, 766-778.

27. Vasil'ev, S. and Bruce, D. (2006) *Biophysical Journal 90*, 3062-3073.

28. Phillips, J. C., Braun, R., Wang, W., Gumbart, J., Tajkhorshid, E., Villa, E., Chipot, C., Skeel, R. D., Kale, L., and Schulten, K. (2005) *Journal of Computational Chemistry 26*, 1781-1802.

29. Humphrey, W., Dalke, A., and Schulten, K. (1996) *Journal of Molecular Graphics 14*, 33-&.

30. Vasil'ev, S., Wiebe, S., and Bruce, D. (1998) *Biochimica et Biophysica Acta-Bioenergetics 1363*, 147-156.

31. Vasil'ev, S. and Bruce, D. (1998) *Biochemistry 37*, 11046-11054.

32. Vasil'ev, S. and Bruce, D. (2000) *Biochemistry 39*, 14211-14218.

33. Mimuro, M., Tomo, T., Nishimura, Y., Yamazaki, I., and Satoh, K. (1995) *Biochimica et Biophysica Acta-Bioenergetics 1232*, 81-88.

34. Melis, A. (1989) *Philosophical Transactions of the Royal Society of London Series B-Biological Sciences 323*, 397-409.

35. Cser, K. and Vass, I. (2007) *Biochimica et Biophysica Acta-Bioenergetics 1767*, 233-243.

36. Rappaport, F., Guergova-Kuras, M., Nixon, P. J., Diner, B. A., and Lavergne, J. (2002) *Biochemistry 41*, 8518-8527.

37. Veerman, J., Bentley, F. K., Eaton-Rye, J. J., Mullineaux, C. W., Vasil'ev, S., and Bruce, D. (2005) *Biochemistry 44*, 16939-16948.

38. Vasilev, S., Bergmann, A., Redlin, H., Eichler, H. J., and Renger, G. (1996) *Biochimica et Biophysica Acta-Bioenergetics 1276*, 35-44.

39. Veerman, J., Bentley, F. K., Eaton-Rye, J. J., Mullineaux, C. W., Vasil'ev, S., and Bruce, D. (2005) *Biochemistry 44*, 16939-16948.

40. Broess, K., Trinkunas, G., van der Weij-de Wit, C., Dekker, J. P., van Hoek, A., and van Amerongen, H. (2006) *Biophysical Journal 91*, 3776-3786.

41. Krausz, E., Hughes, J. L., Smith, P. J., Pace, R. J., and Arskold, S. P. (2005) *Photosynthesis Research 84*, 193-199.

42. Vasil'ev, S. and Bruce, D. (2006) *Biophysical Journal 90*, 3062-3073.

43. Veerman, J., Vasil'ev, S., Paton, G. D., Ramanauskas, J., and Bruce, D. (2007) *Plant Physiology 145*, 997-1005.

44. Vasil'ev, S. and Bruce, D. (2004) *Plant Cell 16*, 3059-3068.

45. Vassiliev, S. and Bruce, D. (2008) *Photosynthesis Research 97*, 75-89.

CONCLUSIONS AND IMPLICATIONS

PSII Repair is an Overriding Consideration in the Structure of the Complex

The investigations of the structures and related processes during this thesis were performed in order to delineate the link between PSII structure and function. Structures that were investigated included the PBS, a long-wavelength quencher and various states of PSII disassembly and/or inactivation as related to compartmentalized repair as well as PSII complexes containing point mutations to specific ligands of co-factors/pigments. Although the structures and processes studied were in many ways disparate, in each Chapter the results illustrate the importance of PSII repair as a factor in the structure of the complex and associated antennae.

In Chapter 1, we showed that the deletion of PsbU resulted in the PBS decoupling from PSII, likely a result of the increased rate of inactivation of the OEC in the mutant (*1*). This decoupling of the PBS would serve to protect PSII from further damage by lowering the excitation energy flowing into the complex from the PBS. In Chapter 2, the importance of PSII repair was outlined explicitly, with the compartments of the thylakoid membrane showing the extent of coordinated and compartmentalized PSII repair. Certainly, it can be surmised that the superstructure of the thylakoid membrane, with the grana stacks and intervening stroma might exist in large part to facilitate such compartmentalized repair. In Chapter 3, drastic and novel quenching via a long wavelength antennae appear to be primarily responsible for the resistance of desiccated *Parmelia sulcata* to PSII damage. This quencher is so important that it was found to be present and coupled to PSII under all conditions, apparently serving as both auxiliary antennae and quencher as the conditions dictate. In Chapter 4, the Q130E mutation, which represents the key difference between D1:1 and D1:2, apparently increases the rate of non-radiative decay of the radical pair. This increase in the rate of non-radiative charge

recombination serves to decrease the rate of photodamage to PSII and is at least partially responsible for the diminished photoinhibition observed in D1:2 substituted PSII centers. This change in electron transfer kinetics might well reduce the overall quantum yield of primary photochemistry, while at the same time allowing for greater overall production via attenuated damage rates.

In all the investigations presented in this thesis, PSII repair was repeatedly shown as a key factor when considering the structure of PSII and associated complexes as well as the interactions of these elements. Even structural components endemic to PSII in the reaction center were subject to these considerations, with the Q130E mutation appearing to be an adaptation serving to reduce the rate of damage. This is an important point since the high quantum yield of PSII(>90%) is often cited as a measure of PSII efficiency (*2;3*). However, the rate of PSII damage and thus repair is high and the overall 'economics' of photosynthesis appears to be heavily dependent on this. PSII repair is also a key factor in the evolution of PSII and related elements and structures, such as quenchers, thylakoid membrane ultrastucture and auxiliary antennae. Thus, it can be concluded that understanding the link between structure and function in PSII will ultimately require that the PSII repair system be delineated in detail. If the PSII repair system is well defined this will facilitate the identification of structures in PSII or those related to the complex that are present to reduce the rate of damage or to facilitate repair.

Regulation of PSII is of Paramount Importance

PSII efficiency can be expressed by the quantum yield of primary photochemistry within the context of a fully functional complex and this model of PSII is represented in many simulations and explanations present in the literature (*3-6*). Certainly, the present thesis expounds on these ideas with the utilization of models which include quantum yield within the

context of a single representative fully functional complex (*7*). The yield of primary photochemistry is an integral part of the thought process and invariably the importance of each component in PSII is placed in this context. However, the 'economics' of photosynthesis and particularly PSII function are not limited to the quantum yield of primary photochemistry. The previous section outlined the importance of PSII repair/damage which is largely a matter of regulation. There are other reasons for regulation besides PSII repair based considerations, such as balancing the activity of PSII/PSI or optimizing the absorbance profile of the photosynthetic apparatus for existing light conditions. The regulation of PSII can be performed via alteration of the complex itself or through methods that do not require modification of PSII structure. This has led to probable compromises in the structure of PSII between the efficiency of primary photochemistry and regulation. As well, the ability of Eukaryotic photosynthetic organisms such as higher plants to regulate PSII using external elements shows that supporting elements such as antennae/quenchers and even the ultrastructure of the thylakoid membrane are of comparable significance to the structure of PSII itself.

Chapter 1 showed that the PBS PSII coupling was disrupted by the luminal side protein subunit deletion of PsbU, it is probable that this disruption was due to the increased chance of inactivation of the OEC (*8*). PBS decouples from PSII with an inactive OEC to protect PSII from damage, this also occurs under high light conditions along with PBS quenching (*9*). From this data it becomes clear that a key element in PBS function is to not only supplement PSII light harvesting capacity but also to closely regulate excitation energy influx into the complex. State transitions balance the excitation energy between PSII and PSI but the PBS must also be able to rapidly energetically decouple from PSII complexes. Therefore, this might factor into the structure of both the PBS and PSII, possibly competing with the demands of quantum yield of

the PBS-PSII supercomplex. It is conceivable that the stromal surface of PSII has been optimized to facilitate the PBS-PSII postulated weak charge-charge interactions(*10*) for instance. Although these considerations are reasonable there remains the issue of the high yield of PSII primary photochemistry, which has been cited as being >90% (*3;11*). Such a highly efficient process might bring into question whether or not there exists any significant compromise between quantum yield of primary photochemistry and regulation, or if the small differences in quantum yield implied by such compromises would be significant enough to affect selection during evolution. It does appear that within the context of the existing structure of PSII, the most significant pigments with respect to energy transfer have orientations that are optimized for efficiency and this efficiency gain is on the order of only 0.3-1% (*11*). In addition, chlorophylls key to exciton transfer are conserved in PSII and PSI (*2*). Considering the modest increase in quantum yield conferred by such chlorophyll orientations the existence of compromises between regulation and quantum yield seems likely.

In Chapter 2, the compartmentalized repair system showed the significance and extent of PSII heterogeneity resulting from repair in higher plants. Interestingly, higher plants contain PSII complexes that are remarkably similar to cyanobacteria and the repair strategy is essentially unchanged: D1 replacement (*12*). It is interesting to note that higher plants use their larger gene complement and metabolic/structural complexity to provide an array of supporting elements for PSII, both logistical as in the case of compartmentalized PSII repair and operational with respect to PSII quenching and light harvesting. For instance, Chapter 2 showed that the antennae size of PSII indicated that LCHII elements in the grana stack acts at least partially as a pool of antennae that is coupled to the pool of PSII complexes effectively maximizing the effective antennae size of the complexes. The superstructure of the thylakoid also facilitates the compartmentalization of

PSII repair, as damaged complexes can be moved from the grana stack to ensure that the PSII present in the stack is for the most part functional and activated. These supporting elements and mechanisms used by higher plants combined with the similarity of PSII in higher plants and cyanobacteria suggest that it is more feasible for the evolution of ancillary strategies to enhance or modify PSII function rather than to modify the PSII complex. Of course, higher plants do possess a longer generation time and do not exhibit the mutation rates that cyanobacteria or their progenitors would likely have possessed and so the development of novel genes or modification of complex enzymes such as PSII would be limited. However, no matter the reason for the conservation of PSII genes in higher plants the fact remains that PSII light harvesting is highly dependent on the regulation of PSII activity independent of the structure of the complex. It seems that higher plants essentially possess conserved D1:2 protein, apparently using the most damage resistant PSII complex available. Then, instead of modifying the complex for regulatory purposes as cyanobacteria do, the progenitors of higher plants evolved elements independent of the structure of PSII to serve the same purpose. This is interesting because this essentially means that the same or at least similar results can be obtained by directly altering PSII structure or through indirect regulation. This suggests that the supporting elements involved, whether it be membrane structure, repair chaperons or quenchers of PSII are in at least some cases tantamount to the structure of PSII itself in regards to primary photochemistry.

In Chapter 3 and Chapter 4, PSII light harvesting activity was shown to be heavily modified by quenching, in the case of the lichens an external quencher is probable while the quenching of PSII in the Q130E mutant was a result of a modification to PSII. This echoes the assertions outlined in the previous paragraph: that PSII primary photochemistry can be modified by changes to PSII or to supporting elements. The mechanisms are different, for the long

wavelength quencher in lichens it appears that excitons are effectively siphoned from PSII and then dissipated as heat. While the Q130E mutant likely includes non-radiative dissipation by way of recombination, effectively quenching P680+ and also decreasing the rate of triplet formation. However, in both cases PSII photodamage is significantly mitigated and resistance to high light level conditions is increased. In the case of the lichens, this resistance to photodamage is pronounced, allowing for extended periods of light exposure with only negligible photoinhibition (*13*). The quenching observed may have also been due to other mechanisms at work in addition to the long wavelength quencher. However, since the rate of dissipation for the quencher was 8 times faster than the rate of charge separation in PSII, the quencher must be significantly or wholly responsible for the resistance to photodamage on a molecular level. This resistance is among the most pronounced known to date (*13*) and it might well be due to a complex external to PSII. Such an example illustrates the principle of such PSII structure independent regulation of primary photochemistry.

The Q130E mutation is not only an example of PSII structure based regulation of PSII activity but also exemplifies the compromises present in the structure of the PSII complex. These compromises between efficiency and regulation might be the source of apparent paradoxical structures/configurations in PSII. Certainly, the H114 ligated chlorophyll stands out as an example of a peculiar element in the structure of PSII, being significantly red-shifted compared to the other chlorophylls present in CP47. This could be due to evolutionary constraints regarding the difficulty of selective pressure reconfiguring complex protein structures because the number/combination of mutations required is prohibitive. Perhaps the shift in the Q_Y transition matches the absorbance more closely to light conditions present during the evolution of the complex or perhaps the shift has a negligible effect on efficiency. These explanations,

while not without merit are all based on the idea of PSII quantum yield as an overriding consideration. What the Q130E mutant shows is that the structure of PSII is also a result of regulation, in this case perhaps a decrease in PSII quantum yield per individual center but an increase in the overall yield of the PSII population by way of a decreased rate of damage. Concordant with these ideas, a recent modeling study has implicated the H114 ligated chl as being important for photoprotection via cartenoid mediated non-photochemical quenching (*6*).

It is also worth noting that the Q130E mutation causes the F_o state of PSII in synechocysitis PCC.6803 to resemble higher plant PSII kinetics. However, closed PSII reaction centers in higher plants still possess much longer fluorescence decay lifetimes than the Q130E mutant (*14*), indicating that regulatory elements likely external to PSII contribute significantly to the kinetics at F_m.

Both the structure independent regulation of PSII and the seemingly counterintuitive elements of PSII structure indicate the complexity of PSII function. Modest changes in the quantum yield of PSII are sufficient to drive evolution but yield is sacrificed in order for the complex to operate in a 'safer' manner. Structure independent regulation of PSII function can induce profound changes to primary photochemistry and illustrates the importance of understanding the structure of PSII in context of the entire photosynthetic apparatus.

Physiologically PSII Must be Considered as a Population

Measurements on populations in science are often performed to reveal information regarding the specific characteristics of individuals in a population. For instance, if a solution of a specific enzyme exhibits a reaction rate with or affinity for specific compounds then the binding pocket is thought to directly reflect the data collected. This assumes that the population of enzymes is homogeneous with respect to structure and interactions. When the

enzyme in question is isolated and exposed to a specific substrate these assumptions regarding homogeneity might be reasonable. However, in the case of PSII, the nature of the enzyme means that a number of complexes will be in various states of repair or rather disassembly and/or inactivation and there will also be a proportion damaged. *In vivo*, PSII is also associated with a number of antennae complexes as well as quenchers in various permutations, further adding to the heterogeneity of the PSII population. For this reason PSII complexes must be considered as a heterogeneous population rather than representative of a single standard complex. This is a significant problem as models of PSII often aim to be representative of individual complexes rather than the entire population, so that reaction mechanisms can be attributed and the population data can be reconciled on a molecular level.

Chapter 1 is a clear example of the difficulties surrounding PSII measurements and the application of measurements to models of PSII function. Deletion of PsbU caused a decoupling of the PBS from PSII and this also altered the kinetics of the PSII/PBS. This could be due to the physical coupling of the PBS being affected in a subtle manner that decreased the level of energy transfer to the PSII complex from the PBS. Alternatively, the PBS might have been decoupling from PSII due to an increase in the proportion of inactivated OEC, which is rendered relatively vulnerable with the deletion of PsbU. A subsequent study (*1*), indicated that the PBS decouples from PSII upon inactivation of the OEC, which supports the idea of a larger proportion of PBS decoupled from PSII. This would essentially mean a shift in the population of PBS towards a higher proportion decoupled from PSII, rather than a specific change to the interactions between PSII and the PBS on an individual basis. If this is true, then the data obtained from the PBS-PSII population is that of at least two subpopulations, PSII complexes decoupled from the PBS and PSII coupled to the PSB. Thus, if we don't know in what proportion these populations occur then

our models that are derived from such data will represent an average PSII complex rather than a physiologically relevant one.

In Chapter 2, itself a study of PSII heterogeneity, in large part represented an attempt to reconcile the aforementioned difficulties using previously published proteomic data to determine the antennae size of PSII supercomplexes. The antennae sizes were then cross referenced with the absorbance data collected to determine the relative level of assembly of the PSII populations in the different compartments of the thylakoid membrane. This was shown to be a valid approach as the two data sets did correspond to each other closely, showing that the sizes of PSII supercomplexes obtained from the proteomic data were representative of the spectrally determined antennae sizes of the PSII populations. However, the proteomic data still showed that each compartment contained a number of PSII populations in various states of disassembly. As well, the model used, although it included the antennae sizes, assumed that the reaction pathway was identical for all PSII centers even though the different centers in states of damage/inactivation and/or repair might possess reaction pathways quite different from fully functional centers. The methods used did include fairly homogeneous populations of active and inactive PSII supercomplexes in the form of the Y100(purified stroma) and BS(purified grana) fractions and the fluorescence decay kinetics were consistent with reaction kinetics similar to standard models of PSII function. There was also a gradual shift from highly functioning PSII to inactivated and disassembled PSII as the sample origin moved from grana to stroma, demonstrating that there was a decided gradient with respect to PSII kinetics and assembly when moving from one compartment to another. Thus, Chapter 2 was a successful attempt to account for the fact that PSII exists as a heterogeneous population in that the attributes of the PSII population in each fraction of the thylakoid membrane were delineated. However, the treatment

of heterogeneity was incomplete as the PSII population likely exists as a distribution with a multitude of structural/functional states far in excess of those used in the model. As such, Chapter 2 illustrates both the facility of considering PSII as a population and the rather daunting level of complexity involved when attempting to account for the heterogeneity of such a population.

In Chapter 3 PSII complexes were shown to be coupled with a long wavelength quencher, this state of PSII was apparently true under all conditions. From the data it was apparent that under desiccation the quencher was actively quenching PSII and under F_o conditions the quencher was probably supplementing the light harvesting capacity of PSII. It would appear that the level of quenching was variable and rapid as reported in previous studies, dynamically adjusting to the conditions. This means that there might be some level of quenching under all conditions, introducing heterogeneity into the PSII population. However, when desiccated, the PSII population likely exists in a relatively homogenous state, at least with respect to reaction kinetics and perhaps structurally as well as every PSII complex appeared quenched in the same manner. Interestingly, this apparent homogeneity occurs in a state of virtual suspended animation with a complete lack of photosynthetic activity.

Chapter 4 represented an attempt that in part, served to ameliorate the difficulties of heterogeneity by changing a single important amino acid in PSII. This ensured that the change in structure was known and discrete. However, point mutants in general impair the assembly of PSII to a degree (*15*). It should also be noted that this impairment has been shown to cause a proportion of PSII centers to fail to assemble but it is also possible that the assembly problems affect assembled complexes in subtle ways as well. In spite of the assembly issue, using point mutations in this manner, much like the use of multiple sources of information in Chapter 2,

increases the certainty of changes observed being representative of changes to the PSII complex itself and not a result of introduced heterogeneity. Although, it should be noted that the Q130E mutation decreases rates of PSII photodamage and thus could alter the ratio of active to damaged/under repair complexes in the PSII population.

The nature of PSII regulation and repair ensures that populations of PSII complexes will almost always represent an array of different PSII subpopulations. This problem can be ameliorated to some extent by utilizing point mutations or using various sources of data pertaining to aspects of PSII heterogeneity and then reconciling such data through cross referencing and modeling. Systems exhibiting relatively homogeneous PSII populations, such as the BS fraction of the thylakoid membrane or desiccated *Parmelia Sulcata* can also be utilized. Heterogeneity of PSII might also be addressed using single molecule measurements (*16*), but many of the techniques proposed alter the PSII complex and suffer from significant difficulties due to lack of signal strength.

Simulations of PSII Hold Promise

This thesis endeavoured to investigate PSII function as it relates to PSII structure by studying altered PSII, using both naturally occurring structures and those produced through mutation. This approach yielded interesting data, such as Chapter 2 showing that the antennae size of the PSII supercomplex significantly contributes to PSII fluorescence decay lifetimes and that PSII photochemistry is slowed down in PSII complexes that are damaged/under repair. In Chapter 1, loss of the PsbU protein caused decoupling of the phycobilisome, consistent with a greater chance of inactivation of the OEC. Although the structure of the long-wavelength quencher is unknown at this time, Chapter 3 illustrated the facility of exciton trapping by the quencher and that the exciton trapping was capable of protecting PSII from damage. In Chapter

4, point mutations pointed toward specific co-factors as unique or capable of significantly altering the kinetics of primary photochemistry in PSII. These results provide glimpses into the mechanisms and processes involved: in Chapter 2 enough information was available for modeling of the populations of PSII in each thylakoid compartment. It was found that integrating the data from various sources yielded a reasonable model of the populations of PSII in question. Certainly, the results from the other 3 Chapters in this thesis might be integrated into a model in much the same manner. If the PBS-PSII interaction could be better understood along with the changes to PSII involved with OEC inactivation then the precise effect of PSII removal might be modeled. Similarly, if the structure of the long wavelength quencher from Chapter 3 could be determined or better yet the PSII-quencher complex, then the mechanism of this rather drastic example of PSII down regulation might be delineated. In Chapter 4, such modeling was attempted with a MD simulation of PSII and yielded a reasonable red-shift in the Q_Y transition in the D1:Ph of the Q130E mutant.

The approaches outline above, even the potential modeling as a result of likely future directions, would serve to study a specific instance or instances of PSII function. There is a lack of reconciliation between differing studies and approaches, certainly the results are compared but a comprehensive model is lacking. The MD simulation of PSII introduced in a previous study(*17*) and utilized in the present thesis, although still used at this point for modeling specific instances of PSII function still represents a step toward this type of consolidation. The simulation includes a protein environment and at present also includes the protonation states of amino acids involved (Vasil'ev, unpublished). Such a model or at least the general objectives tacitly highlight the interconnected nature of the differing structures and interactions related to PSII. This connectedness is illustrated by comparing Chapter 1 and 2, if the PBS decouples from PSII upon

inactivation of the OEC and the OEC is the source of PSII damage then it follows that this decoupling might be a result of PSII damage. Thus, the potential structural changes that occur in PSII are the initial stages of PSII disassembly and repair, and since the structures of higher plant PSII and cyanobacteria are very similar, it is likely that such a change occurs in higher plants as well. This damage/repair based reduction in antennae size was evident in Chapter 2 and such damage induced reductions in PSII antennae size have also been observed in higher plants previously (*18;19*). Thus, the structural changes brought on due to the inactivation of the OEC might be quite similar in both cyanobacteria and plants so a simulation of PSII modeling this change would be applicable to both and likely to all organisms containing PSII.

The approaches used in this thesis, such as point mutations and assaying physiological states of PSII remain limited in facility. Each experiment requires considerable resources to perform and the possible permutations, particularly in regards to point mutations is prohibitively high. A comprehensive PSII simulation might be used to decide which point mutations to employ, much as the structure of PSII and list of conserved residues have been used in the past (*20;21*). Such a simulation might also be used to run virtual experiments and then carry out the successful experiments in the laboratory using standard techniques to validate the simulation. As more information and predictive powers are developed, the simulation would be revised in a cyclic manner and synergistically with 'wet' lab work. This building of a model would reduce the need for further experiments or at least target improved experimental strategies. This type of modeling is certainly not exclusive to this field as many areas now use comprehensive computer modeling to explore experiments which are infeasible (*22*) or to enhance and supplement more conventional methods (*23*). However, the application of such comprehensive models to PSII remains an exciting area and appears to hold considerable promise.

References

1. Hwang, H. J., Nagarajan, A., McLain, A., and Burnap, R. L. (2008) *Biochemistry 47*, 9747-9755.

2. Vasil'ev, S. and Bruce, D. (2004) *Plant Cell 16*, 3059-3068.

3. Merry, S. A. P., Nixon, P. J., Barter, L. M. C., Schilstra, M., Porter, G., Barber, J., Durrant, J. R., and Klug, D. R. (1998) *Biochemistry 37*, 17439-17447.

4. Holzwarth, A. R., Muller, M. G., Reus, M., Nowaczyk, M., Sander, J., and Rogner, M. (2006) *Proceedings of the National Academy of Sciences of the United States of America 103*, 6895-6900.

5. Dekker, J. P. and Van Grondelle, R. (2000) *Photosynthesis Research 63*, 195-208.

6. Raszewski, G. and Renger, T. (2008) *Journal of the American Chemical Society 130*, 4431-4446.

7. Veerman, J., McConnell, M. D., Vasil'ev, S., Mamedov, F., Styring, S., and Bruce, D. (2007) *Biochemistry 46*, 3443-3453.

8. Hwang, H. J., Nagarajan, A., McLain, A., and Burnap, R. L. (2008) *Biochemistry 47*, 9747-9755.

9. Wilson, A., Ajlani, G., Verbavatz, J. M., Vass, I., Kerfeld, C. A., and Kirilovsky, D. (2006) *Plant Cell 18*, 992-1007.

10. Mullineaux, C. W. (2008) *Photosynthesis Research 95*, 175-182.

11. Vasil'ev, S., Shen, J. R., Kamiya, N., and Bruce, D. (2004) *Febs Letters 561*, 111-116.

12. Aro, E. M., Suorsa, M., Rokka, A., Allahverdiyeva, Y., Paakkarinen, V., Saleem, A., Battchikova, N., and Rintamaki, E. (2005) *Journal of Experimental Botany 56*, 347-356.

13. Heber, U. (2008) *Planta 228*, 641-650.

14. Roelofs, T. A., Lee, C. H., and Holzwarth, A. R. (1992) *Biophysical Journal 61*, 1147-1163.

15. Shen, G. Z. and Vermaas, W. F. J. (1994) *Biochemistry 33*, 7379-7388.

16. Vacha, F., Bumba, L., Kaftan, D., and Vacha, M. (2005) *Micron 36*, 483-502.

17. Vasil'ev, S. and Bruce, D. (2006) *Biophysical Journal 90*, 3062-3073.

18. Danielsson, R., Albertsson, P. A., Mamedov, F., and Styring, S. (2004) *Biochimica et Biophysica Acta-Bioenergetics 1608*, 53-61.

19. Danielsson, R., Suorsa, M., Paakkarinen, V., Albertsson, P. A., Styring, S., Aro, E. M., and Mamedov, F. (2006) *Journal of Biological Chemistry 281*, 14241-14249.

20. Lupinkova, L., Metz, J. G., Diner, B. A., Vass, I., and Komenda, J. (2002) *Biochimica et Biophysica Acta-Bioenergetics 1554*, 192-201.

21. Shen, G. Z. and Vermaas, W. F. J. (1994) *Biochemistry 33*, 7379-7388.

22. Lamb, R., Crossley, M., and Waller, S. (2009) *Proceedings of the Institution of Civil Engineers-Water Management 162*, 363-370.

23. Huang, H. W., Shih, T. C., Liauh, C. T., and Horng, T. L. (2009) *Journal of Medical and Biological Engineering 29*, 252-258.